EFFECTS OF INORGANIC MERCURY ON DEVELOPING ZEBRAFISH (*DANIO RERIO*) LARVAE

A Thesis Submitted to the College of
Graduate Studies and Research
In Partial Fulfillment of the Requirements
For the Degree of Doctor of Philosophy
In the Toxicology Graduate Program
University of Saskatchewan
Saskatoon

By
TRACY CLARYLINDA MACDONALD

PERMISSION TO USE STATEMENT

In presenting this thesis in partial fulfillment of the requirements for a postgraduate degree from the University of Saskatchewan, I agree that the Libraries of this University may make it freely available for inspection. I further agree that permission for copying of this thesis in any manner, in whole or in part, for scholarly purposes may be granted by the professor or professors who supervised my thesis work or, in their absence, by the Head of the Department or the Dean of the College in which my thesis work was done. It is understood that any copying or publication or use of this thesis or parts thereof for financial gain shall not be allowed without my written permission. It is also understood that due recognition shall be given to me and to the University of Saskatchewan in any scholarly use which may be made of any material in my thesis.

Requests for permission to copy or to make other use of material in this thesis in whole or part should be addressed to:

Chair of the Toxicology
Graduate Program Toxicology Centre
University of Saskatchewan
44 Campus Drive
Saskatoon, Saskatchewan, Canada S7N 5B3

ABSTRACT

Mercury (Hg) compounds are some of the most toxic compounds of any heavy metal on earth. Due to long-range transport from point sources Hg can be found world-wide in air, soil, water, and living organisms. Mercury compounds can cause a number of adverse effects, with the unborn fetus, infants, and children being most susceptible. Zebrafish (*Danio rerio*) are an excellent vertebrate model system for toxicological studies, including developmental effects. The overall objective of this research was to investigate the effects of inorganic forms of Hg in zebrafish larvae.

Unique accumulation patterns were observed using synchrotron X-ray fluorescence imaging after zebrafish were exposed to one of four Hg compounds (i.e. mercuric chloride, mercury bis-L-cysteineate, methylmercury chloride, methylmercury L-cysteineate). Specifically, we noted chemical form dependant and tissue-specific Hg accumulation including the sensory cells of the olfactory epithelia and the neuromasts.

Phenylthiourea (PTU) is commonly used to block zebrafish melanogenesis to generate transparent larvae to aid with enhanced visualization of immunohistochemical and vital stains. It was determined that PTU dramatically alters Hg toxicity through chemical interaction with Hg so that further studies were conducted in the absence of PTU. To investigate the effects of Hg on primary neurons, the immunohistochemistry protocol using anti-acetylated tubulin was performed and the results demonstrated that mercuric chloride damages primary neurons particularly in the olfactory pits.

To study potential detoxification of Hg in zebrafish we examined the efficacy of two sequestration agents, dimercaptosuccinic acid and alpha lipoic acid, as well as endogenous selenium. The levels of Hg were not significantly lower following treatment with either sequestration agent under the conditions used in this research. Previous work examining the antagonistic relationship between Hg and selenium has been conducted by dosing animals with both Hg and selenium (Se). We discovered a mixed chalcogenide of the general form $HgS_xSe_{(1-x)}$ forming in vivo following exposure to mercuric chloride without the addition of selenium. Indeed the selenium may have been remobilized from natural stores in the pigment spots.

The research presented herein demonstrates that the target tissues for Hg depend strongly on chemical form. In particular inorganic Hg can accumulate in a number of important tissues

including sensory systems. The formation of insoluble and non-toxic $HgS_xSe_{(1-x)}$ in zebrafish larvae suggests that endogenous selenium may play critical roles in modulating toxicity.

ACKNOWLEDGEMENTS

My thesis work would not have been possible without guidance, patience, and support from a number of people. I am very grateful for my supervisors, Dr. Graham George and Dr. Pat Krone, who gave me the opportunity to complete my PhD in their research groups. They challenged and encouraged me to become a better scientist. I would also like to thank my committee members, Dr. Barry Blakley, Dr. Dave Janz, Dr. Phyllis Paterson, and Dr. Ingrid Pickering, who helped me improve my research by always leaving their doors open when I needed advice and suggestions. I am also appreciative of the beamline support provided by Dr. Robert Gordon and Dr. Sam Webb.

I would like to acknowledge the support I received from the Natural Sciences and Engineering Research Council of Canada (NSERC), the Canadian Institutes of Health Research (CIHR), and CIHR-THRUST.

I owe a debt of gratitude to all of my friends and colleagues for their ongoing encouragement and for making my graduate studies an enjoyable experience. I would like to thank Dr. Gosia Korbas for taking me under her wing and teaching me about many aspects of her research. I would also like to thank my group members and friends, especially Dr. Brian Bewer, Tanner Bodnarik, Dr. Sally Caine, Dr. Julien Cotelesage, Dr. Mark Hackett, Ashley James, Eden Marchand, Susan Nehzati, Kurt Nienaber, Dr. Jake Pushie, Kelly Summers, Nicole Sylvain, Dr. Cynthia Swan, Mylyne Tham, and Justin Tse, for providing their scientific expertise, advice, and thoughtful comments.

Finally, for their unconditional love and support throughout my education, I would like to send a special thank-you to my grandma, my parents, and my sister.

DEDICATION

I dedicate my dissertation to my grandpa, Harold Campbell (1920-2014), who taught me the importance of pausing and “havin’ a look” to appreciate the world around me. My achievements were made possible by his constant love and encouragement. His accomplishments and the person he was will continue to inspire me.

TABLE OF CONTENTS

PERMISSION TO USE STATEMENT i
ABSTRACT ii
ACKNOWLEDGEMENTS iv
DEDICATION v
TABLE OF CONTENTS vi
LIST OF TABLES x
LIST OF FIGURES xi
LIST OF ABBREVIATIONS xiv
CHAPTER 1. INTRODUCTION 1
1.1. Mercury 1
1.1.1. Types of Mercury Compounds 1
1.1.2. Sources 2
1.1.3. Absorption, Distribution, and Excretion of Mercury 6
1.1.4. Effects of Mercury on Organisms 7
1.1.5. Mercury and Selenium 9
1.2. Zebrafish 11
1.2.1. A Model System for Studying Toxins 11
1.2.2. An Introduction to the Olfactory System 12
1.2.3. An Introduction to the Lateral Line System 14
1.2.4. Potential Effects on Developing Sensory Systems 15
1.3. Synchrotron Techniques 16
1.3.1. X-ray Fluorescence Imaging 16
1.3.1.1. Overview of X-ray Fluorescence Imaging 16
1.3.1.2. Advantages of X-ray Fluorescence Imaging 17
1.3.1.3. Disadvantages of X-ray Fluorescence Imaging 18
1.3.1.4. Potential Complementary Techniques 18
1.3.2. X-ray Absorption Spectroscopy 20
1.4. Research Objectives and Null Hypotheses 21
1.4.1. Objectives 21
1.4.2. Null Hypotheses 22
CHAPTER 2. METHODS 23
2.1. Zebrafish 23
2.1.1. Maintenance, Husbandry and Embryo Care 23
2.1.2. Zebrafish Exposures 23
2.1.3. Sample Collection and Preparation 24
2.1.3.1. Embedding in Methacrylate 24

2.1.3.2. Sectioning and Staining 25
2.2. General Synchrotron Introduction 26
2.2.1. X-ray Fluorescence Imaging 27
2.2.2. X-ray Absorption Spectroscopy 32
CHAPTER 3. CHEMICAL FORM MATTERS: DIFFERENTIAL ACCUMULATION OF MERCURY FOLLOWING INORGANIC AND ORGANIC MERCURY EXPOSURES IN ZEBRAFISH LARVAE 34
3.1. Preface 34
3.2. Manuscript Author Contributions 34
3.3. Acknowledgements 35
3.4. Abstract 35
3.5. Introduction 36
3.6. Methods 38
3.6.1. Animal Care and Embryo Collection 38
3.6.2. Mercury Treatment Solutions 38
3.6.3. Calculation of Mercury Speciation in Treatment Solutions 39
3.6.4. Preparation of Sections 39
3.6.5. X-ray Fluorescence Imaging (XFI) 41
3.6.6. X-ray Fluorescence Imaging Data Analysis 41
3.7. Results and Discussion 44
3.7.1. Solution Species and the Nature of the Exposure 44
3.7.2. Tissue and Chemically Specific Mercury Accumulation 46
CHAPTER 4. PHENYLTHIOUREA ALTERS TOXICITY OF MERCURY COMPOUNDS IN ZEBRAFISH LARVAE 60
4.1. Preface 60
4.2. Manuscript Author Contributions 60
4.3. Acknowledgements 61
4.4. Abstract 61
4.5. Introduction 62
4.6. Materials and Methods 64
4.6.1. Chemicals 64
4.6.2. Zebrafish 64
4.6.3. Statistical Analysis 65
4.6.4. X-ray Fluorescence Imaging Sample Preparation 65
4.6.5. X-ray Fluorescence Imaging (XFI) 65
4.6.6. X-ray Fluorescence Imaging Data Analysis 66

4.6.7. X-ray Absorption Spectroscopy 66
4.6.8. Density Functional Theory (DFT) 67
4.7. Results and Discussion 67
4.7.1. Toxicological Profiles 67
4.7.2. X-ray Fluorescence Imaging (XFI) 72
4.7.3. Extended X-ray Absorption Fine Structure (EXAFS) and Density Functional Theory (DFT) 77
CHAPTER 5. EFFECTS OF INORGANIC MERCURY ON THE OLFACTORY PITS OF ZEBRAFISH LARVAE 85
5.1. Preface 85
5.2. Author Contributions 85
5.3. Acknowledgements 85
5.4. Abstract 86
5.5. Introduction 86
5.6. Experimental 87
5.6.1. Zebrafish 87
5.6.2. X-ray Fluorescence Imaging (XFI) 88
5.6.3. Tubulin Visualization 88
5.6.4. Optical Microscopy 89
5.7. Results and Discussion 89
CHAPTER 6. DIFFERENTIAL LOCALIZATION OF MERCURY IN THE PRESENCE OF THE PUTATIVE SEQUESTRATION AGENTS DIMERCAPTOSUCCINIC ACID AND α-LIPOIC ACID 94
6.1. Preface 94
6.2. Manuscript Author Contributions 94
6.3. Acknowledgements 95
6.4. Abstract 95
6.5. Introduction 96
6.6. Materials and methods 97
6.6.1. Animal Care and Embryo Collection 97
6.6.2. Mercury Treatment Solutions 99
6.6.3. Preparation of Sections 99
6.6.4. X-ray Fluorescence Imaging (XFI) 100
6.6.5. X-ray Fluorescence Imaging Data Analysis 101
6.7. Results and Discussion 101

CHAPTER 7. INTERACTION OF MERCURY AND SELENIUM IN THE LARVAL STAGE ZEBRAFISH VERTEBRATE MODEL 109
7.1. Preface 109
7.2. Manuscript Author Contributions 109
7.3. Acknowledgements 110
7.4. Abstract 110
7.5. Introduction 111
7.6. Methods 112
7.6.1. Zebrafish 112
7.6.2. X-ray Fluorescence Imaging (XFI) 113
7.6.3. Micro X-ray Absorption Spectroscopy (μ-XAS) 115
7.6.4. Correlation Plots 115
7.7. Results and Discussion 115
7.7.1. X-ray Fluorescence Imaging (XFI) 115
7.7.2. Correlations Plots 122
7.7.3. Micro-X-ray Absorption Spectroscopy (μ-XAS) 126
7.8. Conclusions 128
CHAPTER 8. DISCUSSION, CONCLUSIONS, AND FUTURE DIRECTIONS 129
REFERENCES 137
APPENDIX A – SUPPLEMENTARY MATERIAL FOR CHAPTER 3 154
APPENDIX B – SUPPLEMENTARY MATERIAL FOR CHAPTER 4 157

LIST OF TABLES

Table 3.1 Predicted mercury speciation in zebrafish culture water 40

Table 3.2 Estimated diffusion coefficients and membrane permeabilities for different mercury species 54

Table 4.1 Extended X-ray absorption fine structure (EXAFS) parameters and curve-fitting results of phenylthiourea with mercury compounds at stoichiometry of 10:1 78

Supplementary Table 3.1 All components of mercury treatment solutions in millimolar concentrations included in speciation calculations using MINTEQA2 software 154

Supplementary Table 3.2 Variation in cellular mercury concentrations in liver and somitic muscles between three zebrafish larvae from Supplementary Figure 3.1 156

Supplementary Table 4.1 Statistical significance values for comparison of deaths in $HgCl_2$ versus $HgCl_2$ with phenylthiourea groups 157

Supplementary Table 4.2 Statistical significance values for comparison of deaths in CH_3HgCl versus CH_3HgCl with phenylthiourea groups 157

Supplementary Table 4.3 T-test values 157

LIST OF FIGURES

Figure 2.1 Configuration of beamline 20-ID-B at the Advanced Photon Source, Argonne, IL, USA.....28

Figure 2.2 Concept of X-ray fluorescence imaging of a zebrafish section.....31

Figure 3.1 Quantitative mercury distributions in 5 dpf zebrafish larvae following a 36-hour exposure to 1 μM mercuric chloride $HgCl_2$, 1 μM methylmercury chloride CH_3HgCl, 200 μM mercuric bis-L-cysteineate $Hg(L\text{-}Cys)_2$, or 2 μM methylmercury L-cysteineate.....43

Figure 3.2 Schematic structures of the inorganic and organic mercury species considered in this work 45

Figure 3.3 Quantitative mercury distributions in 5 dpf zebrafish larvae following a 36-hour exposure to 1 μM mercuric chloride $HgCl_2$, 1 μM methylmercury chloride CH_3HgCl, 200 μM mercuric bis-L-cysteineate $Hg(L\text{-}Cys)_2$, or 2 μM methylmercury L-cysteineate.....47

Figure 3.4 Quantitative mercury distributions in 5 dpf zebrafish larvae following a 36-hour exposure to 1 μM mercuric chloride $HgCl_2$, 1 μM methylmercury chloride CH_3HgCl, 200 μM mercuric bis-L-cysteineate $Hg(L\text{-}Cys)_2$, or 2 μM methylmercury L-cysteineate.....49

Figure 3.5 Quantitative mercury distributions in 5 dpf zebrafish larvae following a 36-hour exposure to 1 μM mercuric chloride $HgCl_2$, 1 μM methylmercury chloride CH_3HgCl, 200 μM mercuric bis-L-cysteineate $Hg(L\text{-}Cys)_2$, or 2 μM methylmercury L-cysteineate.....52

Figure 4.1 Schematic structure of the tyrosinase inhibitor 1-phenyl-2-thiourea (PTU).....63

Figure 4.2 Cumulative mortality (%) stacked on top of cumulative deformity (%) (+ SE) of zebrafish larvae over 3 days of exposure to various $HgCl_2$ treatments, with and without phenylthiourea.....70

Figure 4.3 Cumulative mortality (%) stacked on top of cumulative deformity (%) (+SE) of zebrafish larvae over 3 days of exposure to various CH_3HgCl (MeHg) treatments with and without phenylthiourea 71

Figure 4.4 Transverse sections through the olfactory region of zebrafish treated with 4 μM $HgCl_2$ in absence (A, C and E) or presence (B, D and F) of 100 μM phenylthiourea.....73

Figure 4.5 Transverse sections through the trunk region of zebrafish treated with 4 μM $HgCl_2$ in absence (A, C and E) or presence (B, D and F) of 100 μM phenylthiourea.....74

Figure 4.6 Transverse sections through the eye region of zebrafish treated with 0.2 μM CH_3HgCl in absence (A, C and E) or presence (B, D and F) of 100 μM phenylthiourea.....75

Figure 4.7 Transverse sections through the trunk region of zebrafish treated with 0.2 μM CH_3HgCl in absence (A, C and E) or presence (B, D and F) of 100 μM phenylthiourea.....76

Figure 4.8 Mercury LIII-edge extended X-ray absorption fine structure (EXAFS) for phenylthiourea complexes with $HgCl_2$ and MeHgOH at a stoichiometry of 10:1 78

Figure 4.9 Schematic structures of four-coordinate complexes involving phenylthiourea and Hg^{2+}. (A) Hg^{2+} coordinated by two bidentate phenylthiourea ligands 80

Figure 4.10 Density functional theory energy-minimized geometry-optimized structures of the products resulting from reacting phenylthiourea with (A) $HgCl_2$ or (B) CH_3HgOH in aqueous solution....82

Figure 5.1 Olfactory epithelium of a zebrafish larva exposed to 1 µM $HgCl_2$ for 24 hours. The methylene blue stained histological image (left) shows both the olfactory epithelia (oe) and neuromasts (nm)....90

Figure 5.2 High resolution (500 nm) X-ray fluorescence imaging images of olfactory epithelium in zebrafish raised to 3 dpf then exposed to a) system water (control) or b) 2 µM $HgCl_2$ for 72 hours....90

Figure 5.3 Anti-acetylated tubulin staining of zebrafish exposed to a) system water (control) or b) 4 µM $HgCl_2$ for 24h....92

Figure 6.1 Schematic structures for meso-dimercaptosuccinic acid (meso-DMSA) and R-(+) α-lipoic acid (ALA) and R-(+) dihydro α-lipoic acid (DHLA)....98

Figure 6.2 Effects of 20 hour exposure to water (control), 100 µM DMSA and 10 µM ALA on larval stage zebrafish previously exposed for 24 hours to A $HgCl_2$ solutions in fish culture water (2 µM, final Hg) or B 1 µM CH_3HgL-Cys in fish culture water....102

Figure 6.3 Effects of extended exposure (up to 72 hours) to A 100 µM DMSA on larval stage zebrafish exposed to $HgCl_2$ solutions in fish culture water (2 µM, final Hg), or B to 10 µM ALA on larval stage zebrafish exposed to 0.5 µM CH_3HgL-Cys in fish culture water....104

Figure 6.4 Effects of extended ALA exposure (72 hours) on brains of larval stage zebrafish exposed to 0.5 µM CH_3HgL-Cys in fish culture water....105

Figure 7.1 Typical larval zebrafish trunk sections, stained with methylene blue (A) and hematoxylin and eosin (H&E) (B)....114

Figure 7.2 Localization of selenium and mercury in trunk sections of larval zebrafish exposed to system water (control), 2 µM $HgCl_2$, or 1 µM CH_3HgCl....116

Figure 7.3 Localization of sulfur, zinc, selenium, and mercury in pronephros of larval zebrafish exposed to system water (control), 0.5 µM CH_3HgCl, or 2 µM $HgCl_2$....119

Figure 7.4 High resolution XFI of selenium and mercury in zebrafish pronephric duct of the zebrafish exposed to 2 µM $HgCl_2$ shown in Figure 7.3....120

Figure 7.5 Mercury selenium co-localization in zebrafish brain of fish exposed to 2 µM $HgCl_2$. The upper image of the entire section was imaged on APS 20-ID using a step size of 5 µm and a dwell time of 0.6 s per pixel....120

Figure 7.6 High-resolution (500 nm) X-ray fluorescence imaging of larval zebrafish brain imaged at APS beamline 2-ID-D....121

Figure 7.7 Correlation plots of Hg *vs.* Se for selected data sets. (A) shows the kidney section from Figure. 7.3 with $HgCl_2$ treatment, b, and c the brain sections with $HgCl_2$ treatment from Figure 7.5 and 7.6, respectively, and d shows the kidney section from CH_3HgCl-treated larvae from Figure 7.3....123

Figure 7.8 Correlation plot of Hg *vs.* Se for a kidney section from a $HgCl_2$-treated zebrafish showing two distinct correlation domains....124

Figure 7.9 Hg L_{III} micro X-ray absorption near-edge spectra of zebrafish pronephric duct, compared with spectra of selected model compounds. Data were measured on SSRL 2–3 127

LIST OF ABBREVIATIONS

°	degrees
°C	degrees Celsius
λ	cell membrane thickness
α-HgS	red form of mercury sulfide; cinnabar
β-HgS	black form of mercury sulfide; metacinnabar
µg	microgram
µg/cm^2	microgram per square centimetre
µL	microlitre
µm	micrometer
µM	micromolar
µ-XAS	micro X-ray absorption spectrometry
$\chi(k)$	EXAFS oscillations
ε	dielectric value
σ^2	mean square deviation
σ^2_{vib}	vibrational component of the mean square deviation
σ^2_{stat}	static component of the mean square deviation
Å	angstroms
a	areal density
ALA	alpha lipoic acid
AMDEs	Atmospheric Mercury Depletion Events
ANOVA	analysis of variance
Ag	silver
Ar	argon
APS	Advanced Photon Source
AS	Australian Synchrotron
Au	gold
BBB	blood-brain barrier
Bi_n^+	bismuth cation
BPB	blood-placental barrier
C_{60}^+	buckminsterfullerene cation

Ca	calcium
Cd	cadmium
CdSe	cadmium selenide
$[CH_3Hg]^+$	methylmercury cation
CH_3HgOH	methylmercury hydroxide
CH_3HgCl	methylmercury chloride
$CH_3HgC_3H_6NO_2S$	methylmercury cysteineate
Cl	chlorine
CLS	Canadian Light Source
cm	centimeters
CO_3^{2-}	carbonate
COSMO	Conductor-like Screening Model
Cs	cesium
CSD	Cambridge Structural Database
Cu	copper
DFT	density functional theory
DHLA	dihydro-α-lipoic acid
*D*m	diffusion coefficient
DMSA	dimercaptosuccinic acid
dpf	days post fertilization
E_0	threshold energy
EtOH	Ethanol
EXAFS	Extended X-ray Absorption Fine Structure
g	grams
Ga_2O_3	gallium oxide
GDP	guanosine diphosphate
GeV	giga electron volts
GTP	guanosine triphosphate
H&E	Hematoxylin & Eosin
H_2O	water
h	hours

HCl	Hydrochloric acid
HEPES	4-(2-Hydroxyethyl)piperazine-1-ethanesulfonic acid
Hg	mercury
Hg^0	elemental mercury
Hg^{1+}	monovalent mercury cation
Hg^{2+}	mercuric mercury
Hg-Sn	mercury tin
$HgCl_2$	mercuric chloride
Hg_2Cl_2	mercury (I) chloride
$Hg(OH)^+$	mercury (II) hydroxide ion
$Hg(OH)_2$	mercury (II) hydroxide
$Hg(OH)_3^-$	mercury (III) hydroxide ion
HgS	mercuric sulfide
HgSe	mercury selenide
$Hg(C_3H_6NO_2S)_2$	mercury bis-L-cysteineate
hpf	hours post fertilization
I_0	ion chamber prior to sample stage
I_T	ion chamber after sample stage
ICP-MS	Inductively Coupled Plasma Mass Spectrometer
JB-4	plastic embedding kit
K	kelvin
K^+	potassium cation
KB	Kirkpatrick−Baez
keV	kilo electron volts
kJ/mol	kilojoules per mole
K_{ow}	octanol−water partition coefficient
L	litre(s)
L-cys	L-cysteineate
LA-ICP-MS	Laser Ablation Inductively Coupled Plasma Mass Spectrometer
LAT1	L-type amino acid transporter
LINAC	linear accelerator

M	molar
mA	milliamp
MeHg	methylmercury
MeHgOH	methylmercury hydroxide
MeV	milli electron volts
min	minutes
Mg^{2+}	magnesium cation
mg	milligram
$MgSO_4$	Magnesium sulfate
mL	millilitre
mM	millimolar
MRP-2	multidrug resistance protein-2
m_V	molecular volume
N	nitrogen
Na^+	sodium cation
$NaHCO_3$	Sodium bicarbonate
NaH_2PO_4	monosodium phosphate
n	# of larvae per treatment
ng	nanogram(s)
nm	nanometer
NO^{3-}	nitrate
O	oxygen
OAT1	organic anion transporter 1
OH	hydroxide
P	permeability
P	probability
PBS	phosphate buffered saline
PBST	phosphate buffered saline with 0.01% Tween 20
PFA	paraformaldehyde
PO_4^{3-}	phosphate
ppm	parts per million

PTU	1-phenyl-2-thiourea
R	individual bond-lengths
R^2	correlation coefficient
RF	radio frequency
Rh	rhodium
s	seconds
S	sulfur
S_2N_2	dinitrogen disulfide
Se	selenium
Sel P	selenoprotein P
Si	silicon
SIMS	secondary ion mass spectrometry
Sn	tin
SO_4	sulfate
SPEAR	Stanford Positron Electron Accelerating Ring
SRIXE	Synchrotron Radiation Induced X-ray Emission
SSRL	Stanford Synchrotron Radiation Lightsource
Tl	thallium
TlCl	thallium chloride
V	volume
v/v	volume/volume percent
XAS	X-ray absorption spectroscopy
Xe^+	xenon cation
XFI	X-ray fluorescence imaging
XFM	X-ray fluorescence microscopy
z	atomic number
Zn	zinc

CHAPTER 1. INTRODUCTION

1.1. Mercury

1.1.1. Types of Mercury Compounds

Mercury compounds are some of the most toxic compounds (Klassen, 2001; Morel et al., 1998). Significant research has been conducted to try and understand the biogeochemical cycling of mercury; however, there are complex reactions involved and not all aspects of mercury cycling are understood (Gustin et al., 2007). Mercury exists in a variety of chemical species in the environment and the different species confer different levels and different types of toxicity (Clarkson and Magos, 2006). A number of factors influence the speciation of mercury and these factors also influence the ability of mercury to bioaccumulate within species and to biomagnify in the food chain.

Mercury is known to exist in three valence states: Hg^0 (elemental), Hg^{1+} (monovalent cation), and Hg^{2+} (divalent cation) (Morel et al., 1998). Hg^{4+} is an exotic that may exist although only at liquid helium temperatures (Wang et al., 2007). Hg is generally $5d^{10}$ and is not formally a transition metal as its chemistry does not involve d-vacancies; however, if Hg^{4+} does exist then Hg can be a transition element (Wang et al., 2007).

Elemental mercury is the only metal that exists as a liquid at room temperature (Greenwood and Earnshaw, 1984). Unlike the divalent cation, the monovalent cation does not exist naturally in the environment but instead exists as Hg^{2+} with a strong metal-metal bond. Organo-metallic (carbon bound directly to the metal) forms of mercury are the most toxic and are the most well-studied (Clarkson and Magos, 2006). The most abundant forms of naturally occurring mercury are elemental, inorganic, methyl mercury (bound to Cl or OH), dimethyl mercury, and ethyl mercury (Kehrig, 2011). Each form of mercury has unique exposure, metabolic and toxic effects (Clarkson and Magos, 2006).

In regard to location, mercury speciation varies in the atmosphere (primarily elemental form), in sediment (primarily Hg^{2+}), and in water (highly variable) (Morel et al., 1998). Mercury speciation in the water column depends on the location, the season, the depth, and the amount of bacteria and plankton (Morel et al., 1998). When seasonal temperature increases, a corresponding increase in methylation of mercury is observed (Sigel and Sigel, 1997). Elemental mercury is found in higher concentrations closer to the air-water interface whereas total mercury and methylmercury (MeHg) exist in greater concentrations near the sediment-

water interface (Morel et al., 1998). Depth in the water column also affects mercury speciation because surface water tends to be oxic or aerobic and deeper water tends to be anoxic or anaerobic (Morel et al., 1998). Deep, anoxic waters often have higher levels of MeHg and Hg^{2+} due to sedimentation of mercury with iron and manganese oxides (Morel et al., 1998). The form of mercury depends on the pH and the chloride concentration and can exist as $[Hg(OH)]^{+}$, $Hg(OH)_2$, $[Hg(OH)_3]^{-}$, $[HgCl]^{+}$, HgClOH, $HgCl_2$, $[HgCl_3]^{-}$, or $[HgCl_4]^{-}$ (Morel et al., 1998). In aerobic conditions, MeHg is usually present as CH_3HgCl or CH_3HgOH (Morel et al., 1998).

Biotransformation of mercury by bacteria is another important factor affecting speciation. Desulfovibrio desulfuricans bacteria, in laboratory cultures containing elevated mercury concentrations, have been found to produce MeHg (Morel et al., 1998). One of the reasons that methylation is greater in anaerobic environments (Sigel and Sigel, 1997) is that sulfate-reducing bacteria are obligate anaerobes and are believed to be involved with methylation of mercury in the environment (Kehrig, 2011). It is hypothesized that acidification of surface waters could also play a role in increasing MeHg production due to increased levels of sulfate (Sigel and Sigel, 1997). However, some oceans and estuaries may have concentrations of sulfate that are too high for sulfate-reducing bacteria to methylate mercury efficiently (Morel et al., 1998).

1.1.2. Sources

Mercury is a global pollutant spread by both natural and anthropogenic activities. It is estimated that only 10% of annual atmospheric mercury is from natural emissions while 30% of annual emissions are from anthropogenic sources and the remaining 60% are from re-emission of mercury that was deposited in soils and water primarily from previous anthropogenic contributions (UNEP, 2013). Some common anthropogenic point sources include chlor-alkali plants, pulp industries, cement manufacturing, waste handling, treatment and incineration, and burning of fossil fuels (Morel et al., 1998). Many manufacturing processes, including some currently operating, use elemental mercury and are thus sources of elemental mercury in the environment (Sigel and Sigel, 1997). Some of these processes include the manufacture of barometers, thermometers, switches, fluorescent lamps, X-ray tubes, and dental amalgam (Sigel and Sigel, 1997). Mercury amalgamation is used in artisanal and small-scale gold mining to purify gold because it is simple, cheap, and effective for gold extraction (Sigel and Sigel, 1997). By adding mercury to the ore that contains small particles of gold, an amalgam of mercury and

gold forms. The amalgam is then heated which volatilizes the Hg and leaves pure gold behind; however, this process releases mercury vapour into the atmosphere (Sigel and Sigel, 1997; Bose-O'Reilly et al., 2008). Although there are many different anthropogenic sources of atmospheric mercury, artisanal and small-scale gold mining represents 37% of all atmospheric emissions (UNEP, 2013). An estimated 800 tonnes of mercury waste are released annually into the land and water surrounding artisanal gold mining operations (UNEP, 2013). Artisanal gold mining practices occur in over 50 countries including Peru, Brazil and the Philippines and an estimated 10 to 15 million people are conducting this practice (WHO, 2008). Unfortunately, children and women are often found to conduct this procedure thus exposing themselves to high levels of mercury vapour (Bose-O'Reilly et al., 2008). Additionally, some people heat the gold and mercury amalgam in their homes for convenience and/or to prevent theft of the gold, resulting in exposure to everyone in the home (WHO, 2003). It is important to note that artisanal gold mining has been banned in some countries yet many people continue the illegal practice as it is often their primary source of income (Bose-O'Reilly et al., 2008). For example, it has been banned in China and they report no emissions from artisanal gold mining; however, it is likely that people are still continuing the practice and this may affect the estimated global emissions (UNEP, 2013). The burning of coal is the second greatest contributor of atmospheric emissions at 24% (UNEP, 2013). Specifically, East Asia, Southeast Asia and South Asia release nearly 50% of all annual mercury emissions (approximately 931 tonnes of Hg; UNEP, 2013). Sub-Saharan Africa and South America contribute approximately 16% and 12.5% respectively (UNEP, 2013).

Methylmercury is the most common form of organic mercury and the primary source of exposure to humans is through the ingestion of fish, shellfish, and marine mammals (WHO, 2008). Both inorganic and organic forms of mercury had various uses such as in pesticides (Sigel and Sigel, 1997) especially ethyl- and methylmercury which were often used as antifungal agents in seed grain (Clarkson and Magos, 2006). Mercuric chloride was used in photography laboratories, embalming and taxidermy (Sigel and Sigel, 1997). Mercury is an effective disinfectant, which is why calomel, mercuric oxide, and ammoniated mercury have been used as disinfecting agents and preservatives (Sigel and Sigel, 1997). Some countries have also used mercury for medicinal purposes and some are in use today. For example, methoxypropylmercury was used as a diuretic and phenyl mercury was used as a vaginal contraceptive (Sigel and Sigel, 1997) and Hg_2Cl_2 (calomel) was used in teething powder

(Weinstein and Bernstein 2003). Thimerosal (ethylmercury thiosalicylate) is currently used as a preservative in many multidose vaccines around the world (Clarkson and Magos, 2006). In some parts of the world other organic forms of mercury are still used in paints, fungicides, antiseptics, preservatives, and topical disinfectants (WHO, 2008).

Natural point sources include volcanoes and forest fires (Morel et al., 1998). Although the contribution of mercury to the atmosphere from forest fires is poorly understood it does represent an important factor in mercury emission (Morel et al., 1998). Soils reportedly contain over 90% of the total ecosystem mercury and certain plants can accumulate mercury depending on the plant age and species (Gustin et al., 2008). Wind moving dust particles and degassing from water surfaces are the most common non-point sources of mercury (Morel et al., 1998). There is increased transfer of mercury in soil to water during flooding events, especially in new surface impoundments (Sigel and Sigel, 1997). However, the mechanisms involved in moving mercury from the water to sediments are not well understood (Sigel and Sigel, 1997).

As previously mentioned, mercury is found worldwide in air, soil, water and organisms yet the amount varies depending on the chemical form. Approximately 95% of the total mercury in the atmosphere is in the elemental form (Morel et al., 1998). Elemental mercury is slowly oxidized (likely by ozone) to Hg^{2+} at the solid-liquid interface of fog and cloud droplets (Morel et al., 1998). Adsorption of mercury on aerosols, such as soot, promotes deposition of mercury from the air as well (Morel et al., 1998). Natural waters are normally super-saturated with elemental mercury compared to the air above causing it to volatilize to the atmosphere and remain there for up to a year (Morel et al., 1998). This explains how mercury can affect remote or previously pristine regions through long-range transport.

The arctic acts as a sink for many contaminants, including mercury, from all the continents in the northern hemisphere (Douglas et al., 2012). Atmospheric Mercury Depletion Events (AMDEs) occur in both the artic and in Antarctica (Sprovieri et al., 2010). In the three months after polar sunrise, elemental mercury can be converted to reactive or water-soluble forms of mercury that are rapidly deposited in the snow and ice, resulting in an increase of mercury deposition from the atmosphere (Sprovieri et al., 2010). The sea ice in the arctic is an area that varies seasonally providing an interface for gas and contaminant exchange (Douglas et al., 2012). Because multi-year sea ice is being replaced by seasonal ice it may cause significant

changes in mercury cycling and further research must be done to understand the potential effects (Douglas et al., 2012).

Bioaccumulation and biomagnification of mercury depend on the chemical form. Elemental mercury and dimethyl mercury are not reactive and therefore do not bioaccumulate whereas methylmercury does bioaccumulate and biomagnify (Kehrig, 2011, Morel et al., 1998, Sigel and Sigel, 1997). Bioaccumulation is related to bioavailability, speciation, lipid solubility, relative concentration, and efficiency of assimilation by grazers (Morel et al., 1998). The single greatest contribution of mercury to the food chain is from MeHg bioconcentrating from the water to plankton (Kehrig, 2011). MeHg then further accumulates up to one million times from plankton to predatory fish and mammals (i.e. biomagnifies) (Kehrig, 2011). Generally, larger and older animals have more MeHg (WHO, 2008). While MeHg is lipid soluble, it is most commonly found in muscle tissue of fish suggesting that lipid solubility is not the only variable at play (Morel et al., 1998). Previous models had assumed that the chemical form was CH_3HgCl which is more lipophilic and more toxic (Harris et al., 2003). Harris et al. (2003) found that the mercury in swordfish and orange roughy was bound to an aliphatic sulfur and most likely cysteine therefore previous models estimating toxicity that had assumed the primary form to be CH_3HgCl may be inaccurate.

Bioaccumulation and biomagnification of inorganic mercury is much more complicated than MeHg (Morel et al., 1998). $HgCl_2$ and CH_3HgCl both diffuse through membranes at approximately the same rate and both are retained by microorganisms (Morel et al., 1998). However, MeHg is transferred four times more than Hg^{2+} from marine diatoms to copepods because Hg^{2+} is bound to the particulate cellular material of diatoms which are excreted by the copepod whereas the MeHg is bound to the soluble fraction of diatoms and is thereby absorbed in copepods (Morel et al., 1998). Phytoplankton do not readily assimilate Hg^{2+} and thus do not transfer it up the food chain; however, zooplankton can accumulate both organic and inorganic mercury from both food and water leading it to be passed on to the next predator (Kehrig, 2011).

Biomagnification of mercury can be reduced through bloom dilution in eutrophic systems (Kehrig, 2011). When algal biomass increases, the concentration of mercury per cell decreases which subsequently reduces dietary mercury to zooplankton (i.e. bioaccumulation in zooplankton) (Kehrig, 2011). The decreased bioaccumulation naturally leads to reduced trophic transfer and decreased rate of biomagnification (Kehrig, 2011).

Tropical ecosystems have not been well studied because they are often considered less contaminated (especially in the South Atlantic) (Kehrig, 2011). As humans are using increasingly more land in tropical areas, more research will have to be conducted to better understand mercury in these ecosystems (Kehrig, 2011). Tropical systems may tend to have less mercury deposition than the north and south poles; however, tropical ecosystems also have warmer temperatures, more solar radiation, and high levels of dissolved organic carbon, which can all affect methylation of mercury (Kehrig, 2011).

As previously discussed, even remote regions far from point sources of mercury pollution are likely to contain some level of mercury due to long range atmospheric transport. Water bodies are complex and various factors affect mercury speciation. In lakes, methylated mercury originates from anoxic water near the sediment-water interface whereas in oceans and Great Lakes not much MeHg comes from deep waters (Morel et al., 1998). In oceans, some MeHg could be from partial demethylation of dimethyl mercury upwelled from deep waters (Morel et al., 1998). Although methylation occurs primarily in anoxic water or sediments, the significant levels of MeHg in surface waters of the ocean lead researchers to believe that some MeHg must be produced in oxic water as well (Morel et al., 1998).

In summary, mercury is found in various chemical forms in air, soil, water and living organisms around the world. While significant research has been conducted to understand how mercury is mobilized, stored and transported on earth, we still do not fully understand these processes. With rapidly developing countries like China and India burning more coal for fuel, mercury emissions are rising despite efforts of other countries to minimize emissions (Sprovieri et al., 2010). Mercury emissions, transport, and storage must continue to be researched in order to understand how changes may affect the earth and all living systems on it.

1.1.3. Absorption, Distribution, and Excretion of Mercury

The WHO (1991) estimates that humans ingest 2.4 µg of organometallic mercury daily primarily through ingestion of fish, shellfish and marine mammals (WHO, 2008). It forms water-soluble complexes with thiol groups and can then cross the blood-brain and blood-placental barriers (Clarkson and Magos, 2006). Once in the brain mercury can remain as methylmercury cysteineate or it can be converted to inorganic mercury and is often bound to selenium thus creating a highly insoluble compound (Korbas 2010a). Methylmercury can be transformed in the

intestinal tract to inorganic mercury but the mechanism is unknown (Clarkson and Magos, 2006). The major route of excretion of methylmercury is through feces (Clarkson and Magos, 2006).

Inorganic mercury salts are primarily absorbed via oral exposure whereas elemental mercury exposure is primarily via inhalation (WHO, 2003). An estimated 80% of the inhaled dose of elemental mercury is absorbed by the lungs through diffusion (WHO, 2003). The amount of inorganic mercury that is absorbed from oral exposure appears to be dependent on many factors including dose, age, diet and chemical form (WHO, 2003). Inorganic mercury has been detected in the urine of people using skin lightening creams containing inorganic mercury compounds therefore dermal absorption is another important route of exposure to consider (WHO, 2003). The lipophilic nature of elemental mercury results in its ability to readily cross the blood-brain and blood-placental barriers and can be excreted through breastmilk (Clarkson and Magos, 2006; WHO, 2003). Both elemental mercury and inorganic mercury salts accumulate in the kidneys and liver and are primarily excreted via the feces for approximately the first week and then urinary excretion becomes the main pathway (Clarkson and Magos, 2006; WHO, 2003). A smaller proportion of inorganic and elemental mercury can also be excreted through expired air, sweat and saliva (WHO, 2003).

1.1.4. Effects of Mercury on Organisms

Exposure to different forms of mercury can cause a range of effects including kidney damage, gastrointestinal effects, cardiovascular effects, respiratory effects, reproductive and developmental abnormalities, and central nervous system effects including paresthesia, impaired vision, and deafness (Clarkson and Magos, 2006; WHO, 2003; WHO, 2008). Methylmercury exposure in adults can cause serious neurological damage and result in sensory, motor, opthalmological, and audiological impairment (WHO, 2008). Irreversible damage to the central nervous system can occur when exposure to methylmercury occurs in utero as this is the most sensitive period in the lifecycle to methylmercury exposure (Clarkson and Magos, 2006; WHO, 2008). Interestingly, the brains of adults that had been exposed to methylmercury by eating contaminated wheat had lesions in the focal region of the brain whereas infants that died shortly after birth (due to prenatal exposure) had lesions affecting the entire brain (Clarkson and Magos, 2006). Some of the effects noted were inhibition of neuronal migration and distortion of the cortical layers of neuronal cells (Clarkson and Magos, 2006). Children exposed to non-lethal

levels of methylmercury were found to have adverse effects including developmental delays, exaggerated reflexes, blindness, deafness, cerebral palsy, physical growth disturbance, and limb deformities (Clarkson and Magos, 2006; WHO, 2008).

Humans are primarily exposed to methylmercury through ingestion of fish; however, the correlation between adverse effects and the ingestion of methylmercury containing fish is still unclear despite decades of research (Clarkson and Magos, 2006). Several cohorts including people in the Faroe Islands, the Seychelle Islands and New Zealand have been studied with differing results (Clarkson and Magos, 2006). It appears that people in New Zealand and the Faroe Islands experience a number of adverse effects while those in the Seychelle Islands have little or no adverse effects and overall health outcomes are positively correlated with fish intake (Clarkson and Magos, 2006). The differences may be due to a number of factors such as concomitant exposures to other contaminants, differences in methodology and end points, smoking habits, alcohol consumption, overall diet, and the amounts of mercury in the seafood (Clarkson and Magos, 2006). Raymond and Ralston (2009) note that the ratio of mercury to selenium is also likely important and must be considered when creating safety regulations. For example, in the Faroe Island cohorts the mercury: selenium ratio in the cord blood was 1:1 suggesting that there would be little selenium in the blood that would be accessible by the fetus (Raymond and Ralston, 2009). Berntssen et al. (2004) fed rats a diet of either salmon that had been raised on methylmercury contaminated feed ("natural contamination") or salmon fillets that had been spiked with methylmercury chloride. Mercury levels in the blood, brain and kidneys were significantly higher in the rats that ingested the mercury spiked salmon than the rats that were fed the "naturally contaminated" salmon (Berntssen et al., 2004). The rats fed the mercury spiked salmon also had significantly lower fecal excretion of mercury (Berntssen et al., 2004). Although dietary factors such as amount of selenium and vitamin E are known to affect mercury toxicity, Berntssen et al. (2004) controlled for these variables therefore other variables such as lipophilicity must be involved in the differences in accumulation and excretion. In conclusion, further work must be conducted to elucidate the mechanisms of toxicity of the different chemical forms of organic mercury.

Although inorganic mercury is less toxic than organic mercury there are many serious adverse effects caused by exposure to inorganic and elemental mercury. The estimated daily intake of inorganic mercury for the average adult is 4.3 µg (WHO, 2003). Calomel containing

products have been used in teething powder and have been known to cause acrodynia (a pink discolouration on the hands and feet) as well as emotional lability, insomnia, memory impairment (Weinstein and Bernstein, 2003), weight loss, weakness and photophobia (Clarkson and Magos, 2006). Because mercury can block the degradation of catecholamines, excessive sweating and hypertension can manifest as well (Weinstein and Bernstein, 2003). The estimated average daily intake of mercury vapour ranges from 1.2-27 µg primarily based on exposure to dental amalgams (WHO, 2003); however, occupational exposure to mercury vapour could result in higher exposures. Several adverse effects can result from elemental and inorganic mercury exposure including a variety of cognitive, sensory, motor and personality changes (WHO, 2003). Elemental and inorganic mercury salts can both result in the following effects on the central nervous system: tremors, emotional lability, memory loss, headaches, paresthesia, unsteady walking, muscle twitching, blurred vision, reduced hand-eye coordination, and decreased scores in cognitive skills tests (WHO, 2003). Respiratory effects (such as dyspnea, pneumonitis, cough, and reduced vital capacity) and cardiovascular effects (such as tachycardia and hypertension) have been found in people exposed to both elemental mercury vapour and ingestion of inorganic mercury compounds (WHO, 2003). Following exposure to high levels of elemental or inorganic mercury has been found to cause abdominal pain, nausea, vomiting and diarrhea (WHO, 2003). As inorganic mercury is known to primarily accumulate in the kidneys it is not surprising that renal effects including proteinuria, haematuria, degeneration of the proximal convoluted tubules, and renal failure have been observed following exposure to inorganic mercury (WHO, 2003).

1.1.5. Mercury and Selenium

Selenium is an essential trace element required for major divisions of living organisms. In almost all of its functional forms in enzymes (selenoenzymes), selenium is found as the 21st amino acid, selenocysteine (Chen and Berry, 2003) with a very few but notable exceptions in which selenide is found directly bound to metal ion (Pushie and George, 2014). Selenium is available in essentially all foods, but is especially high in ocean fish (Ralston, 2008). Selenate and selenite can both be converted to selenocysteine *in vivo* (Chen and Berry, 2003) although the latter is metabolized quite slowly (Gailer et al., 2002). Selenium can also replace sulfur in methionine to create selenomethionine (Chen and Berry, 2003). It can then be incorporated into proteins in place of methionine, and can be ultimately catabolically converted to selenocysteine

(Chen and Berry, 2003), depending on the protein involved and nutritional status. Research has demonstrated that selenium can play a role in the prevention in cardiovascular disease, viral infections, and certain cancers (Chen and Berry, 2003). Three main categories of selenoenzymes are important in vertebrates; glutathione peroxidases, thioredoxin reductases and iodothyronine deiodinases (Raymond et al., 2014). Glutathione peroxidases are detoxifying enzymes that protect cells from reactive oxygen species by removing hydrogen peroxide., Thioredoxin reductases function to reduce disulfide bonds in cellular proteins and plays roles in regulation of gene expression, in cell viability and in cellular proliferation (Chen and Berry, 2003). Research has shown that selenium levels are higher in the areas of the brain with more grey matter and selenium tends to be preferentially conserved in the brain compared to blood, liver, and muscle tissues following selenium depletion (Chen and Berry, 2003). Selenoprotein P (SelP) is a glycoprotein produced in most tissues with 17 selenocysteines in zebrafish (Chen and Berry, 2003). SelP appears to be important for both selenium homeostasis and detoxification and is the primary transporter of selenium to the brain (Chen and Berry, 2003).

The antagonistic relationship between mercury and selenium has been known for decades (Parízek and Ostádalová, 1967). Many studies have utilized mice, rats, rabbits, birds, fish and human and animal cell lines to study the interactions between pre-, co-, and post-exposure of selenium with mercury (Luque-Garcia et al., 2013). Carvalho et al. (2008) found that both inorganic and organic mercury target the thioredoxin reductase system which can result in increased reactive oxygen species. Amlund et al. (2015) demonstrated increased methylmercury elimination from muscle in zebrafish supplemented with selenomethionine (SeMet). MeHg was found to down-regulate a number of selenoprotein-coding genes important in antioxidant pathways as mercury binds selenium at enzyme active-sites (Penglase et al., 2014b; Ralston et al., 2010; 2012). These selenoprotein-coding genes have been found to be susceptible to selenium deficiency (Penglase et al., 2014b). Because selenium is an essential trace element, mercury toxicity may be partly due to selenium deficiency resulting from the sequestration of selenium by mercury, known as the selenium depletion hypothesis (Ralston et al., 2007). Indeed, Ralston and coworkers (2008) showed that increasing molar ratios of Hg:Se in the blood are a better predictor of harm than blood mercury concentrations alone. Although mercury has a high binding affinity for sulfur, mercury's affinity for selenium is approximately a million times

greater (Ralston, 2008). Methylmercury binds to selenocysteine in vivo and prevents the selenocysteine from participating in its typical metabolic cycle (Ralston, 2008).

One study reported that although SeMet prevented reduced growth and survival of adult female zebrafish exposed to methylmercury, the combination of elevated SeMet and methylmercury in adult females resulted in reduced fecundity and embryo survival (Penglase et al., 2014a). Additional selenium in the diet may indeed confer some protection from mercury toxicity; however, the chemical form and concentration must be carefully considered to avoid selenium toxicity. Thomas et al. (2011; 2014) report altered behavioural and physiological responses in adult zebrafish exposed to SeMet as well as increased mortality and developmental toxicity in offspring of these fish. As many other researchers have suggested, selenium may help ameliorate some aspects of mercury toxicity; however, more work needs to be conducted to understand the ideal exposure period, dose, and chemical form of selenium.

1.2. Zebrafish

1.2.1. A Model System for Studying Toxins

Zebrafish (*Danio rerio*) embryos are often used as a model vertebrate system to study the toxic effects of compounds on early life stages (Kari et al., 2007; Dai et al., 2014). The high fecundity and small size of both the adults and embryos make zebrafish a highly cost effective option for experiments requiring a large number of replicates (Lele and Krone, 1996). Once the eggs are fertilized the embryos develop rapidly, hatching from their chorions at approximately 3 days post fertilization (dpf). Zebrafish receive nutrition from their yolk sac until it is completely absorbed (around 6 dpf). Because zebrafish do not begin to feed until approximately 5 dpf, food does not need to be supplied until about 7 dpf and thus eliminates a potential confounding factor from experiments conducted during this stage (Yang et al., 2009). Zebrafish have many organs including brain, heart, liver, pancreas, kidney, intestines, bone, muscles, nerve systems and sensory organs which are very similar at the anatomical, physiological and molecular level (McGrath and Li, 2008).

Unlike mammals, zebrafish embryos are transparent and develop outside their mother. Coupled with a well characterized developmental staging series, these factors allow researchers to carefully follow development (Kimmel et al., 1995). For example, researchers have exposed zebrafish embryos and larvae to a variety of compounds including mercury, cadmium, lead,

nickel, and copper and characterized changes in development including time to hatch, physical deformities, and mortality (Dave and Xiu, 1991; Blechinger et al., 2007). More subtle changes in cellular function can be studied using transgenic zebrafish, vital stains, immunohistochemistry, and behavioural assays (Dai et al., 2014).

Many highly efficient protocols have been developed to induce mutations in zebrafish which has led to the identification of several thousand genes and developmental processes (Yang et al., 2009). Additionally, access to the genome sequence allows researchers to search for specific genes and regulatory sequences. Many genes and regulatory sequences have been found to be conserved between humans and zebrafish (Yang et al., 2009). Zebrafish also have many similar mechanisms for enzyme induction and oxidative stress response (McGrath and Li, 2008). Recently, bacterial clustered regularly interspaced short palindromic repeats (CRISPR)/CRISPR-associated (Cas) 9 system (CRISPR/Cas9) was developed as a knock in technique for zebrafish (Li et al., 2015). CRISPR/Cas9 allows the insertion of exogenous genes while maintaining the expression and function of targeted endogenous genes (Li et al., 2015).

Although there are many advantages to using zebrafish for developmental research there are some disadvantages. Zebrafish differ from mammals in that they do not have placentas and development occurs outside the adult therefore any compounds that can cross the blood-placental barrier and expose the embryo during gestation cannot be accurately studied. Experiments often expose zebrafish to a compound(s) by addition to the water thus this route of exposure may not accurately represent a typical human exposure and there may be differences in absorption, distribution, metabolism, and excretion (McGrath and Li, 2008). Despite some drawbacks, overall zebrafish are an excellent model system to study how toxins can affect the developing organism.

1.2.2. An Introduction to the Olfactory System

The olfactory organs are comprised of olfactory pits that connect to olfactory bulbs of the forebrain via the olfactory nerves. Proper functioning of the olfactory organs is crucial for daily functioning of many species, especially in fish. Olfactory organs are diverse across species and even within fish species depending on ecological habits and level of development (Pitcher, 1993). The number, arrangement, and shape of lamellae (folds) of the olfactory epithelium vary among species (Pitcher, 1993). The lamellae increase the surface area for more receptors in the

olfactory pit. On average, 5 – 10 million olfactory receptor cells can be found on each side of the nasal cavities in teleost fish (Pitcher, 1993). Teleost fish also typically have paired olfactory pits on the dorsal side of the head with an anterior inlet and a posterior outlet (Pitcher, 1993). In contrast to terrestrial vertebrates, there is no connection between the olfactory and respiratory systems in teleost fish (Pitcher, 1993). The normal functioning of olfactory organs in teleost fish (e.g. zebrafish) is critical for numerous behavioural activities including finding food, courtship, and avoiding predators (Pitcher, 1993). For example, the release of zebrafish ovarian pheromones can elicit courtship and inhibit fighting (likely due to a mixture of estradiol-17B and testosterone glucuronides) (Pitcher, 1993). When the skin of a fish is damaged, "club cells" are broken and release an alarm substance, which is detected by the olfactory system, to warn other fish (Pitcher, 1993).

Significant development occurs rapidly in early olfactory differentiation, followed by subsequent development of the olfactory bulbs and organs occurring more slowly (Nusslein-Volhard and Dahm, 2002). The zebrafish olfactory system is initially formed as the central portion of cloverleaf shaped outgrowths from the brain, with the lateral growths forming eyes and the centre forming the olfactory placodes (Hansen & Zeiske, 1993). Between the 10 and 20 somite stages, the placode cells proliferate and fill the area between the eyes and forebrain (Hansen and Zeiske, 1993). During this proliferation phase, most of the cells facing the forebrain send out axons and the placode cells begin to elongate once the axons project into the brain (Hansen and Zeiske, 1993; Nusslein-Volhard and Dahm, 2002). The olfactory epidermis forms a pit with a series of lamellae to form a rosette (Pitcher, 1993). Small slits, surrounded with spherical epidermal cells on the outside and microvilli and kinocilia inside, make up the olfactory pits (Hansen and Zeiske, 1993). By 50 hours post fertilization (hpf) the olfactory pits have cilia, microvillous receptor cells, support cells and nonsensory cells (Hansen and Zeiske, 1993). By 4 dpf all major cell types including basal cells, ciliated and microvillous receptor cells, support cells and ciliated non-sensory cells have formed (Nusslein-Volhard and Dahm, 2002). The olfactory bulb is made up of the following four laminae: olfactory nerve, glomerular, mixed mitral cell/plexiform, and granule cell layers (Nusslein-Volhard and Dahm, 2002).

1.2.3. An Introduction to the Lateral Line System

The lateral line of fish and amphibians is comprised of mechano-sensory organs called neuromasts and a corresponding set of neurons extending to the hindbrain (Dambly-Claudière et al., 2003). Neuromasts contain sensory hair cells surrounded by support cells and can be found superficially or enclosed in pouches, canals or vesicles (Alexandre and Ghysen, 1999). Neuromasts in fish and amphibians act as a "water displacement detecting system" to detect movements and vibrations within a radius of their body length (Alexandre and Ghysen, 1999). The lateral line system plays a critical role in predator and obstacle avoidance, prey detection and schooling behaviour (Alexandre and Ghysen, 1999; Collazo et al., 1994; Dambly-Claudière et al., 2003). It is very similar to the sensory hairs in insects and thus is likely derived from a common ancestral mechano-sensory organ (Dambly-Claudière et al., 2003).

In zebrafish, the lateral line develops in a consistent pattern during larval development (Dambly-Claudière et al., 2003). While the lateral line is functional in zebrafish at 5 dpf (days post fertilization), at 10 dpf apoptosis of hair cells occurs and support cells divide to form new hair and support cells (Dambly-Claudière et al., 2003). Hair cells in zebrafish are easily observed when stained with the vital fluorescent marker 2-Di-4-Asp (Dambly-Claudière et al., 2003). The lateral line continues to develop in adults in a reproducible pattern of 50 neuromasts in four lines (Dambly-Claudière et al., 2003). Adult fish, amphibians and birds can generate new hair cells through dividing support cells. While the mammalian auditory system and cochlear hair cells are believed to have evolved from the lateral line system of fish and amphibians (Alexandre and Ghysen, 1999), mammals do not possess the ability to regenerate new hair cells within the cochlea (Dambly-Claudière et al., 2003).

The anterior lateral line is composed of neuromasts on the head whereas the neuromasts on the body and tail make up the posterior lateral line (Dambly-Claudière et al., 2003). The neuromasts on the head and body of fish develop from epidermal placodes on the head whereas the tail neuromasts develop from placodes caudal to the otic capsule (Collazo et al., 1994). Neural crest cells form the peripheral nervous system, pigment cells, and the skeletal parts of the head (Collazo et al., 1994). Because neural crest cells migrate to areas near neuromasts, it is believed that some neuromasts may develop from neural crest cell differentiation (Collazo et al., 1994).

1.2.4. Potential Effects on Developing Sensory Systems

Chemoreception by the olfactory system and mechano-sensory reception by the lateral line are critical for feeding, defense, reproduction, schooling, orientation and migration. Therefore it follows that if the olfactory organs or lateral lines are impaired by toxicants, serious adverse effects may be elicited. For example, in a properly functioning olfactory system in fish, stimulant molecules bind to receptors causing altered membrane permeability through protein conformational changes (Hara, 1982). The increased permeability leads to nerve impulses being conducted to the central nervous system and behavioural response begins (Hara, 1982). Toxicants could interfere at any stage of this process and potentially cause unwanted side effects (Hara, 1982). The lateral line, olfactory pits and eyes of fish are all prime targets for toxins because they are directly exposed to the environment (Hara, 1982). Although receptor cells are continuously renewed in adults (and recovery is more likely once the toxicant is removed), functionality may never fully recover (Hara, 1982; Pitcher, 1993; Blechinger et al., 2007). Additionally, certain toxicants may enter the body via one route and affect one or more sensory system. Accumulation and effects of heavy metals may directly disrupt normal fish activities including schooling, predator avoidance, and prey detection (Sandahl et al., 2007).

Hara (1982) notes that most pollutants can mask or inhibit biologically important odours, or damage chemoreception. Cell death in the olfactory epithelium and behavioural changes (i.e. lack of response to alarm substance) following acute exposure have been found in juvenile zebrafish (40 – 50 dpf) exposed to cadmium (Blechinger et al., 2007). One study found that whitefish exposed to mercuric chloride displayed a decreased response to food extract (Hara, 1982). Certain compounds can also result in avoidance or preference for a site depending on the amount of damage to the olfactory cells. For example, fish exposed to cadmium or mercury were not found to avoid sublethal or lethal concentrations while some fish even preferred the site (Hara, 1982). Studies of fish exposed to mercury have demonstrated that severe degenerative changes occurred in the neurosensory cells of these fish (Hara, 1982). Dissolved copper associated with habitat degradation has been shown to impair lateral line function and olfaction in chinook salmon, rainbow trout, brown trout, fathead minnows, Colorado pikeminnows, and tilapia (Sandahl et al., 2007).

Korbas et al. (2008) found that 3.5 dpf zebrafish larvae exposed to methylmercury L-cysteineate preferentially accumulated mercury in the lens epithelium. This level of mercury in

the lens epithelium was the highest in the entire larvae whereas in 10 dpf zebrafish the levels of mercury in the liver were comparable to those in the lens epithelium (Korbas et al., 2008). Another significant finding by Korbas et al. (2010b) was that mercury continued to accumulate in the lens epithelium even after removal from the mercury contaminated water. Korbas et al. discovered that in zebrafish larvae treated with CH_3HgCl, mercury preferentially accumulates directly in the cells of the eye. Initially it appeared that the mercury was accumulating in the outer layer of rapidly dividing epithelial cells of the lens (2010b); however, using higher resolution imaging techniques it was determined that the mercury targets in the secondary fibre cells immediately under the epithelial cells as well as in the outer segments of the retinal photoreceptors (Korbas et al., 2013). Previously, it was believed that impaired vision in people exposed to mercury was caused by mercury's effects on the visual cortex; however the research by Korbas et al. (2008, 2010b, 2013) suggests that mercury may be directly acting on the cells of the eye. Research has not yet demonstrated if inorganic mercury can cause these same effects in the eye lens or potentially in other sensory organs such as the olfactory organs or lateral line system.

1.3. Synchrotron Techniques

1.3.1. X-ray Fluorescence Imaging

1.3.1.1. Overview of X-ray Fluorescence Imaging

Synchrotron X-ray fluorescence imaging (XFI) is a relatively new technique for imaging metals in biological systems which enables researchers to create element specific maps of samples imaged (Pushie et al., 2014). XFI is sometimes referred to as X-ray fluorescence microscopy (XFM) or synchrotron radiation induced X-ray emission (SRIXE) (Pushie et al., 2014). XFI uses X-rays to excite elements and detect characteristic X-ray fluorescence from such elements (Qin et al., 2011; Pushie et al., 2014). This technique is a simple but accurate method of determining elemental distributions and concentrations in whole cell and tissue sections (Paunesku et al., 2006; Pushie et al., 2014). A specific element is "windowed" or focused on using computer software at the beamline. Computer software allows researchers to analyze individual elements or to overlay up to three elements on one image. Software programs can be used to examine correlation of different elements. Many different XFI imaging beamlines exist around the globe at synchrotrons including but not limited to the Canadian Light Source (CLS),

the Advanced Photon Source (APS), the Stanford Synchrotron Radiation Lightsource (SSRL), the Australian Synchrotron (AS) and SPring-8. Only third generation synchrotron sources have high enough brilliance at high-photon energies to collect images with subcellular resolution of biological samples with trace elements (Paunesku et al., 2006). However, not all studies require subcellular resolution or have low levels of trace elements. In such cases, other imaging beamlines can provide elemental localization maps and element concentrations can be determined.

1.3.1.2.Advantages of X-ray Fluorescence Imaging

Three of the main advantages to this technique are high spatial resolution, element specificity, and the ability to simultaneously collect data on all elements in the sample (Paunesku et al., 2006). Depending on the synchrotron and the beamline, spatial resolution can be as high as 150 nm for XFI and 0.1 - 1μm for micro X-ray absorption near edge spectroscopy (Lobinski et al., 2006; Qin et al., 2011). Each element fluoresces at a discrete energy resulting in a relatively simple method to determine which element(s) are in the sample.

XFI differs from other techniques in that it does not require pre-treatment of the sample prior to analysis. XFI is the only available technique to quantitatively image elements in hydrated whole cells using submicron resolution (Paunesku et al., 2006; Petibois and Guidi, 2008). Methods such as ICP-MS (inductively coupled mass spectroscopy) require acidification of samples prior to analysis and simply determine the total quantity of an element in the sample rather than the location the element accumulated in. An XFI image is created using the information from the full spectrum of all fluorescent photons collected from each pixel of the image (i.e. all elements in the sample can be examined individually). If standard films of known concentration are imaged using the same settings as the sample, the amount of element per pixel ($\mu g/cm^2$) can be determined. Each beamline has different components and configuration thus allowing researchers to use XFI for many different projects. Macro (e.g. human brain sections), micro (e.g. zebrafish sections) and nano (e.g. cellular detail) imaging are possible depending on the beamline configuration and equipment.

Chemically selective spectroscopic imaging can provide information on speciation of a particular element (Pushie et al., 2014). Rather than collecting multiples images of different elements multiple images are collected at various energies related to one element. For example,

Pickering et al. (2000) were the first to publish a paper using chemically selective XFI by imaged live plants at SSRL using two different energies that corresponded to two different selenium species (Se-methyl-L-selenocysteine and selenate) and were able to determine where each form of selenium accumulated within the plant.

1.3.1.3.Disadvantages of X-ray Fluorescence Imaging

Some of the drawbacks of XFI include having to apply for beamtime, cost, time to travel to the synchrotron, and time to run the samples. The sample should be relatively uniform thickness (i.e. sectioned tissue) for traditional XFI; however, this is not necessary for all studies and synchrotron XFI could be used to provide topographic information (Qin et al., 2011). Additionally, XFI cannot yet be done on many living organisms due to their size and ethical considerations related to pain and radiation dose. While it is often possible to collect simultaneous images of each element within the sample this process can be complicated if there are two elements in the sample with fluorescence peaks at neighbouring energies. For example, the mercury $L\alpha_1$ peak is at 9,988 eV and the zinc $K\beta$ peak is at 9,572 eV. If both mercury and zinc exist in the sample and there is a significant amount of zinc compared to mercury then care must be taken to separate the "windows" collecting the counts from each element so that you do not have counts from zinc overflowing into the mercury counts (which would result in a falsely high mercury concentration). Setting narrower windows will ensure there is no 'leaking' of counts into the other window; however, this is at the expense of missing some actual counts.

Some beamlines can collect data for a small number of elements (e.g. 8-16 elements on beamline 10-2 at SSRL) while other beamlines have the capability of collecting the full set of elements (e.g. beamline 20 ID-B at APS and 2-3 at SSRL). The advantage of collecting the full spectrum of elements for each pixel in an image is the ability to look at other elements after the experiment is complete.

1.3.1.4.Potential Complementary Techniques

Several complementary techniques are available to collect various types of information each with its own advantages and disadvantages. Mercury probes offer potential in labs that require rapid turnaround, low cost, only general information on mercury accumulation, and a

large number of samples (Yoon et al., 2005). However, not all mercury probes can be used at room temperature and actually require heating and digestion of the sample in nitric acid (Song et al., 2009; Yoon et al., 2005). Typically, standards are measured using atomic absorption spectroscopy and the fluorescence emission of the standards can be compared to the fluorescence of the samples for quantification (Yoon et al., 2005). Many other techniques are not very element specific and may cause a false reading. For example, fluorescent probes ideally bind to one specific element; however, in the case of mercury, a probe may fluoresce in the presence of calcium in fish tissue because calcium is a divalent cation that naturally exists in very high quantities compared to the mercury levels in the fish (Yoon et al., 2005). In addition to selectivity issues, many fluorescent probes must bind to the mercury in order to fluoresce and this binding causes a chemical modification of the mercury (Yoon et al, 2005; Yoon et al., 2007). Many of the probes currently in use are not ideal and could be improved by creating probes with better metal and oxidation state specificity, brighter fluorescence signal, and the ability to target subcellular areas (Domaille et al., 2008).

Secondary ion mass spectrometry (SIMS) involves bombarding the top few atomic layers of the sample surface with primary ions such as Ar^+, Xe^+, Cs^+, Bi^+, or C_{60}^+ (Lobinski et al., 2006; Moore et al., 2012). Laser ablation inductively coupled plasma mass spectrometry (LA-ICP-MS) is a technique that uses a focused laser beam to evaporate the sample (Lobinski et al., 2006; Qin et al., 2011). Argon, as a carrier gas, transports the ionized material to the ICP where the formed ions are extracted and separated based on their mass-to-charge ratio (Lobinski et al., 2006; Qin et al., 2011).

Both SIMS and LA-ICP-MS are highly sensitive chemical imaging methods that allow for isotopic analysis (Lobinski et al., 2006). Both techniques are also available in nano imaging versions to improve the sample resolution to the nanometer scale; however, the nano-LA-ICP-MS is very new and has not been thoroughly tested (Qin et al., 2011). As with synchrotron XFI, SIMS and LA-ICP-MS can essentially detect all elements in each analysis point in the sample but NanoSIMS can only collect 5 to 7 elements (Qin et al., 2011). LA-ICP-MS is significantly more cost effective and easier to use than both SIMS and synchrotron XFI (Qin et al., 2011). Additionally LA-ICP-MS can also be used to quantify the elements within biological samples using solution-based calibration or matrix-matched laboratory samples (Qin et al., 2011).

Quantification in SIMS analysis is possible but is complicated by the yield of secondary ions from each element, by the matrix effect in biological samples, and by the topography of the sample (Moore et al., 2006). Spatial resolution varies from 0.1 – 10 μm for SIMS and >50 nm for NanoSIMS to 5 – 200 μm for LA-ICP-MS (Qin et al., 2011). In terms of sample preparation, SIMS samples should be semi-thin or thin sections of embedded material and must be run under high vacuum and therefore water must be removed from the cells (Moore et al., 2006; Qin et al., 2011). The removal of water could alter the distribution of elements or the chemical state of the elements in biological samples (Moore et al., 2006). Ideally, samples should be run using cryoSIMS or high-pressure freezing and subsequent freeze-substitution (Moore et al., 2006). LA-ICP-MS uses 10 – 40 μm cryo-sectioned samples that do not require prior treatment other than laser ablation (Qin et al., 2011). Unfortunately, both SIMS and LA-ICP-MS damage the sample during testing either for the top 1-10 nm in the case of SIMS or the entire section in the case of LA-ICP-MS (Moore et al., 2006; Qin et al., 2011).

In summary, XFI is a synchrotron technique that provides high resolution elemental distribution maps of biological samples. XFI has a number of advantages over other complementary techniques including high chemical specificity, little to no pre-treatment of sample, and simultaneous collection of elements in the sample.

1.3.2. X-ray Absorption Spectroscopy

X-ray absorption spectroscopy (XAS) can be used to collect information about the speciation of an element, the bond lengths of ligands, the number of nearby atoms, and the approximate size of the nearby atoms (Pushie et al., 2012). Like XFI, XAS is an element specific technique that can be used to study a wide range of elements (George and Pickering, 2007). Each element has an absorption edge at a discrete energy dependent on the amount of energy required to eject an electron from a specific orbital. By analyzing the spectral shape and position of the absorption edge and the region just prior to it (collectively referred to as the near edge), details are provided on the oxidation state of the element of interest. To examine an atom's radial structure, the energy range is extended further past the absorption edge, and before another element's absorption edge, also known as extended X-ray absorption fine structure (EXAFS) spectroscopy (George and Pickering, 2007). One particular advantage of XAS over other techniques is that it can be performed on solids, liquids or gases with little or no pre-treatment necessary

(George and Pickering, 2007). EXAFS can provide very accurate bond lengths between the element of interest and the ligands (Pushie et al., 2012). EXAFS can also provide information on the neighbouring atoms; however, it is difficult to distinguish between atoms of a similar atomic number (e.g. between sulfur and chlorine) (George and Pickering, 2007).

A complementary synchrotron technique called micro X-ray absorption spectroscopy (µ-XAS) can be used to determine chemical speciation within the sample (Paunesku et al., 2006; Pushie et al., 2014). This method involves collecting an XFI image and then moving to a particular point of interest and then recording a spectrum (Pushie et al., 2014). The sample must be sufficiently concentrated in order to obtain a good signal to noise ratio to collect the EXAFS. The primary advantage of this technique is the ability to collect images and EXAFS on the same sample at the same beamline during the same allocation of beamtime. Normally, EXAFS is run on a separate beamline. Overall, XAS and µ-XAS can be very useful in providing additional information that is not obtained from XFI.

1.4. Research Objectives and Null Hypotheses

1.4.1. Objectives

The overall objective of this research was to study the effects of inorganic mercury exposure in zebrafish larvae. More specifically the objectives of this study include the following:

A. Use synchrotron X-ray fluorescence imaging to determine mercury accumulation patterns of four mercury compounds (mercury bis-L-cysteineate ($Hg(C_3H_6NO_2S)_2$), mercuric chloride ($HgCl_2$), methylmercury L-cysteineate ($CH_3HgC_3H_6NO_2S$), methylmercury chloride (CH_3HgCl)) in zebrafish larvae.
B. Examine the effects of phenylthiourea on mercury toxicity in zebrafish larvae exposed to mercuric chloride and methylmercury chloride.
C. Map the accumulation of mercury and investigate the effects on the primary neurons in the olfactory system following exposure to mercuric chloride.
D. Evaluate the efficacy of the mercury sequestration agents alpha lipoic acid (ALA) and dimercaptosuccinic acid (DMSA) on zebrafish larvae exposed to mercuric chloride and methylmercury chloride.

E. Study the accumulation of selenium and mercury in zebrafish larvae exposed to mercuric chloride.

1.4.2. Null Hypotheses

A. Synchrotron X-ray fluorescence imaging will not demonstrate any differences in accumulation patterns of the four different chemical forms of mercury.
B. Phenylthiourea will have no effect on mercury toxicity and accumulation in zebrafish larvae exposed to mercuric chloride or methylmercury chloride.
C. Mercuric chloride exposure will not affect the primary neurons in zebrafish larvae.
D. Neither ALA nor DMSA will cause an increase or decrease in mercury levels in zebrafish larvae exposed to mercuric chloride and methylmercury chloride.
E. There will be no evidence of co-localization between mercury and selenium in zebrafish larvae exposed to mercuric chloride.

CHAPTER 2. METHODS

2.1. Zebrafish

2.1.1. Maintenance, Husbandry and Embryo Care

Adult wild type zebrafish were purchased from a local pet store and maintained in Dr. Patrick Krone's lab in an Aquatic Habitats Flow-Through System (Apopka, FL). All research was conducted with the approval of the University of Saskatchewan's Ethics Board. Zebrafish were housed in a room maintained at 28ºC with a light: dark cycle of 14:10 hours to mimic natural conditions. Fish were fed a diet of brine shrimp and chironomids (Hikari, Hayward, CA) at least once per day. Floating pellets were used to supplement the diet prior to breeding (Aquatic Eco-Systems, Apopka, FL).

Adult zebrafish were bred in 4.5 litre breeding tanks according to standard methods (Westerfield, 1995). Approximately 5-8 adult zebrafish were placed in each tank (with a greater number of females than males) with glass marbles at the bottom, an artificial plant and an air stone. The fertilized embryos sink to the bottom of the tank, below the marbles, which protects them from predation by the adult zebrafish. Embryos were collected approximately one hour following light stimulus to ensure a large collection of embryos (typically 250 embryos per tank). The adult fish were first returned to their home tank, the marbles were removed, and finally the water was poured through a fine mesh net to collect the embryos. All embryos were rinsed three times with fresh system water (carbon-filtered tap water) to remove debris and stored in 25 cm Petri dishes with a dilute methylene blue wash to protect embryos from fungal growth (1 mL methylene blue per litre of carbon filtered system water). Approximately 100 zebrafish embryos were placed in each Petri dish to prevent overcrowding. All embryos and larvae were kept in an incubator at 28˚C when not being treated or cleaned. Dead embryos (opaque white rather than transparent) were removed and remaining embryos were rinsed once more on the day of collection and every 24 hours thereafter.

2.1.2. Zebrafish Exposures

Zebrafish larvae were exposed to test compounds at 3 dpf. If the larvae had not emerged from their chorions at 3 dpf the fish were carefully dechorionated using fine forceps. All larvae were rinsed three times in system water following dechorionation or removal from the methylene

blue wash. Larvae were then randomly assigned to control (system water) or treatment groups until each Petri dish contained 25 larvae. Each group was comprised of four Petri dishes for a total of 100 larvae per treatment group. Treatment solutions of $HgCl_2$ and $Hg(C_3H_6NO_2S)_2$ were diluted daily from stock solutions to desired concentrations using fresh system water. Dead larvae were recorded and removed prior to preparation and addition of fresh solution.

2.1.3. Sample Collection and Preparation

Twenty living fish from each treatment group were collected at each time point, rinsed three times in system water to remove any mercury from the surface of the fish (approximately 5 minutes), placed in 2 mL Eppendorf microcentrifuge tubes (Fisher Scientific, Ottawa, ON), then fixed in 4% paraformaldehyde (PFA) for two hours at room temperature or overnight at 4˚C. The fish were dehydrated in a graded series from 100% PBST (phosphate buffered saline with 0.01% Tween-20), 75% PBST: 25% ethanol (EtOH), 50% PBST: 50% EtOH, 25% PBST: 75% EtOH, to 100% EtOH. For each rinse, larvae were placed on a gentle shaker for 5 minutes, then the solution was removed and the next solution added. Dehydrated embryos were stored in 100% EtOH at -20˚C overnight or until time to embed embryos using JB-4 methacrylate kit (PolySciences Inc., Warrington, PA).

2.1.3.1.Embedding in Methacrylate

Embryos were rehydrated using the reverse solution series of dehydration, washed in PBST and then larvae were placed in each plastic mold for embedding in agarose. Embryos were embedded in 1% low melting point agarose and oriented using fine forceps. Once hardened, the agarose block was trimmed and placed in a 15 mL Falcon tube (Fisher Scientific, Ottawa, ON). Agarose blocks were dehydrated in 100% EtOH for 5-8 hours at 4˚C with gentle shaking. Dehydrated blocks were infiltrated overnight at 4˚C using infiltration solution comprised of Solution A (from the JB-4 methacrylate kit; Polysciences Inc., Warrington, PA, USA) and a benzoyl peroxide catalyst (ratio of 1mL Solution A: 0.0125g catalyst). Infiltration solution was replaced the following morning and falcon tubes were gently shaken for 5-6 hours at 4˚C. To prepare mounting solution, Solution B (accelerant) was added to fresh infiltration solution (ratio of 1 mL Solution B: 25 mL infiltration solution), mixed and placed on ice. Infiltrated blocks were placed in separate molds and 2 mL of mounting solution was poured over each block. An

aluminum chuck was placed in each mold and the tray of molds was left at room temperature for approximately 20 minutes to begin polymerization process. Molds were placed on ice, wrapped in plastic and stored at 4˚C overnight to complete polymerization. The following morning each block was gently removed from its mold and allowed to dry completely before sectioning.

2.1.3.2.Sectioning and Staining

Unless specified otherwise, 6 µm transverse serial sections were cut using a microtome and glass knife. Sections of interest were placed in a triple-distilled water bath to transfer to a glass slide and the adjacent section was placed on a metal free plastic cover slip (Thermanox, Thermo Scientific). Sections on glass slides were stained with methylene blue-azure II stain for histological analysis (13 µg/mL methylene blue, 2 µg/mL Azure II, 1% glycerol (v/v), 1% methanol (v/v), 1% phosphate buffer (0.1 mM NaH_2PO_4, 0.67 mM KH_2PO_4; v/v)). Glass slides were placed in a slide holder and methylene blue solution was poured over slides. The slide holder was placed in an incubator at 65˚C for 15 seconds. Excess methylene blue was removed and slides were rinsed with distilled water for approximately 5 minutes then placed on a hot plate to dry.

When interested in examining very small structures (e.g. cells within a neuromast), a 6 µm thick section was deemed too thick and instead 3 µm thick sections were collected, floated in a room temperature water bath, and mounted on silicon nitride windows for XFI. All 3 µm sections were stained with Hematoxylin & Eosin (H&E) using an adapted protocol from Sullivan-Brown et al. (2011). Hematoxylin yields a purple stain in basophilic structures such as nucleic acids which are concentrated in the nucleus whereas eosin yields a pink stain in eosinophilic, protein-rich regions such as the cytoplasm (Sullivan-Brown et al, 2011). Glass staining slides were placed in glass slide racks that could be dipped into each solution and easily transferred to the next solution. Slides were first dipped in Gill's number 2 hematoxylin (Polysciences) for 7 minutes, then rinsed in running distilled water for 2 minutes. Destaining occurred in acid water (120 mM HCl) for 5 seconds. Slides were rinsed again for 1 minute then dipped in Scott's Tap Water Substitute (0.8 g $NaHCO_3$, 8 g $MgSO_4 \cdot 7H_2O$, 400 mL distilled H_2O) for 45 seconds to correct the pH and enhance the purple of the nuclei. All slides were rinsed again for 3 minutes. Slide racks were dipped in eosin-Y (0.5%; Polysciences) for 1.5 minutes and rinsed for an additional 5 minutes before being placed on a hot plate to dry (at least

10 minutes). Plastic cover slips were adhered to all stained slides using a xylene based material (Cytoseal XYL, Richard-Allen Scientific, Kalamazoo, MI). Adjacent sections on cover slips were used for X-ray fluorescence imaging without any further treatment.

2.2. General Synchrotron Introduction

Synchrotrons are very intense sources of light that are primarily used to study very small things including animal tissues, proteins, and molecules or smaller parts of large things (such as the hoof of a horse). Third generation synchrotron sources are distinguished from first or second in having decreased electron beam emittance which makes for improved performance for demanding applications such as imaging. Most third generation synchrotrons like the Canadian Light Source, the Stanford Synchrotron Radiation Light Source, and the Advanced Photon Source consist of an electron gun, a linear accelerator (LINAC), a booster ring, and a storage ring. At the CLS the source of the electron gun is a heated tungsten-oxide disk (to over 1000ºC). A large amplitude positive charge potential then accelerates the electrons and passes them to the next accelerating section. The LINAC increases the energy of the electrons to a given energy, at which point the electrons are traveling at a speed 99.9998% the speed of light. Electromagnetic fields generated in the Radio Frequency (RF) Cavity of the booster ring 'boost' the electrons in energy from 250 MeV to 2.9 GeV (in the case of the CLS). An injection system then transfers the electrons to the storage ring that contains a series of magnets to direct the electrons around the ring. The electrons travel in discrete bunches and the radiation from an RF Cavity in the storage ring is synchronized to crest as a bunch of electrons enter the cavity in order to accelerate the electrons with peak amplitude. At each dipole magnet the path of the electrons is bent which results in the emission of synchrotron light (photons) tangential to the electrons' orbit (Winick, 1994). Finally, an insertion device (i.e. a wiggler or an undulator) can be placed in a straight stretch of the storage ring to create a more focused beam with higher flux (more photons per second reaching the sample). Both types of insertion devices are composed of a series of alternating magnetic poles (Winnick, 1994). Wigglers create a broad range of high energy X-rays that are more intense than those from a bend magnet (Winick, 1994) whereas undulators create a narrower range of X-rays with higher flux through constructive interference (Winick, 1994).

The photon beam then arrives in the beamline, first passing through the optics hutch where a monochromator is used to select the wavelength and mirrors are used to focus the beam,

then moving into the experimental hutch where researchers can mount samples and conduct their experiment using the appropriate technique such as X-ray fluorescence imaging or X-ray absorption spectroscopy.

2.2.1. X-ray Fluorescence Imaging

X-ray fluorescence imaging (XFI) is a technique used to create images of elemental localization within samples. X-ray fluorescence images of zebrafish were collected on beamlines 20-ID-B, 2-ID-D, and 2-ID-E at the Advanced Photon Source (APS) in Argonne, IL (see Figure 1 for layout of beamline 20-ID-B). APS is a third generation synchrotron with a 7 GeV electron storage ring and an operating current of 102 mA. All beamlines utilized for XFI employed an undulator to create a high flux beam and Si(111) double crystal monochromators with Rh-coated mirrors for focusing and harmonic rejection.

In order to decide what incident energy to set the monochromator to one must consider which elements are likely to be found in the sample and then set the incident energy above the absorption edges of all elements of interest. Each element has an absorption edge at a discrete energy and fluoresces at a discrete energy, based on the photoelectric effect (Pushie et al., 2014). The incident energy must be such that it is high enough to eject an inner core electron thus creating an unstable vacancy. This vacancy is filled by the decay of an outer shell electron. As this core hole is filled, a concomitant release of a fluorescent photon occurs and can be detected by the detector. Each fluorescent photon occurs at an energy related to which element it was produced from and what shell the electron decayed from. For example, calcium K edge requires an incident energy of 4.039 keV and the fluorescent photons Ca $K\alpha_1$ will be detected at 3.692 keV (Thompson, 2009). The K edges of high Z elements are often unreachable therefore lower energy edges are utilized instead. In the case of mercury, the K edge requires an incident energy of 83.102 keV which is unachievable at most synchrotrons (Thompson, 2009). Instead, the L_{III} edge is probed using an incident energy of 12.284 keV and the $L\alpha_1$fluorescence peak at 9.989 keV and the $L\alpha_2$ at 9.898 keV (Thompson, 2009). The $L\alpha_1$ and $L\alpha_2$ peaks are so close in energy they are often grouped together; however, the $L\alpha_2$ has a relative intensity of 11% whereas the $L\alpha_1$ has a relative intensity of 100% and is the strongest (Thompson, 2009). The incident X-ray energy in all experiments was set to 13.45 keV because it is above the elements of interest (i.e. sulfur, calcium, zinc, mercury and selenium) and below the excitation

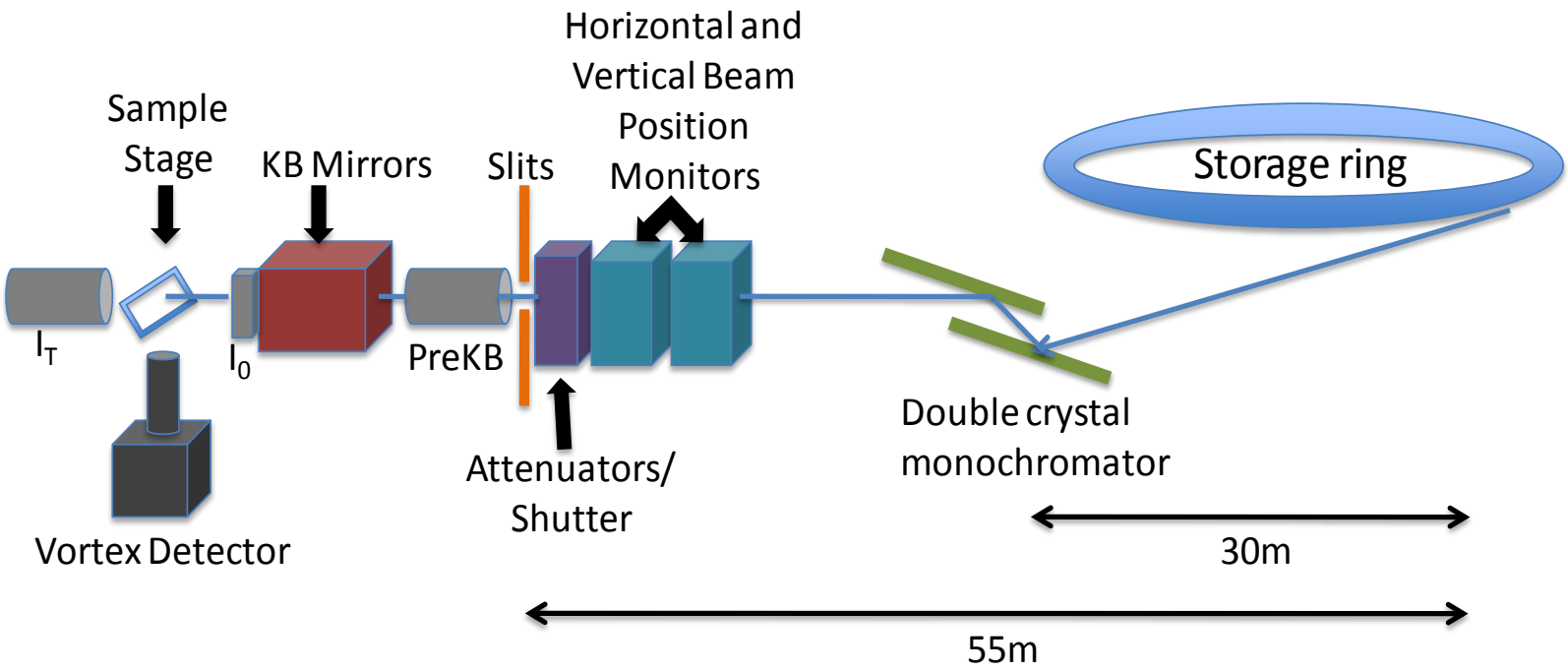

Figure 2.1 Configuration of beamline 20-ID-B at the Advanced Photon Source, Argonne, IL, USA. PreKB= ion chamber prior to the KB mirrors, I0= ion chamber prior to sample stage, IT= ion chamber after sample stage.

energy of bromine (13.474 keV; Thompson, 2009) which is found in many plastic components at the beamline. Additionally, essentially any element in the sample with an absorption energy below the incident energy would be detected because the detector collects any fluorescent photons that reach the detector.

Beamline 20-ID-B uses Kirkpatrick-Baez (KB) mirrors (which have a typical resolution of 2-20 µm; Pushie et al., 2014) to focus the beam to a minimum spot size 5 µm x 5 µm. The high-resolution micro-focused beams approximately 250 nm in diameter on 2-ID-D and 2-ID-E were generated by Fresnel zone plates (which have a typical resolution of 150-300 nm; Pushie et al., 2014) (X-radia, Pleasanton, CA). Samples at all beamlines used were mounted at 45˚ to the incident X-ray beam because this configuration allows the detector to be mounted at 90˚ to the incident X-ray beam which is the angle for minimum X-ray scattering which helps eliminate background noise and minimize detector saturation (Pushie et al., 2014).

Once the beamline configuration has been determined and the monochromator has been set to a specific energy then a region of interest in the sample is selected. This region is raster scanned from left to right and from the bottom of the sample to the top (Pushie et al., 2014). The beam illuminates a particular pixel for a specified amount of time and the detector collects the fluorescent photons from that pixel (Pushie et al., 2014; see Figure 2.2 panel A). X-ray fluorescence was monitored using a silicon-drift Vortex detector (Hitachi High-Technologies Science America Inc., Northridge, CA, USA). The computer is used to 'window' on the peaks created by the various amounts of fluorescent photons (see Figure 2.2 panels B and C). A window is set up for each element found in the sample (including unexpected elements). The computer can then display images of the distribution of each element in the sample (see Figure 2.2 panel D).

Although each element fluoresces at a discrete energy the fluorescence peak covers a certain area and depending on the width could overlap with elements that fluoresce at a similar energy. One such issue arises with zinc which has Kβ peak at 9.572 keV (Thompson, 2009).

Zinc naturally occurs in zebrafish larvae at relatively high levels compared to the levels of mercury observed following exposure to mercury compounds. Care must be taken when setting windows around the Zn K_{β} and the Hg $L_{\alpha 1,\,2}$ peaks to ensure that they do not overlap. If the tails of the peaks overlap and there is an abundance of Zn it could register in the Hg window and create a falsely elevated count of Hg. The disadvantage is that some real counts of Hg may

be excluded. The windows created for the experiments discussed in this thesis were carefully defined to avoid any overlap of Zn in the Hg window. All peaks in the full spectra collected were examined to determine if any unexpected elements were located in samples. Finally, all elements of interest were windowed on and images of the distribution of each element were created. XFI data were analyzed using SMAK software (http://home.comcast.net/~sam_webb/smak.html). Quantification of the elements can be completed using one of three methods. Peak fitting is a more accurate method of quantification (if the energy dispersive data are available) and is particularly useful in the case of dilute samples (Pushie et al., 2014). A common method for quantification is to run a standard of known composition and to relate the peak areas of the standard to those in the sample. Finally, if a standard of known concentration is unavailable for a particular element then standards of elements adjacent on the periodic table (Z±1) can be used along with linear interpolation to determine the quantity of the element. For example, standards containing Hg were found to slowly decrease in concentration over time and could not be guaranteed by the manufacturer. Instead, certified standards of gold (Au) and thallium (Tl) were used as they are the elements adjacent to Hg on the periodic table. Standards and samples should be as similar as possible in terms of thickness, smoothness, and interaction with the beam (Bewer, 2015). Standards should be run under the same conditions (detector solid angle, X-ray incident angle, X-ray incident energy, beam spot size, and material path lengths) as the sample otherwise one must account for the changes (Bewer, 2015). The samples discussed in this thesis adhered to these conditions therefore there was no need for mathematical adjustments and linear interpolation was utilized for quantification of Hg concentrations. Following these quantification methods the units used in XFI are $\mu g/cm^2$ which expresses the amount of the element within the sample as a function of the surface area (Pushie et al., 2014).

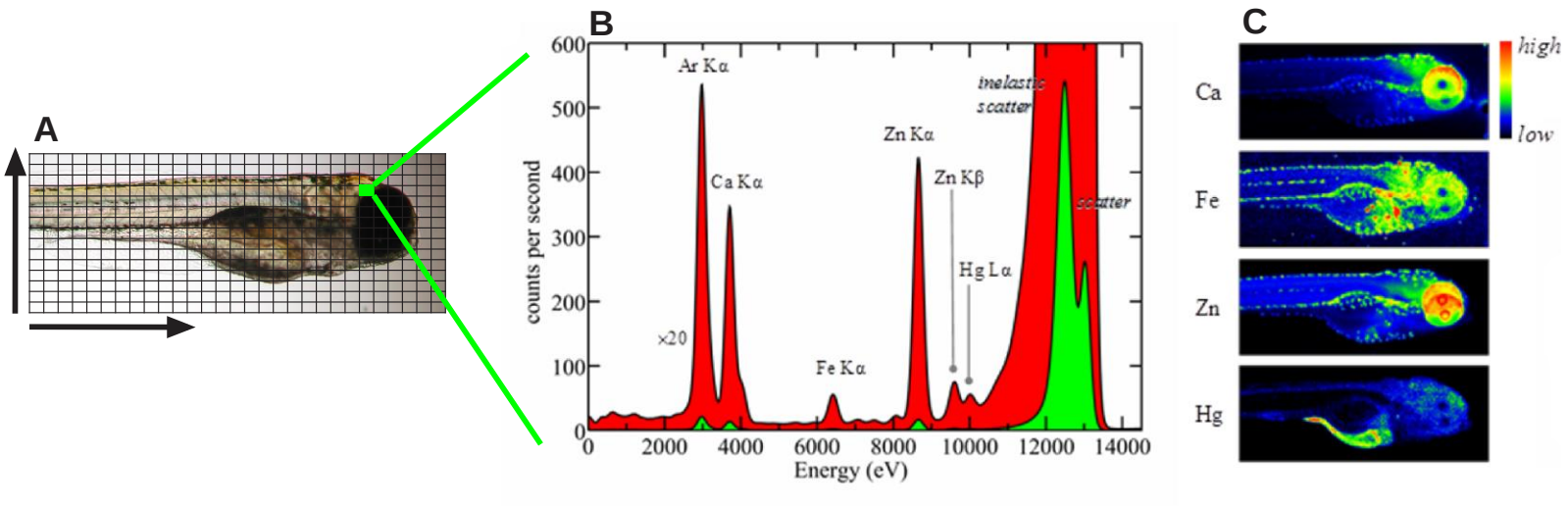

Figure 2.2 Concept of X-ray fluorescence imaging of a zebrafish section. A) Section of zebrafish with a grid showing the raster scanned region (from left to right, starting at the bottom and moving to the top) with individual pixels. A full spectrum of elements is collected for each pixel. B) A spectrum from one pixel, the green spectrum shows the small peaks of fluorescent photons and the large scatter peaks and the red spectrum shows everything enlarged 20 times. C) Image focused on the fluorescence peaks with 'windows' around elements of interest. D) Individual maps of elemental localization of select elements (e.g. calcium, iron, zinc, and mercury) with the highest amount of each element shown in dark red and the lowest amount shown in black.

2.2.2. X-ray Absorption Spectroscopy

As with XFI, XAS depends on the photoelectric effect and the absorption edge of the element of interest. In contrast to XFI in which the monochromator is set to one energy, to study the near edge structure the energy of the monochromator is set to start below the absorption edge and scan through the edge and slightly beyond. To study the extended X-ray absorption fine structure the beam must be set to scan above the absorption edge.

Samples can be run in transmission mode if they are highly concentrated. However, this is not often an option with biological samples as they are usually lower in concentration. Dilute samples are run in fluorescence mode which detects the fluorescent photons ejected from the sample while the energy is scanned from below to above the absorption edge.

XAS was carried out at SSRL with the storage ring operating at 500 mA at 3 GeV on beamlines 2-3 and 7-3. SSRL beamline 2-3 is primarily used for XFI of samples. Once a region of interest is located, micro XAS can be conducted on a particular spot to collect EXAFS (Pushie et al. 2014). A sample run on 2-3 used a micro-focused X-ray beam of approximate diameter of 2 μm that was obtained by using Rh-coated Kirkpatrick-Baez mirrors, with samples mounted at 45° to the incident X-ray beam and a silicon-drift Vortex detector. Beamline 7-3 employs a wiggler and a Si(220) double-crystal monochromator whereas beamline 2-3 has an undulator and a Si(111) double-crystal monochromator. Fluorescent photons are collected by a 30-element germanium detector mounted at 90° to the incident X-ray beam on beamline 7-3. XAS is conducted at very low temperature (e.g. 10 K) to minimize damage from the beam and to decrease thermal vibrations (George and Pickering, 2007; Cotelesage et al., 2012).

All XAS data were analyzed using EXAFSPAK program suite (George, 2000). The phase-corrected Fourier transforms of the EXAFS oscillations were routinely computed. Fourier transforms provide preliminary inter-atomic distances between the absorber and nearby atoms; however, quantitative data analysis uses curve-fitting of a theoretical model to the EXAFS oscillations. The inter-atomic distances are very accurately determined from the EXAFS curve-fitting analysis and the number and size (atomic number) of the nearby atoms can also be approximately determined from the EXAFS data (Pushie et al., 2012). EXAFS analysis is a model building type of analysis. One postulates a model and then refines the parameters until a good fit is achieved. Because an erroneous model may fit the

data reasonably well one must also determine if the parameters are physically reasonable or not. Despite a reasonable fit to physically unlikely parameters, the correct model will always have the best fit. After determining some likely candidates that could be bound to the element of interest, density functional theory (DFT) is often used by our research group to determine additional information that EXAFS alone cannot provide. DFT is a relatively rigorous quantum mechanical method of determining energy minimized and geometry optimized structures to best model which structures are most stable.

CHAPTER 3. CHEMICAL FORM MATTERS: DIFFERENTIAL ACCUMULATION OF MERCURY FOLLOWING INORGANIC AND ORGANIC MERCURY EXPOSURES IN ZEBRAFISH LARVAE

3.1. Preface

Worldwide, people are exposed to different chemical forms of mercury via the air, soil, and water in the environment. Methylmercury is known to cross the blood-brain and blood-placental barriers and to cause various negative effects on the developing organism; however, most research focuses on methyl mercury regardless of the ligand to which it is bound to. Research has shown that inorganic forms of mercury are less toxic than organometallic forms of mercury and therefore there is less emphasis on understanding effects of different ligands bound to mercuric mercury (Hg^{2+}). This chapter focuses on differences in uptake and accumulation patterns of mercury following exposure to different chemical forms including two inorganic and two organometallic forms of mercury. X-ray fluorescence imaging was used to map the localization of mercury in a variety of tissues to elucidate target tissues/organs of each chemical form. The results of this study demonstrate that different chemical forms of mercury can accumulate differentially in a tissue-specific manner, particularly in the case of sensory cells.

3.2. Manuscript Author Contributions

This chapter was published in *ACS Chemical Biology* and was reformatted to follow the guidelines for a manuscript style thesis.

Korbas, M.,[¶] MacDonald, T.C.,[¶] Pickering, I.J., George, G.N., and Krone, P.H. (2012). Chemical form matters: differential accumulation of mercury following inorganic and organic mercury exposures in zebrafish larvae. *ACS Chem. Biol.*, 7(2), 411–420. [¶] These authors contributed equally to this work.

M. Korbas carried out experiments on organic mercury, analyzed XFI data, completed calculations in MINETEQ and drafted the manuscript.

T.C. MacDonald carried out experiments on inorganic mercury, analyzed data, and assisted in drafting the manuscript.

I.J. Pickering, G.N. George, P.H. Krone provided scientific input and guidance, commented on and edited the manuscript, and provided funding for the research.

3.3. Acknowledgements

This research used resources of the Advanced Photon Source (APS), a U.S. Department of Energy (DOE) Office of Science User Facility operated for the DOE Office of Science by Argonne National Laboratory under Contract No. DE-AC02-06CH11357. Data for this chapter were collected from beamline 20-ID-B. Sector 20 facilities at the APS, and research at these facilities, are supported by the U.S. DOE, Office of Basic Energy Sciences (OBES), the Canadian Light Source and its funding partners, the University of Washington, and the APS.

3.4. Abstract

Mercury, one of the most toxic elements, exists in various chemical forms each with different toxicities and health implications. Some methylated mercury forms, one of which exists in fish and other seafood products, pose a potential threat, especially during embryonic and early postnatal development. Despite global concerns, little is known about the mechanisms underlying transport and toxicity of different mercury species. To investigate the impact of different mercury chemical forms on vertebrate development, we have successfully combined the zebrafish, a well-established developmental biology model system, with synchrotron-based X-ray fluorescence imaging. Our work revealed substantial differences in tissue-specific accumulation patterns of mercury in zebrafish larvae exposed to four different mercury formulations in water. Methylmercury species not only resulted in overall higher mercury burdens but also targeted different cells and tissues than their inorganic counterparts, thus revealing a significant role of speciation in cellular and molecular targeting and mercury sequestration. For methylmercury species, the highest mercury concentrations were in the eye lens epithelial cells, independent of the formulation ligand (chloride *versus* L-cysteine). For inorganic mercury species, in absence of L-cysteine, the olfactory epithelium and kidney accumulated the greatest amounts of mercury. However, with L-cysteine present in the treatment

solution, mercuric bis-L-cysteineate species dominated the treatment, significantly decreasing uptake. Our results clearly demonstrate that the common differentiation between organic and inorganic mercury is not sufficient to determine the toxicity of various mercury species.

3.5. Introduction

Compounds of heavy elements are often toxic, and excluding radioactive elements, compounds of mercury are generally the most toxic. In natural systems mercury is found in elemental, inorganic, and organometallic forms. The nature and extent of mercury toxicity depend largely on its molecular form (Clarkson and Magos, 2006). Relatively benign mercury compounds include mercuric sulfides which have very low solubilities; α-HgS is widely used in traditional Chinese medicines (Huang et al., 2007) and in red tattoo ink (Mortimer et al., 2003), while β-HgS occurs on the surface of aged dental amalgam restoratives (George et al., 2009). In contrast, organo-mercury compounds are extremely toxic to vertebrates, for example dimethylmercury is one of only a few compounds formally classified as supertoxic (Nierenberg et al., 1998).

Human populations are exposed to different forms of mercury from a wide variety of sources. Exposure to elemental and inorganic mercury comes mainly from dental amalgams and inhalation of ambient air during occupational activities (chlor-alkali plants, mercury mines, mercury-based gold and silver mining), as well as from direct contact with mercury-containing products (*e.g.*, thermometers and other measuring equipment, batteries, fluorescent light bulbs) and ingestion of mercury-contaminated food and water (Poulin and Gibb, 2008). Exposure to elemental and inorganic mercury is especially high in Asia, the region with both the largest mercury emissions (UNEP, 2008) and the highest demand for this metal (UNEP, 2006). In some Asian countries the continuous use of traditional, folk, or herbal medicines containing metallic or inorganic mercury also contributes to elevated exposures (Martena et al., 2010).

The dominant organic mercury form to which humans are exposed is thiolate-bound methylmercury (Harris et al., 2003). This compound is present in virtually all fish and seafood products and exposure is therefore more widespread than to other forms of mercury. Concentrations of mercury in fish vary between species and habitats, with generally higher levels in carnivorous and older fish or fish from polluted areas. The levels of human exposure to methylmercury strongly depend on fish and seafood eating habits and may be elevated among

populations reliant on these foodstuffs for their daily nutrition (Bravo et al., 2010; Trasande et al., 2010; Cheng et al., 2009).

The adverse effects of mercury on health depend on chemical form and dose; however, mercury vapor and organic mercury have one common characteristic. They readily cross the blood-brain (BBB) and blood-placental barrier (BPB) causing irreversible damage to the nervous system especially in early stages of development (Clarkson and Magos, 2006). In contrast, inorganic mercury (*e.g.*, mercuric mercury, Hg^{2+}) has limited capacity to cross the BBB and BPB but is avidly accumulated by the kidneys (Clarkson and Magos, 2006). Although mercuric mercury is generally less toxic than organic forms, it plays a key role in mercury toxicology. The mercuric ion is produced in tissues after inhalation of mercury vapor. It is also a product of methylmercury demethylation in the intestines and the brain (Korbas et al., 2010a). The WHO have estimated that the average daily mercury intake in North America and Europe is approximately 4.3 and 2.4 μg for inorganic and organometallic forms, respectively, with most of the latter arising from fish (IPCS, 1991). Even though these levels are not high, mercury accumulation within the human body over time may be a problem. A recent study confirmed that inorganic mercury deposition within the body due to chronic exposure increases with age and correlates significantly with biological markers of the main mercury targets: pituitary, immune system, and liver (Laks, 2009).

Early life stages are particularly susceptible to mercury's adverse effects; however, the mechanisms of mercury disposition within the developing body are poorly understood. Zebrafish makes an excellent model vertebrate to study mercury toxicity in developing organisms (Yang et al., 2009), especially due to an endothelial-based BBB, which exhibits characteristics comparable to its mammalian counterpart as early as 3 days post fertilization (dpf) (Jeong et al., 2008). Previously we successfully utilized zebrafish with synchrotron-based X-ray fluorescence imaging to study the localization, dynamic accumulation, and redistribution of mercury in developing zebrafish embryos and larvae following waterborne exposure to methylmercury L-cysteineate (Korbas et al., 2008; Korbas et al., 2010b). Here we investigate the uptake of different organic and inorganic mercury species in zebrafish larvae, showing that mercury accumulation patterns vary tremendously with the chemical form.

3.6. Methods

3.6.1. Animal Care and Embryo Collection

Adult fish were kept at 28°C in carbon-filtered tap water with a photoperiod of 14 hours (h). Embryos were collected and staged following standard procedures. After collection, embryos and larvae were reared in 25 mL Petri dishes with culture water changed daily. This work was approved by the University of Saskatchewan's Animal Research Ethics Board and adhered to the Canadian Council on Animal Care guidelines on the care and use of fish in research, teaching, and testing.

3.6.2. Mercury Treatment Solutions

Methylmercury compounds are extremely toxic, and thus appropriate precautions must be taken to prevent any inhalation of or skin contact with these compounds or solutions thereof. All reagents, except when specifically mentioned, were purchased from Sigma-Aldrich as the highest quality available. A 1 mM stock solution of mercuric chloride was made from mercuric chloride crystals dissolved in triple-distilled water. A stock solution of 1 mM mercuric bis-L-cysteineate was prepared from 2 mM stock solution of mercuric chloride and 5 mM solution of L-cysteine in 100 mM HEPES buffer by mixing equal aliquots of those two (1:2.5 molar ratio) to ensure each mercury atom was bound to two cysteine molecules. Methylmercury chloride was purchased as a 1000 ppm aqueous solution from Alfa Aesar and further diluted in triple-distilled water to give a 1 mM stock solution. Methylmercury hydroxide was purchased as a 1 M aqueous solution from Strem Chemicals Inc. and diluted in triple-distilled water to give a 4 mM stock solution. A 4 mM stock solution of L-cysteine was prepared in 30 mM phosphate buffered saline (PBS; 153.3 mM NaCl, 4.8 mM $NaH_2PO_4 \cdot H_2O$ and 25 mM Na_2HPO_4). A 1 mM stock solution of methylmercury L-cysteineate was prepared by mixing suitable aliquots of methylmercury hydroxide and L-cysteine solutions to give a 20% molar excess of L-cysteine (*i.e.*, a molar ratio of 1:1.2) with addition of 30 mM PBS as needed.

Mercury solutions for treatment of zebrafish were prepared from the above solutions by dilution in fish culture water (carbon-filtered tap water). All stock and treatment solutions were freshly made prior to each exposure.

All exposures were at 28 °C for 36 h starting at 3.5 dpf. Larvae were placed in 25 mL Petri dishes containing 1 μM mercuric chloride (1:1000 dilution of stock solution in culture water), 200 μM mercuric bis-L-cysteineate (1:5), 1 μM methylmercury chloride (1:1000), 2 μM methylmercury L-cysteineate (1:500), or control dishes with no added mercury. For each mercury formulation (Table 3.1) three replicate treatments (3 × 25 larvae) were carried out. After exposure, larvae were rinsed several times in fresh carbon-filtered water to remove any remaining mercury.

3.6.3. Calculation of Mercury Speciation in Treatment Solutions

Mercury equilibrium speciation calculations were performed using MINTEQA2 (version 4.03), a U.S. EPA equilibrium speciation program for dilute aqueous systems (http://www.epa.gov/ceampubl/mmedia/minteq/). The simulations were computed for 28 °C and pH 7.8, the conditions under which larvae were reared. The fish culture water was analyzed in the environmental analytical laboratory of the Saskatchewan Research Council for major components (bicarbonate, chloride, nitrate, sulfate, calcium, magnesium, potassium, sodium), and these were included in the calculations together with all of the external components originating from mercury stock solutions and PBS and HEPES buffers. The detailed list of concentrations for all of the constituents in the calculations is shown in Supplementary Table S3.1. Since HEPES is not included in the MINTEQA2 components, database literature values were incorporated to simulate its potential effects (Delnomdedieu et al., 1992).

3.6.4. Preparation of Sections

Larvae were fixed in 4% paraformaldehyde (PFA) for 2 h at room temperature immediately following the exposures. The fixed larvae were dehydrated in a graded series (0%, 25%, 50%, 75%, and 100%) of ethanol in PBST buffer (30 mM PBS, 0.01% Tween 20) for 5

Table 3.1 Predicted mercury speciation in zebrafish culture water[a]

Formulation [b]	Mercury Species	Mole %
1 μM $HgCl_2$	$Hg(OH)_2$	90.0%
	HgClOH	9.5%
	$HgCO_3$	0.3%
	$HgCl_2$	0.2%
1 μM CH_3HgCl	CH_3HgOH	96.1%
	CH_3HgCl	3.3%
	CH_3HgCO_3	0.6%
200 μM $HgCl_2$ + 500 μM L-Cys	$Hg(L\text{-}Cys)_2$	100.0%
2 μM CH_3HgOH + 2.4 μM L-Cys	$CH_3Hg(L\text{-}Cys)$	100.0%

[a] Computed at 28°C and pH 7.8 using MINTEQA2

[b] Other components originating from system water, phosphate buffered saline (PBS) formulation and HEPES buffer are given in Table S3.1 (Supplementary Information).

minutes (min) each and stored in 100% ethanol at −20 °C until needed. For sectioning, the fixed and dehydrated larvae were rehydrated into PBST by 5 min washes in the reversed ethanol gradient. Selected larvae were properly oriented and embedded in 1% agarose gel. The blocks of gel containing the fish were cut out and dehydrated in 100% ethanol by gentle shaking for 5−8 h at 4 °C. Following dehydration the blocks were infiltrated overnight on a rotating stirrer at 4 °C with JB-4 catalyzed solution A (10 mL solution A:0.125 g catalyst; Polysciences Inc., Warrington, PA, USA). The infiltration process with fresh infiltration solution continued on the following day for 5−6 h. The infiltrated samples were placed in embedding molds filled with a mixture of JB-4 solution B and fresh infiltration solution (1 mL solution B: 25 mL infiltration solution) and left overnight at 4 °C to polymerize. Sections of 6 μm thickness were cut on a microtome using glass knives. Of two adjacent sections, one was mounted on a glass slide and stained with methylene blue, while the other, intended for synchrotron X-ray fluorescence imaging, was fixed on a Thermanox plastic coverslip (Gibco BRL) without any further processing.

3.6.5. X-ray Fluorescence Imaging (XFI)

X-ray fluorescence images were collected at the Advanced Photon Source (Argonne, IL, USA) using beamline 20-ID-B (PNC/XOR) with the storage ring operating in continuous top-up mode at 102 mA and 7.0 GeV. The incident X-ray energy was set to 13.45 keV and the Hg $L\alpha_{1,2}$ fluorescence lines, as well as the intensity of the total scattered X-rays, were monitored using a silicon-drift Vortex detector (SII NanoTechnology USA Inc.). Incident and transmitted X-ray intensities were measured with nitrogen-filled ion chambers. Experiments used a Si(111) double crystal monochromator and Rh-coated silicon mirrors for focusing and harmonic rejection. The microfocused beam of 5 μm diameter was generated by Kirkpatrick−Baez (K−B) Rh-coated focusing mirrors. Samples were mounted at 45° to the incident X-ray beam and were spatially rastered in the microbeam with a step size of 5 μm. Beam exposure was 0.6 seconds (s) per step.

3.6.6. X-ray Fluorescence Imaging Data Analysis

The XFI data were processed using SMAK software. Windowed fluorescence counts were normalized by the incident X-ray intensity and background-corrected by subtracting the average intensity obtained of pixels outside the tissue. Quantities of Hg per pixel were calibrated

using two certified highly uniform thin film standards on 6.3-μm-thick mylar substrates (Micromatter, Vancouver, BC, Canada) containing 16.3 and 17.1 μg/cm^2 Au and TlCl, respectively. Using standards of gold and thallium, adjacent to mercury in the periodic table, was preferable to employing a mercury amalgam standard because the latter decreased in mercury content slowly over time, presumably due to loss of elemental mercury vapor. Average background intensities for windowed fluorescence from the standards were estimated from the X-ray fluorescence image of the 6.3 μm thick mylar film. The background-corrected Au and Tl L$\alpha_{1,2}$ fluorescence intensities were used to interpolate a Hg L$\alpha_{1,2}$ fluorescence intensity, which was applied to the background-corrected Hg distribution maps to obtain the quantities of Hg per pixel in μg/cm^2. The use of this unit is widespread in the XFI literature because it directly relates to what is being measured. These units can be simply related to mercury concentration in mM by assuming that the sections are uniformly 6 μm thick and by multiplying the aerial Hg densities (in μg/cm^2) by 8.3. Another useful unit is the number of moles of Hg per cell, which is sometimes used in *in vitro* uptake studies. Assuming that the average diameter of a cell is 10 μm and the thickness of the sections is 6 μm, the number of moles of Hg per cell can be calculated by multiplying the aerial Hg density (in μg/cm^2) by 4×10^{-15}. To verify the biological relevance of the aerial densities obtained with our method, we compared them to the previously reported number of moles of Hg taken up by a K-562 cell in the cell culture study following 48-h treatment with 35 μM $HgCl_2$ (Frisk et al., 2001). On average, the number of moles of Hg per K-562 cell was 0.5×10^{-15}, which is only slightly higher than the respective number reported here for the zebrafish olfactory epithelial cells following 36-h exposure to 1 μM $HgCl_2$ (~0.1 μg/cm^2 of Hg in Figure 3.1, corresponding to 0.4×10^{-15} mol Hg/cell).

Statistics on large sample numbers are precluded by the long data acquisition times and limited availability of synchrotron time. Instead, we examined the reproducibility in mercury levels of the liver and somitic muscles in three trunk sections following the same methylmercury L-cysteineate treatment. For different fish with identical treatments, the variation in anatomically similar sections was less than 20% (see Appendix A for Supplementary Figure 3.1 and Supplementary Table 3.2).

In the results presented below, ranges in mercury levels refer to the observed variation from pixel to pixel in a particular area of a single sample.

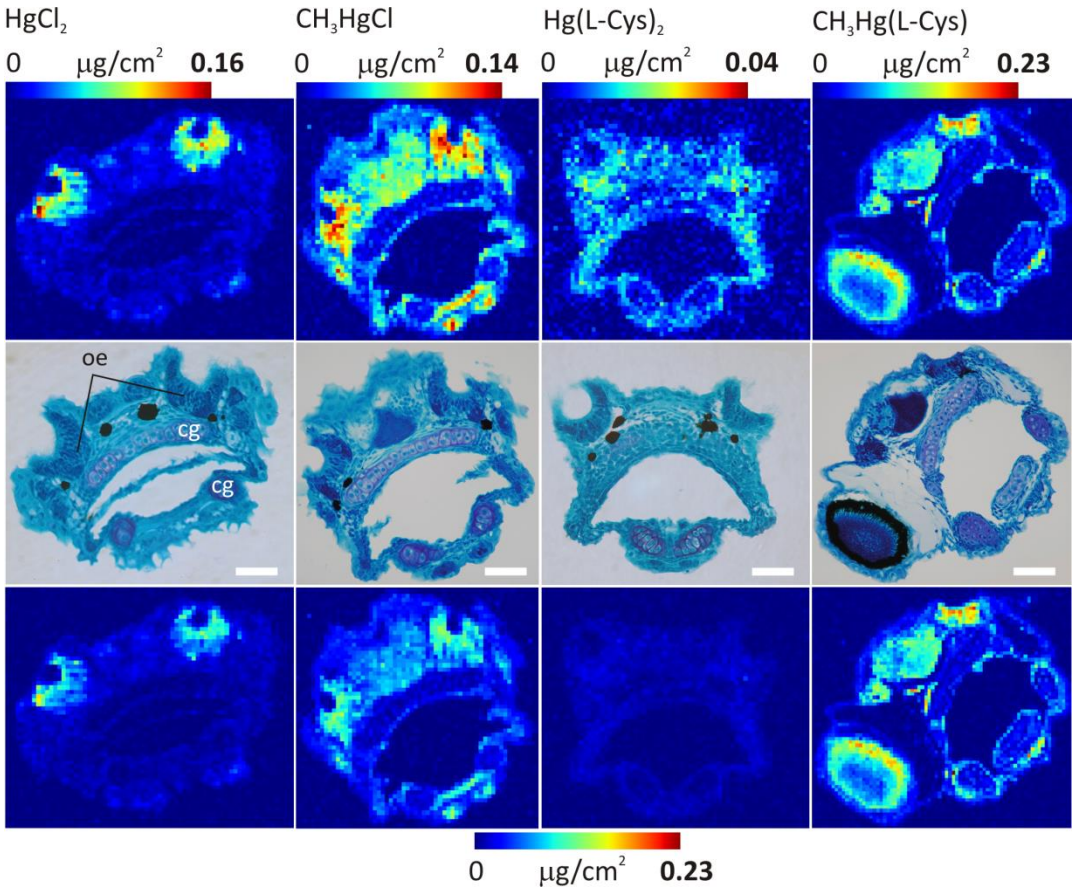

Figure 3.1 Quantitative mercury distributions in 5 dpf zebrafish larvae following a 36-hour exposure to 1 µM mercuric chloride $HgCl_2$, 1 µM methylmercury chloride CH_3HgCl, 200 µM mercuric bis-L-cysteineate $Hg(L\text{-}Cys)_2$, or 2 µM methylmercury L-cysteineate. The dominant mercury species in the treatment solutions are shown in Table 3.1. Histological images (middle panel) of olfactory epithelium are compared with the mercury distributions of the adjacent sections. The first row mercury maps are scaled separately to the highest level of mercury in each of the images, whereas the ones in the third row are scaled to the highest level of mercury among all four images. Scale bar 50 µm, *oe*-olfactory epithelium, *cg*-cartilage.

3.7. Results and Discussion

3.7.1. Solution Species and the Nature of the Exposure

Zebrafish larvae at 3.5 dpf were exposed for 36 h to four different mercury formulations in water: 1 μM mercuric chloride, 1 μM methylmercury chloride, 200 μM mercuric bis-L-cysteineate, and 2 μM methylmercury L-cysteineate. The mercury treatment concentrations were chosen to be non-lethal over the exposure period and to facilitate detection in larval tissues. Preliminary range-finding experiments demonstrated considerable differences in toxicity with chemical forms, especially for the L-cysteine based forms, thus precluding the use of identical concentrations for all mercury forms. In particular, mercuric bis-L-cysteineate showed very low toxicity to developing larvae; even at 200 μM it did not cause any deformities or behavioral changes, although low death rates were observed with longer exposures in some experiments (96 h).

The complex water chemistry potentially present in the exposure solutions was estimated using the simulation program MINTEQA2 (http://www.epa.gov/ceampubl/mmedia/minteq/). Consistent with previous work, solution mercury speciation was predicted to depend on pH and the concentrations of chloride and L-cysteine (Delnomdedieu et al., 1992; Mason et al., 1996; Dyrssen and Wedborg, 1991).

Due to low chloride content in the zebrafish culture water (~0.31 mM) and the slightly basic pH (7.8), the predominant inorganic and organic mercury forms (in absence of L-cysteine) were predicted to be uncharged hydroxide complexes, $Hg^{-}(OH)_2$ and CH_3HgOH (Table 3.1). The total concentration of $Hg(OH)_2$ was well below its water solubility of 0.25 mM (Sillen, 1964); consistent with this no precipitation was observed. Figure 3.2 shows structures of the different mercury species considered. These species are in equilibrium, with differing uptake rates of the specific equilibrating species; removal of one species from solution by uptake will drive the equilibrium to replenish that species. To study the effects of individual equilibrating components would require variation of conditions such as chloride and pH, which would affect the larvae in complex ways; this is outside the present scope. For the L-cysteine complexes, essentially all of the mercury was predicted to be thiol-bound (Table 3.1) as expected from the high affinities of mercury for thiolates (Webb, 1966). This is illustrated by the formation constant for methylmercury L-cysteineate of $10^{15.7}$, compared with $10^{5.45}$ and $10^{9.5}$ for chloride and hydroxide forms, respectively (Webb, 1966).

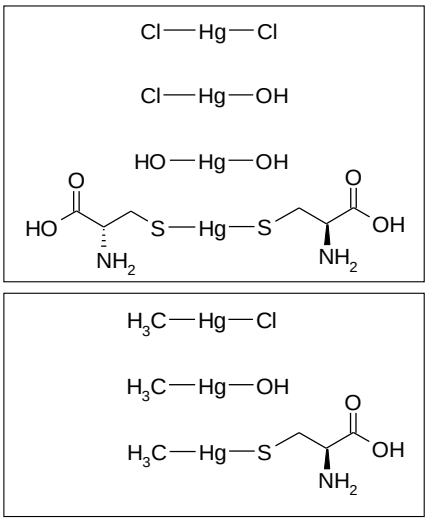

Figure 3.2 Schematic structures of the inorganic and organic mercury species considered in this work. Inorganic mercury compounds in top panel are mercuric chloride, mercuric hydroxy-chloride, mercuric hydroxide, and mercury bis-L-cysteineate. Organic mercury compound in lower panel are methylmercury chloride, methylmercury hydroxide, and methylmercury L-cysteineate.

3.7.2. Tissue and Chemically Specific Mercury Accumulation

For each exposure condition, four transverse sections representing different tissues and organs were imaged and analyzed for mercury distribution. In all cases, untreated control fish showed no mercury signal. The use of the high flux 5 μm size synchrotron X-ray beam from 20-ID-B at the Advanced Photon Source significantly improved mercury detection at lower concentrations and with higher spatial resolution than our previous work (Korbas et al., 2008; Korbas et al., 2010b). Figure 3.1 compares 5-μm-resolution X-ray fluorescence images showing mercury distributions in 6-μm-thick olfactory epithelium sections of exposed zebrafish larvae. The mercury distribution substantially varied with the exposure chemical form. Despite the extremely high concentration for the mercuric bis-L-cysteineate exposure (200 μM), mercury levels in treated larvae were extremely low (less than 0.04 $\mu g/cm^2$) with no specific tissue targeted (Figure 3.1). In contrast, uptake in mercuric chloride-treated larvae was highly efficient and selective with highly elevated mercury only in olfactory epithelium (up to four times that from mercuric bis-L-cysteineate exposure). The olfactory epithelium contains the sensory hair cells required for olfaction. Organic mercury uptake in the olfactory section was more widespread than for mercuric chloride. In both methylmercury chloride solution and methylmercury L-cysteineate-treated larvae, significant mercury accumulated not only in the olfactory epithelium (up to 0.14 and 0.21 $\mu g/cm^2$, respectively) but also in other tissues (Figure 3.1). Despite these differences, all four mercury forms showed very low mercury uptake by cartilage cells accompanied by higher mercury uptake by surrounding connective tissue (Figure 3.1), possibly due to the relatively low cell density and avascularity of cartilage.

Given the known toxic effects of mercury on the brain, mercury distributions in transverse sections through the brain and eye were next examined (Figure 3.3). Figure 3.3A shows striking differences in mercury uptake between inorganic and organic species. Overall mercury levels were significantly lower for inorganic compared to organic mercury species. Following exposure to mercuric chloride solutions (Figure 3.3A), mercury specifically concentrated in the neuromasts, epiphysis (pineal gland), and brain ventricular region. Trace mercury was detected in other tissues including the optic nerve. With mercuric bis-L-cysteineate exposure, the brain area appeared preferentially targeted; tissues with the highest mercury levels included the epiphysis, ventricular region, habenula, and optic nerve (Figure 3.3A).

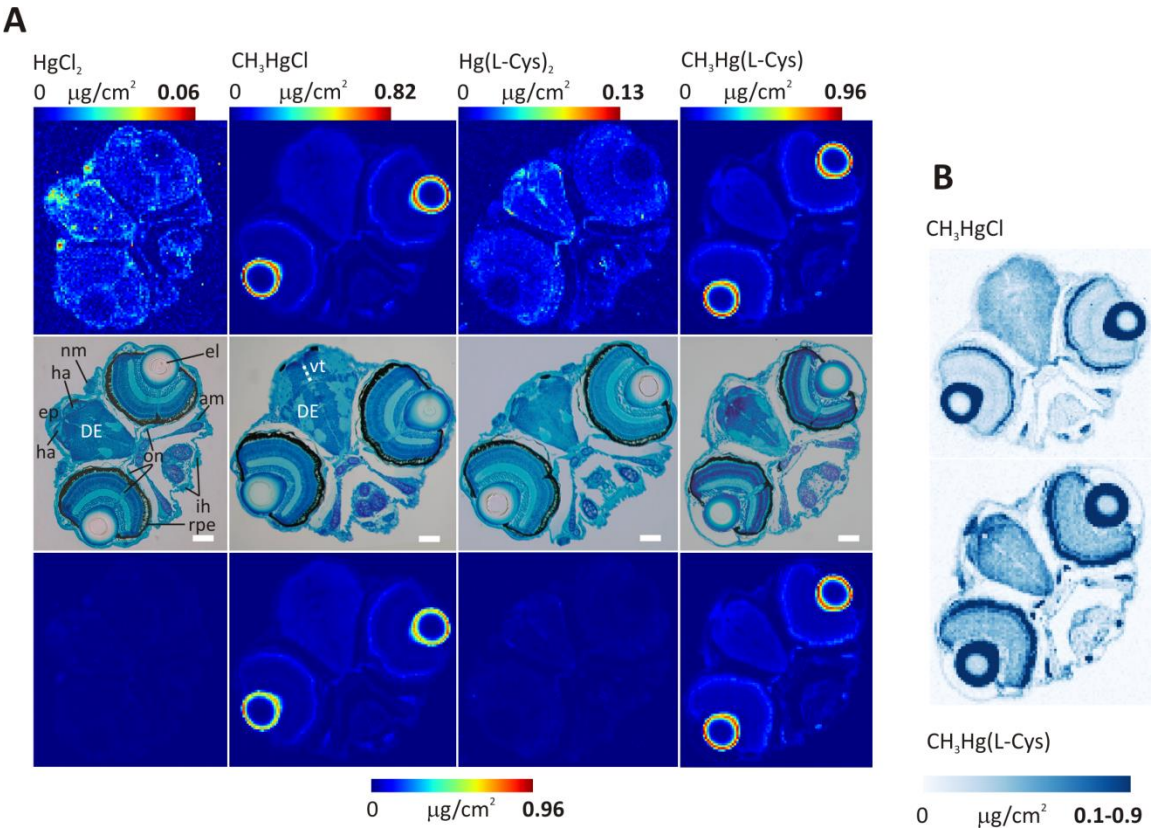

Figure 3.3 Quantitative mercury distributions in 5 dpf zebrafish larvae following a 36-hour exposure to 1 µM mercuric chloride $HgCl_2$, 1 µM methylmercury chloride CH_3HgCl, 200 µM mercuric bis-L-cysteineate $Hg(L\text{-}Cys)_2$, or 2 µM methylmercury L-cysteineate. The dominant mercury species in the treatment solutions are shown in Table 3.1. Histological images (middle panel) of the brain and the eye are compared with the mercury distributions of the adjacent sections (A). The first row mercury maps are scaled separately to the highest level of mercury in each of the images, whereas the ones in the third row are scaled to the highest level of mercury among all four images. Scale bar 50 µm, *el*-eye lens, *rpe*-retinal pigmented epithelium, *on*-optic nerve, *nm*-neuromast, *ih*- interhyoideus, *am*- adductor mandibulae, *ep*-epiphysis, *ha*-habenula, *vt*-ventricular region, *DE*-diencephalon. Mercury distribution maps for organic mercury exposures were scaled to 0.1 µg/cm^2 to better illustrate the variations in the mercury levels in the brain region (B).

The mercury accumulation patterns following exposures to organic mercury were very distinct from those from the inorganic species and virtually independent of the bound ligand (Figure 3.3). For both methylmercury chloride and methylmercury L-cysteineate solutions, the highest mercury levels were detected in the outer layer of the eye lens (Figure 3.3A; up to 0.82 and 0.96 μg/cm^2, respectively), corresponding to the lens epithelium, a single layer of dividing cells that gives rise to fibers within the lens; these data confirm these cells as a major target organ for organic mercury (Korbas et al., 2008; Korbas et al., 2010b). Levels in lens epithelium were on average 3−5 times higher than in the outermost layers of the retina (most likely retinal pigmented epithelium and/or photoreceptor layer), the second highest mercury uptake site within the eye section. Similar mercury levels to those found in the retina were also observed in the cranial muscles, namely, adductor mandibulae and interhyoideus. However, consistent with the olfactory sections, very low mercury uptake was observed in the cartilage tissue. Significant mercury also accumulated in the optic nerve with maximum mercury levels for chloride or L-cysteine bound methylmercury exposures at 0.085 and 0.19 μg/cm^2, respectively. Interestingly, mercury accumulation in the brain region was more diffuse but showed overall significantly higher mercury levels than for inorganic mercury exposures (Figure 3.3). Following organic mercury exposures, mercury accumulated in the diencephalon of the forebrain region with progressively higher levels with increasing distance from the ventricle. However, no mercury was present within the ventricular region itself, again in striking contrast to the inorganic mercury exposures. Due to a slight difference in the sectioning planes of the two specimens, specific mercury accumulation in the habenula and epiphysis could be observed only in the methylmercury L-cysteineate-treated larva (Figure 3.3B). The mercury levels in these two were at least 2-fold higher than those of the gray matter of the diencephalon.

Consistent with findings from the olfactory epithelium and eye sections, transverse sections of the heart region showed mercury levels in the inorganic mercury-treated fish that were significantly lower than those treated with the organic forms (Figure 3.4). Among the two inorganic forms, mercury uptake from mercuric chloride solution was more efficient as similar levels in larvae were observed for the 200 μM mercuric bis-L-cysteineate solutions compared to the 1 μM mercuric chloride solutions. The ventricular region was a common target for both inorganic mercury treatments with maximum mercury levels at 0.03 and 0.05 μg/cm^2 for mercuric chloride solution and mercuric bis-L-cysteineate exposures, respectively (Figure 3.4).

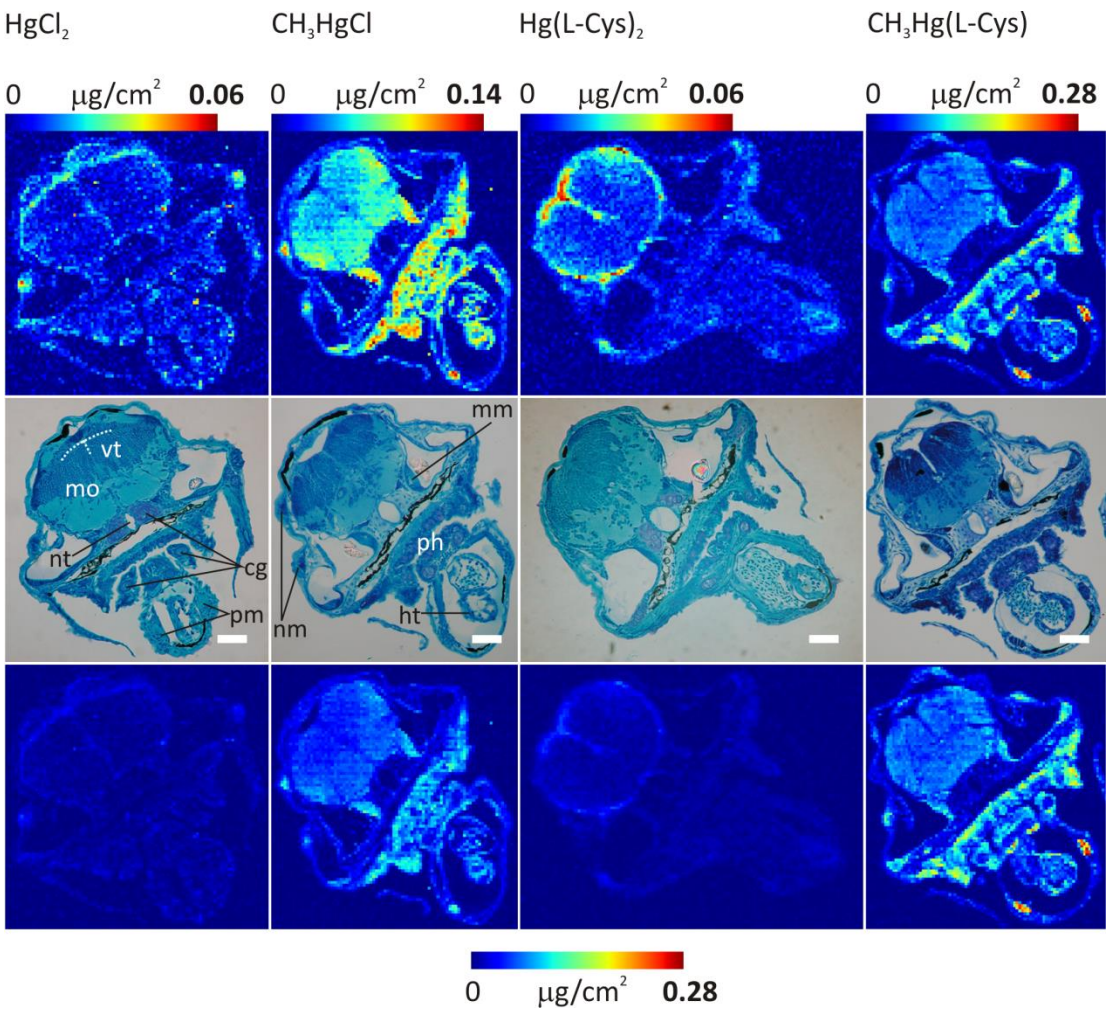

Figure 3.4 Quantitative mercury distributions in 5 dpf zebrafish larvae following a 36-hour exposure to 1 µM mercuric chloride $HgCl_2$, 1 µM methylmercury chloride CH_3HgCl, 200 µM mercuric bis-L-cysteineate $Hg(L\text{-}Cys)_2$, or 2 µM methylmercury L-cysteineate. The dominant mercury species in the treatment solutions are shown in Table 3.1. Histological images (middle panel) of the heart region are compared with the mercury distributions of the adjacent sections. The first row mercury maps are scaled separately to the highest level of mercury in each of the images, whereas the ones in the third row are scaled to the highest level of mercury among all four images. Scale bar 50 µm, *vt*-ventricular region, *mo*-medulla oblongata, *nt*-notochord, *pm*-pericardial muscles, *cg*-cartilage, *nm*-neuromast, *mm*-median macula, *ph*-pharynx, *ht*-heart.

For the latter treatment, mercury lined the periphery of the medulla oblongata in the hindbrain region protruding in certain areas toward its interior. Other organs such as the pharynx or heart showed only trace levels (below 0.02 μg/cm^2) of accumulated mercury when exposed to inorganic mercury forms. Following organic mercury exposures, the mercury distribution was again higher and more widespread, with notable differences compared to inorganic mercury (Figure 3.4). Organic mercury treated larvae showed significant mercury throughout the medulla oblongata region. For methylmercury L-cysteineate the distribution was nearly uniform, with mercury levels between 0.04 and 0.09 μg/cm^2. However, for methylmercury chloride solution, the white matter of the medulla oblongata showed slightly higher mercury levels than the gray matter (0.05−0.1 *vs* 0.03−0.06 μg/cm^2). Interestingly, overall mercury levels in the medulla oblongata for the two organic mercury forms were similar despite the double molar excess of mercury in the methylmercury L-cysteineate solutions compared to the methylmercury chloride solutions. Similarly, comparable mercury levels (0.07−0.13 μg/cm^2) were detected in the median macula (sensory epithelium) of the inner ear following the two organic mercury exposures.

A significant and noteworthy difference between inorganic and organic mercury-exposed larvae was that the former showed specific mercury accumulation in the ventricular region of the brain, whereas the organic mercury was excluded from this region (Figure 3.4). In addition, the pharyngeal epithelium, the heart, and the pericardial muscles showed significantly elevated mercury levels only with the organic mercury exposures (Figure 3.4). Interestingly, none of the mercury exposures gave rise to mercury in the notochord or cartilage tissue. Both are highly hydrated, avascular tissues that provide structural support to the developing larva through the development of hydrostatic pressure.

The presence of neuromasts in the heart sections of the organic mercury-treated larvae (Figure 3.4) and in the eye section of the inorganic mercury-treated larvae (Figure 3.3) allowed us to compare mercury accumulation in a second type of sensory organ containing sensory hair cells. Unlike the olfactory epithelium, neuromasts are mechano-sensory organs responsible for detecting pressure changes in water. By far the highest mercury levels were detected in the neuromasts from larvae treated with organic mercury (0.11 and 0.16 μg/cm^2 for methylmercury chloride and methylmercury L-cysteineate solutions, respectively). The neuromast mercury levels with mercuric chloride solutions (0.02−0.06 μg/cm^2) were on average half of those of the

organic counterparts (Figures 3.3 and 3.4). The lowest neuromasts mercury accumulation was detected for the mercuric bis-L-cysteineate solutions (less than 0.02 μg/cm^2).

Liver sections showed even more pronounced differences in mercury uptake and accumulation between inorganic and organic mercury exposures (Figure 3.5). Organs especially highlighting those differences included medulla oblongata, the somitic muscles, the gut, and the yolk. In these tissues the levels of mercury following inorganic mercury exposures were negligibly low or even close to zero.

In the case of the mercuric chloride solutions, mercury specifically accumulated in the pronephric ducts, in the yolk sac wall (but not inside the yolk), and in the liver. Mercuric bis-L-cysteineate solutions had similar target organs, but overall levels were significantly higher, especially in the yolk sac wall.

Following exposure to organic mercury solutions, mercury specifically accumulated in the pronephric ducts, the liver, the yolk sac wall, and the somitic muscles (Figure 3.5). Mercury levels in the pronephric ducts and the liver were similar for both methylmercury chloride solution and methylmercury L-cysteineate exposures, reaching 0.25 and 0.19 μg/cm^2, respectively. Despite the higher mercury exposure concentrations used for methylmercury L-cysteineate compared with methylmercury chloride, the latter resulted in higher mercury levels in the yolk, the gut, and the medulla oblongata.

In summary, inorganic mercury exposures resulted in overall lower mercury burdens than organic mercury exposures. The difference was especially pronounced for mercuric bis-L-cysteineate, which despite the highest concentration (200 μM) of all four forms, showed mercury levels lower than those of the organic mercury larvae, except for the yolk sac wall (Figure 3.5). Exposures to inorganic mercury species not only gave generally lower mercury levels but also targeted different cell types in the developing larvae. In mercuric chloride solution, the highest mercury levels were in the olfactory epithelial cells (0.05−0.16 μg/cm^2) (Figure 3.2). For mercuric bis-L-cysteineate, the target cells were those of the yolk sac wall (0.05−0.15 μg/cm^2) (Figure 3.5). However, by far the highest mercury levels were detected in the eye lens epithelial cells in the larvae exposed to solutions of methylmercury chloride and methylmercury L-cysteineate (0.4−0.82 and 0.4−0.96 μg/cm^2) (Figure 3.3).

Higher bioaccumulation levels of organic mercury toxicants have been observed previously and sometimes attributed to their enhanced lipid solubility and thus higher

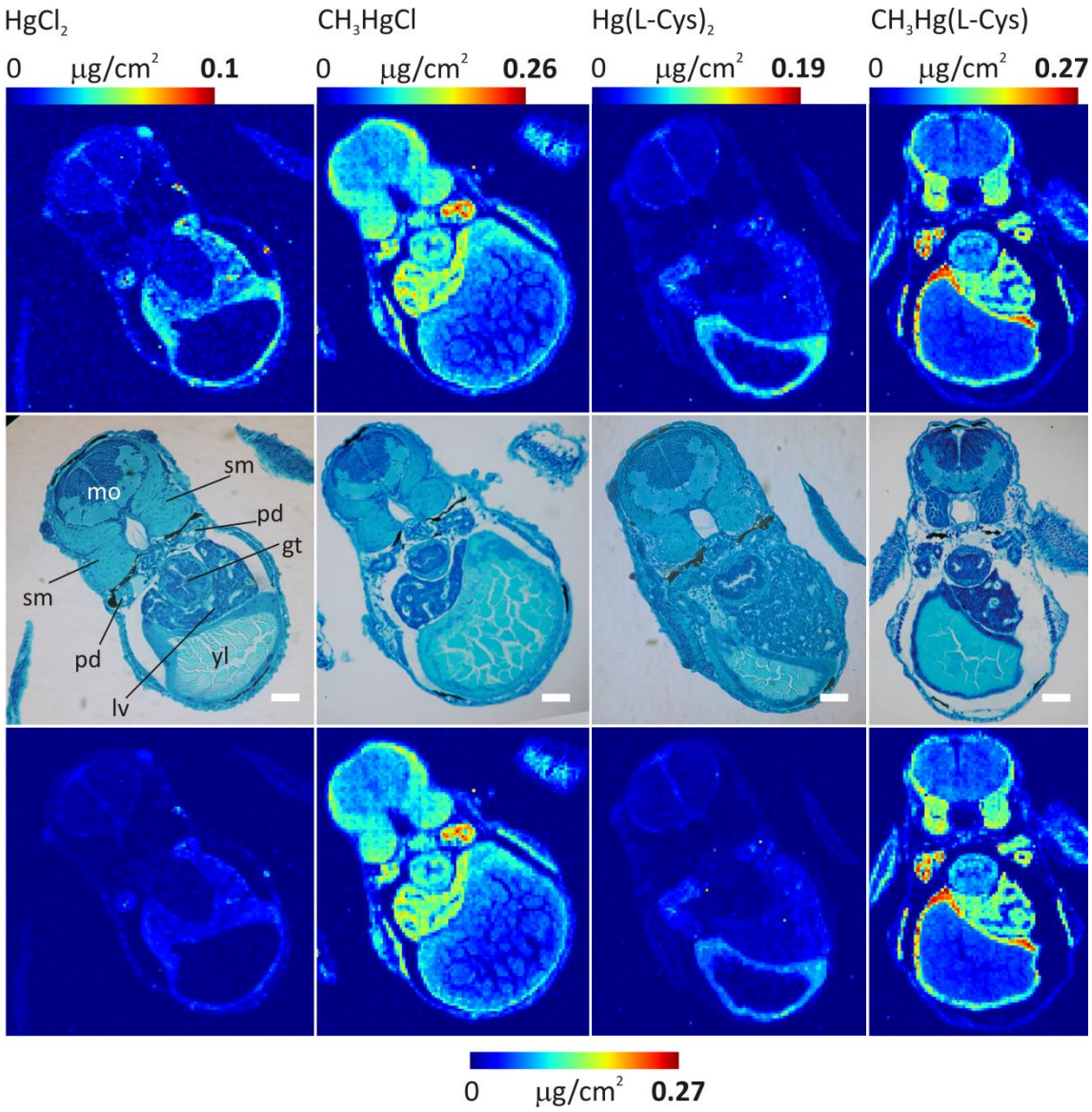

Figure 3.5 Quantitative mercury distributions in 5 dpf zebrafish larvae following a 36-hour exposure to 1 µM mercuric chloride $HgCl_2$, 1 µM methylmercury chloride CH_3HgCl, 200 µM mercuric bis-L-cysteineate $Hg(L\text{-}Cys)_2$, or 2 µM methylmercury L-cysteineate. The dominant mercury species in the treatment solutions are shown in Table 3.1. Histological images (middle panel) of the liver region are compared with the mercury distributions of the adjacent sections. The first row mercury maps are scaled separately to the highest level of mercury in each of the images, whereas the ones in the third row are scaled to the highest level of mercury among all four images. Scale bar 50 µm, *mo*-medulla oblongata, *sm*-somitic muscles, *pd*-pronephric duct, *gt*-gut, *lv*-liver, *yl*-yolk.

permeability across the cell membrane. If passive diffusion of a molecule was the sole uptake mechanism, then differences in cell membrane permeabilities might alone explain the observed differential uptake of inorganic and organic mercury species herein. To test this, we estimated the permeabilities P of dominant mercury species (>1% in Table 3.1) as (Stein and Lieb 1986)

$$(1)\ P = K_{ow} D_m / \lambda$$

where K_{ow} is the octanol−water partition coefficient, D_m is the diffusion coefficient across the cell membrane, and λ is the cell membrane thickness. D_m was estimated using the expression of Stein and Lieb (Stein and Lieb 1986), relating D_m to molecular volume V and two constants, D_0 and m_V, dependent upon the nature of the biological membrane (Stein and Lieb, 1986).

$$(2)\ \log D_m = \log D_0 - m_V V$$

Reliable effective molecular volumes V can be computed from three-dimensional structures (http://pubchem.ncbi.nlm.nih.gov/), and all such calculations herein were done using Accelrys Discovery Studio v3.0.0. We assumed that D_0 and m_V for zebrafish larvae approximate those for human erythrocytes, for which required data have already been reported. D_m values were calculated for 10 different nonelectrolyte species using eq 1 with published values of P and K_{ow} and assuming λ = 40 Å (Stein and Lieb, 1986). D_0 and m_V were then computed by linear regression of a plot of logD_m against V giving $D_0 = 3.6 \times 10^{-8}$ cm^2/s and $m_V = 0.0413$ Å^{-3}. These values of D_0 and m_V together with computed molecular volumes V of the various mercury species were then used in eq 2 to estimate diffusion coefficients for the these species (Table 3.2). Permeabilities P were then estimated using eq 1 and previously published K_{ow} values (Table 3.2).

The calculation of D_m and P parameters for the mercury species, though applicable specifically for the red blood cell membrane, provided an important insight into the molecular basis of the differential mercury uptake observed in this study. Mercuric bis-L-cysteineate, though more hydrophobic (higher K_{ow}) than most of the considered mercury species, had significantly decreased permeability due to its high molecular volume (Table 3.2). Its permeability was more than 10^4 times lower than that of the dominant hydroxide species (Table 3.2) thus offering a plausible explanation of its extremely low accumulation in zebrafish larvae. Despite the highest hydrophobicity among all studied forms (K_{ow} = 50), the passive diffusion of methylmercury L-cysteineate was also hindered by its much lower diffusion rate resulting in permeability similar to that of methylmercury hydroxide (Table 3.2).

Table 3.2 Estimated diffusion coefficients and membrane permeabilities for different mercury species[a]

Permeant	K_{ow} [b]	Molecular volume[c] (Å^3)	Diffusion coefficient D_m (x10^{-10} cm^2/s)	Permeability P (x10^{-4} cm/s)
$Hg(OH)_2$	0.05	47.9	3.78	0.47
HgClOH	1.2	55.6	1.82	5.45
CH_3HgOH	0.07	54.9	1.94	0.34
CH_3HgCl	1.7	63.0	0.90	3.8
$Hg(L\text{-}Cys)_2$	3.7	189.4	0.0000054	0.00005
$CH_3HgL\text{-}Cys$	50	124.7	0.0025	0.32

[a] All D_m and P values are estimated for the passive transport across the human red blood cell membrane

[b] See ref. Laporte et al. 2002

[c] Calculated by Accelrys Discovery Studio (v3.0.0) from the three-dimensional geometry-optimized energy-minimized density functional theory structures as the total van der Waals volume of all the atoms subtracted by the overlap volume of bonded atoms, and scaled to 95% .

On the basis of the permeability data alone, one would expect that, in absence of L-cysteine in the treatment solutions, the net rate of movement of inorganic mercury [90% $Hg(OH)_2$/9.5% HgOHCl] across the larval body (*e.g.*, through the gills, the skin, or the gastrointestinal tract) would be similar or even slightly greater (due to a higher fraction of more permeable HgClOH species in the solution) than for organic mercury [96% CH_3HgOH/3.3% CH_3HgCl] (Table 3.2). This in turn would result in similar (or even slightly higher) accumulation of inorganic mercury especially in the tissues directly in contact with the surrounding water (e.g., gut epithelium). However, in contrast to methylmercury-exposed larvae, no significant accumulation of inorganic mercury occurred in the gut of the inorganic mercury-exposed fish, and thus most likely a simple passive diffusion model of a compound across the lipid part of the cell membrane cannot fully explain the differential accumulation of inorganic and organic mercury observed in our study.

Since both Hg^{2+} and $[CH_3Hg]^+$ show high affinities for thiol groups (Webb, 1966), it is likely that upon entering the larval body in their original chemical form the hydroxide or chloride ligands are substituted by thiols. Hence, the likely form of mercury in tissues would be a thiolate-based one, predominantly L-cysteineate complexes, and as such distributed inside the fish body into the target cells. This may explain the observed consistency in the target organs between the chloride and the L-cysteine-based mercury treatment solutions. Significantly lower permeability of mercuric bis-L-cysteineate than methylmercury L-cysteineate may also provide a partial explanation for the generally lower mercury levels after mercuric mercury exposures in internal organs, such as liver, which are not in direct contact with the water (Figure 3.5). It is however clear that the preferential accumulation of extremely high levels of methylmercury in the lens epithelial cells (Figure 3.3) cannot be explained solely in terms of increased permeability of the thiol bound methylmercury *versus* its mercuric mercury counterpart. An active transport mechanism, which is yet to be determined, must be present.

Several potential methylmercury L-cysteineate transporters have been detected or postulated in various organs and cells (Bridges and Zalups, 2010), *e.g.*, system L (Na^+-independent large neutral amino acid transporter) in the blood-brain and blood-placenta barrier and system $B^{0,+}$ (Na^+-dependent neutral and cationic amino acid transporter) and OAT1 (organic anion transporter 1), respectively, in the luminal and basolateral membrane of the renal proximal tubular cells. Since methylmercury uptake by eye tissues has only recently been revealed

(Korbas et al., 2008; Korbas et al., 2010b), no data are available on possible mechanisms of its transport across cell membranes in this organ. However, the most likely candidate is system L, which is universally expressed in cells performing high protein synthesis such as the lens epithelium. Indeed, the presence of system L has been recently demonstrated both in mouse lens fiber cells (Bassnett et al., 2009) and in human retinal pigmented epithelial cells (Yamamoto et al., 2010).

Apart from the eye, organs for which a differential uptake of inorganic and organic mercury was most pronounced were the muscles and gut (Figure 3.5). Despite similar permeabilities between methylmercury and mercuric exposure species in absence of L-cysteine, mercury accumulated only in the gut and somitic muscles of the methylmercury-treated larvae. Moreover, the presence of L-cysteine did not affect that distribution, and only trace levels of mercury were detected in the gut and muscles of the mercury bis-L-cysteineate larvae (Figure 3.5). These results are consistent with previous observations of poorly absorbed inorganic mercury species in the gastrointestinal tract when compared with methylmercury species (Clarkson and Magos, 2006). Mechanisms of mercury uptake by the gut epithelium are not fully understood in either fish or mammals; however, both passive diffusion and active transport have been implied (Bridges and Zalups, 2010; Hoyle and Handy, 2005). The process of mercury uptake in the gut is additionally complicated by the presence of the mucosal microenvironment on the gut epithelial surface. It has been postulated that polyanionic ligands of mucus may interact with the inorganic mercury species in the gut lumen resulting in ligand exchange and transport modification across the mucosal membrane (Hoyle and Handy, 2005). Low inorganic mercury levels observed in the somitic muscles could result directly from low absorption by the gut epithelium and thus low uptake into the blood compartment.

Although mercury accumulation within the brain was not unexpected, different chemical forms displayed very different accumulation patterns. Methylmercury exposures led to generally diffuse, though high, accumulations of mercury. In contrast, inorganic mercury exposures affected only specific areas of the brain with mercury levels significantly lower than those for methylmercury (Figures 3.3 and 3.4). This is consistent with previous studies and the ability of methylmercury to cross the blood-brain barrier on the system L transporter (LAT1) as methylmercury L-cysteineate species.

The most pronounced difference in brain mercury distributions between the organic and inorganic mercury treatments was the preferential accumulation of inorganic mercury in the brain ventricular region (Figures 3.3, 3.4, and 3.5). The cerebrospinal fluid-filled ventricles of the brain as well as the central canal of the spinal cord are lined with the ependymal cells, which are the most likely target cells for the observed inorganic mercury deposition. Mercury deposits in the cytoplasm of these cells were observed previously in rats exposed to mercuric chloride in drinking water (Møller-Madsen and Danscher, 1986). The accumulation of mercury in ependymal cells suggests that these cells may act as a barrier to the transfer of inorganic mercury from cerebrospinal fluid (and thus the blood) to brain. Interestingly, it has been recently found that ependymal cells express high levels of selenoprotein P (Sel P) in human brain (Scharpf et al. 2007). Sel P is an abundant plasma glycoprotein with an unusually high content of selenocysteine and cysteine residues (up to 10 and 17, respectively). Sel P has a significant function in selenium homeostasis (Burk and Hill, 2005), in particular being implicated in selenium transport to brain (Hill et al., 2003). Its expression in zebrafish has recently been reported (Tujebajeva et al. 2000). Sel P appears to have a significant role in mercury sequestration. When mammals (rabbits or rats) are intravenously given equimolar solutions of sodium selenite and $HgCl_2$, the toxic effects of the mercury are relieved (Suzuki et al., 1998). Gailer et al. (2000) used synchrotron-based X-ray absorption spectroscopy to show that the molecular basis of this antagonism is the formation of nanoparticulate HgSe in blood plasma. The formation of such nanoparticles was previously suggested by Suzuki and co-workers (Suzuki et al., 1998), who estimated their approximate size as $(HgSe)_{100}$ and demonstrated that Sel P can sequester up to 35 of these nanoparticles (Suzuki et al., 1998). In light of the binding properties of Sel P, the formation of similar complexes in the ependymal cells is thus plausible.

Despite significant differences in brain mercury distribution between different mercury treatments, we discovered preferential accumulation of mercury in the epiphysis (pineal gland) of both the inorganic and organic mercury-treated larvae (Figure 3.3). Mercury deposits in the pineal gland have been observed in miners exposed to elemental mercury (Falnoga et al., 2000). The pineal gland lies outside the blood-brain barrier and therefore pinealocytes have free access to mercury in the bloodstream. The mechanism of mercury uptake by the pineal gland is not yet known. However, since pineal gland produces melatonin, a hormone affecting the modulation of wake/sleep patterns, the elevated mercury levels therein could be responsible for the sleep

disturbances observed in mercury-intoxicated individuals (Kobal and Grum, 2010). A protective effect of melatonin against methylmercury induced mortality (Kim et al., 2000) and mercuric chloride-induced oxidative damage (Sener et al., 2003) has been also reported.

Similarly to the pineal gland, all molecular forms of mercury led to accumulation in two types of sensory tissues. The olfactory epithelium (olfaction system) contains sensory hair cells responsible for detecting chemicals that elicit an olfactory response. The neuromasts of lateral line system (mechano-sensory system) comprise hair cells, organized into small bundles and distributed on the outside of the fish body, that detect pressure changes in water. The hair cells of both olfactory epithelium and neuromasts are in direct contact with contaminated water, and the presence of mercury is likely related to this fact. The levels of mercury accumulation in the olfactory epithelium reflected the estimated permeabilities of the different mercury species (Table 3.2), suggesting a prevalence of passive transport across the epithelial barrier. However, the same trend was not observed in the neuromasts. Despite similar permeabilities, inorganic mercury concentrations were on average half compared with their organic counterparts, suggesting involvement of an active carrier in the transport of methylmercury species across the cell membrane.

The uptake of inorganic and organic mercury species by the olfactory epithelium has been reported before in fish (de Oliveira Ribeiro et al., 2002). It has even been postulated that the olfactory pathway could be a route of entry for inorganic mercury species into the central nervous system (Henriksson and Tjälve, 1998). In contrast, there are no available data on mercury uptake by the lateral line system; however, the disruptive effects of other heavy metals on neuromasts have been reported (Froehlicher et al., 2009). Interestingly, the hair cells of the neuromasts are physiologically and microscopically very similar to mammalian inner ear hair cells and as such have been recently used to screen for drugs that prevent or cause hearing loss (Ou et al., 2010). It is thus likely that hearing problems reported previously in individuals intoxicated with mercury may be partially due to the accumulation of mercury in the inner ear hair cells. Further studies are clearly needed to confirm that.

In conclusion, synchrotron X-ray fluorescence imaging has revealed striking differences in the accumulation patterns of mercury in zebrafish larvae exposed to four different mercury formulations in water. Exposures to methylmercury species not only resulted in overall higher

mercury burdens but also targeted different cells and tissues, revealing a significant role of speciation in cellular and molecular targeting and sequestration.

CHAPTER 4. PHENYLTHIOUREA ALTERS TOXICITY OF MERCURY COMPOUNDS IN ZEBRAFISH LARVAE

4.1. Preface

Based on the findings in Chapter 3 regarding mercury accumulation in sensory cells, the next logical study aimed to study the effects of mercury on neuromasts in the lateral line of zebrafish. The compound N-phenylthiourea (PTU) is routinely used to block pigment formation in zebrafish embryos to improve visualization of fluorescent stains. Surprisingly, preliminary trials with PTU demonstrated significant alterations in mercury toxicity following the addition of PTU. This chapter focuses on understanding how and why PTU affects the toxicity of both inorganic and organometallic mercury. PTU was found to bind to mercuric chloride and to form large oligometric complexes that would not easily cross membranes and thus decrease the toxicity of mercuric chloride. Conversely, methylmercury chloride binds to PTU and forms a positively charged compound that would more easily be transported across cell membranes and consequently increase toxicity.

4.2. Manuscript Author Contributions

This chapter was published in the *Journal of Inorganic Biochemistry* and was reformatted to follow the guidelines for a manuscript style thesis.

MacDonald, T.C., Nehzati, S., Sylvain, N.J., James, A.K., Korbas, M., Caine, S., Pickering, I.J., George, G.N. and Krone, P.H. (2015b). Phenylthiourea alters toxicity of mercury compounds in zebrafish larvae. *J. Inorg. Biochem*., 151, 10-17.

T.C. MacDonald conducted fish trials with mercuric chloride, collected and analyzed XFI data, worked on statistical analysis, and drafted the manuscript.

S. Nehzati prepared solutions for EXAFS and analyzed the data, and conducted DFT calculations and molecular modeling.

N.J. Sylvain performed preliminary trials to determine the appropriate dose of PTU and assisted with exposures.

A.K. James conducted fish trials for organic mercury and helped collect XFI data.

M. Korbas conducted mortality and deformity fish trials for organic mercury.

S. Caine assisted with statistical analysis.

I.J. Pickering, G.N. George, and P.H. Krone provided scientific input and guidance, commented on and edited the manuscript, and provided funding for the research.

4.3. Acknowledgements

This research used resources of the Advanced Photon Source (APS), a U.S. Department of Energy (DOE) Office of Science User Facility operated for the DOE Office of Science by Argonne National Laboratory under Contract No. DE-AC02-06CH11357. Data for this chapter were collected from beamline 20-ID-B. Sector 20 facilities at the APS, and research at these facilities, are supported by the U.S. DOE, Office of Basic Energy Sciences (OBES), the Canadian Light Source and its funding partners, the University of Washington, and the APS.

4.4. Abstract

In recent years larval stage zebrafish have been emerging as a standard vertebrate model in a number of fields, ranging from developmental biology to pharmacology and toxicology. The tyrosinase inhibitor 1-phenyl-2-thiourea (PTU) is used very widely with larval zebrafish to generate essentially transparent organisms through inhibition of melanogenesis, which has enabled many elegant studies in areas ranging from neurological development to cancer research. Here we show that PTU can have dramatic synergistic and antagonistic effects on the chemical toxicology of different mercury compounds. Our results indicate that extreme caution should be used when employing PTU in toxicological studies, particularly when studying toxic metal ions.

4.5. Introduction

Zebrafish (*Danio rerio*) are fresh-water fish that have been extensively and increasingly used as an animal model in a variety of research areas over the past 30 years (Craig et al. 2006). Key characteristics that make the zebrafish an excellent model vertebrate system include nearly transparent embryos, rapid development outside the mother, large egg clutch, and a fully sequenced genome (Yang et al., 2009). As a model vertebrate system for studying the development of the embryo, researchers have used zebrafish to explore metal toxicity (Yang et al., 2009; Dave and Xiu, 1991; Blechinger et al., 2002; Korbas et al., 2008; Korbas et al., 2010b; Korbas et al., 2012; Korbas et al., 2013) as well as various human diseases (Craig et al., 2006; Kari et al., 2007).

In developmental biology research, zebrafish embryos and larvae offer a particular advantage over other model systems in that they are nearly transparent. Transparency and development outside the mother have allowed researchers to create a well-characterized staging series from fertilized embryo to hatched larva (Yang et al., 2009). Many techniques involve viewing fluorescent stains, probes or proteins using optical microscopy (Karlsson et al., 2001) which can be hindered by natural pigmentation in the fish as they age. Zebrafish develop black melanophores, yellow xanthophores and reflective iridophores (Rawls et al., 2001). One commonly used technique for inhibiting natural pigmentation is the inhibition of tyrosinase activity (Thanigaimalai et al., 2011) by exposing embryos to 1-phenyl-2-thiourea (PTU) (Figure 4.1) which inhibits melanogenesis in the melanophores (Karlsson et al., 2001; Whittaker, 1966). Additionally, normal pigmentation is restored in zebrafish following PTU treatment after a two week recovery period in water with no exogenous agents such as PTU (Karlsson et al., 2001).

When the PTU pigment blocking process was initially developed, no significant effects on hatching or survival were noted when a dose of 75 μM PTU was used (Karlsson et al., 2001). However, concentrations of 200 μM PTU are frequently used (Parker et al. 2013), with such

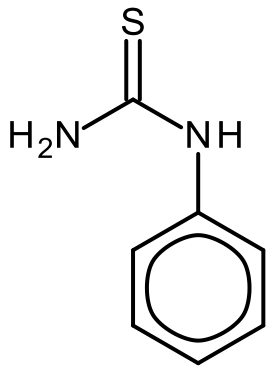

Figure 4.1 Schematic structure of the tyrosinase inhibitor 1-phenyl-2-thiourea (PTU).

concentrations considered standard protocols (Westerfield, 1995). Recently, evidence has been emerging that commonly used doses of PTU may not be as benign as previously had been assumed (Elsalini and Rohr, 2003; Bohnsack et al., 2011; Li et al., 2012). Elsalini and Rohr (2003) found that PTU can interfere with thyroid hormone production and thus may alter normal development after 60 hours post fertilization. PTU also has been reported to affect extraocular muscle development and neural crest development (Bohnsack et al., 2011). Its use has also been seen to result in reduced body size and specifically in smaller eye lenses and more tightly packed eye cells (Li et al., 2012). To date, however, and despite the widespread use of zebrafish, the effects of PTU on the toxicity of exogenous chemical entities have not been studied. In the course of conventional microscopy studies of the effects of mercury compounds on the mechano-sensory apparatus of the zebrafish, we uncovered dramatic changes in toxicology when PTU was used to generate transparent fish. We present herein a study of the effects of PTU in combination with different mercury compounds on larval stage zebrafish and show that PTU substantially perturbs these systems in ways that are totally different for inorganic mercury (Hg^{2+}) species and methylmercury species.

4.6. Materials and Methods

4.6.1. Chemicals

Phenylthiourea (PTU) and mercuric chloride were purchased from Sigma Aldrich (Oakville, ON) and methylmercury hydroxide from Strem Chemicals Inc. (Newburyport, MA). A 1000 ppm (3.98 mM) methylmercury chloride solution was obtained from Alfa Aesar (Ward Hill, MA).

4.6.2. Zebrafish

All procedures were approved by the University of Saskatchewan Ethics Board. Adult zebrafish (*Danio rerio*) were mated using the marble technique (Westerfield, 1995). Embryos were collected and raised to 22 hours post fertilization (hpf) in system water in a 28 °C incubator with a 14:10 hour light: dark cycle.

4.6.3. Statistical Analysis

For comparisons involving deformity and death rates, significance was determined using ANOVA with a Tukey's post-hoc pairwise test to compare treatments within each day. A Student's *t*-test was used to compare Hg values in the livers of fish imaged using XFI. For all statistical analyses a *P*-value <0.05 was considered to be significant.

4.6.4. X-ray Fluorescence Imaging Sample Preparation

Half of the zebrafish were raised in 100 µM PTU until 3 days post fertilization (dpf) while the second half were raised to 3 dpf in system water. All zebrafish were then randomly divided into the following treatment groups: control, 100 µM PTU, both 2 and 4 µM $HgCl_2$ in the presence or absence of PTU, both 0.2 and 0.5 µM CH_3HgCl in the presence or absence of PTU. These doses were selected to represent a high mercury exposure; however, the number of deaths in the 0.5 µM CH_3HgCl group prohibited collection of any samples. The dose 0.2 µM CH_3HgCl was selected because fish in the 0.1 µM CH_3HgCl were found to have few deformities and no deaths. After a 48 hour exposure all fish were rinsed 3 times in fresh system water to remove excess mercury on the surface of the fish. Zebrafish were fixed, embedded and sectioned as previously described (Korbas et al., 2012).

4.6.5. X-ray Fluorescence Imaging (XFI)

XFI data were collected at the Advanced Photon Source (APS) in Argonne, IL, USA on beamline 20-ID-B. The storage ring was operating in continuous top-up mode at 102 mA and 7.0 GeV. An incident X-ray energy of 13.45 keV was selected to avoid the Br K edge while being able to monitor the Hg $L\alpha_{1,2}$ and Zn Kα fluorescence lines. A Si(111) double crystal monochromator and Rh-coated mirrors were used for focusing and harmonic rejection. Samples were mounted at 45° to the incident X-ray beam and raster scanned, with a silicon-drift Vortex detector at 90° to the incident X-ray beam (Pushie et al., 2014). Kirkpatrick-Baez Rh-coated focusing mirrors were used to generate a micro-focused beam of 5 µm diameter. Samples were raster scanned using a step size of 5 µm with a beam exposure time of 0.6 s per point.

4.6.6. X-ray Fluorescence Imaging Data Analysis

Data collected from X-ray fluorescence imaging were processed as previously described (Korbas et al., 2012), with normalization to the incoming beam intensity and removal of background signal by averaging the intensity per element in the area outside of the tissue then subtracting this amount from each pixel in the entire image. Certified highly-uniform thin film standards mounted on 6.3 µm Mylar substrates for zinc, gold, and thallium were obtained from Micromatter Co. (Vancouver, BC). To quantify the amount of zinc per pixel, the zinc standard was imaged, normalized and background subtracted using a blank foil. Because mercury amalgam standards slowly decrease in mercury content over time, mercury was quantified using gold and thallium standards, as they are adjacent to mercury on the periodic table. These standards were imaged, normalized and background subtracted. Linear interpolation was then used to estimate a calibration for the mercury intensity for quantification of the mercury in the zebrafish sections. This method was verified by measurement of a new mercury-silver amalgam standard foil (Micromatter Co., Vancouver, BC). This worked only with a fresh mercury-amalgam standard as the mercury reading was found to decrease on storage, presumably due to loss of mercury as vapour.

Due to time constraints associated with limited allocations of beamtime and long acquisition time (an average of 3.5 h per sample), only a limited number of samples can be run. Therefore 3 representative zebrafish were selected for each treatment group for synchrotron imaging. Following the quantification of mercury in each sample, significant differences were evaluated with a Student's *t*-test on the amount of mercury (in $\mu g/cm^2$) in the livers of each treatment group.

4.6.7. X-ray Absorption Spectroscopy

Samples for X-ray absorption spectroscopy (XAS) were prepared at 10:1 mM PTU: Hg stoichiometries in aqueous solution (using CH_3HgOH or $HgCl_2$). Solution mixtures were incubated for 5 minutes at room temperature then were loaded into 2 mm × 3 mm × 22 mm acrylic cuvettes and were flash frozen in a slurry of liquid nitrogen-cooled isopentane.

Mercury L_{III}-edge spectra was measured on the structural molecular biology beamline 7-3 at the Stanford Synchrotron Radiation Lightsource (SSRL) with the SPEAR storage ring operating at 3.0-GeV with a current of 500 mA. The beamline was equipped with a Si(220)

double-crystal monochromator with harmonic rejection achieved by setting the cut-off energy of an upstream Rh-coated mirror to 15 keV. Incident X-ray intensities were monitored using a nitrogen-filled gas ionization chamber and X-ray absorption of samples was measured as the X-ray fluorescence excitation spectrum using a 30-element germanium detector array (Cramer et al., 1988). Soller slits and Ga_2O_3 X-ray filters were used to attenuate unwanted scattered radiation and to preserve detector linearity. Samples were placed in a liquid helium cryostat to maintain an approximate temperature of 10 K during data collection. Simultaneous absorption of a downstream standard Hg-Sn amalgam metal foil was measured by transmittance. Incident X-ray energy calibration was accomplished using the lowest energy Hg L_{III} inflection point of the standard foil, assumed to be 12,285.0 eV. Each sample was subjected to eight sweeps approximately 22 minutes long.

Extended X-ray absorption fine structure (EXAFS) oscillations $\chi(k)$ were analyzed using the EXAFSPAK program suite (George, 2000), as previously described (George et al., 1996) and assuming a Hg L_{III} threshold energy (E_0) of 12,305.0 eV. Phase-correction of Fourier transforms employed Hg—S backscattering. FEFF version 7 was utilized to compute theoretical phase and amplitude functions.

4.6.8. Density Functional Theory (DFT)

DFT calculations used the program $Dmol^3$ and Biovia Accelrys Materials Studio V7.0 for geometry optimization (Delley, 1990; Delley, 2000). Geometry optimization used the Perdew-Burke-Ernzerhof functionals (Perdew et al., 1996) for both the potential during the self-consistent field procedure and the energy, and employing an all-electron relativistic core treatment. Solvent effects were simulated by using the Conductor-like Screening Model (COSMO) with a dielectric value representing water ($\varepsilon = 78.39$; Klamt and Schüürmann, 1993).

4.7. Results and Discussion

4.7.1. Toxicological Profiles

Prior to examining the effects of mercury, range-finding studies were conducted to determine the PTU dose that combined the best pigment inhibition with the lowest rate of adverse effects. Treatment groups were 0 (control), 25, 50, 75, 100, 200 and 300 µM PTU, each

with 75 larvae at 22 h post fertilization (hpf). Consistent with normal practice, this time was chosen as zebrafish pigment formation begins at ~24 hpf, with rapid progression thereafter (Karlsson et al., 2001) and to inhibit the pigment formation larvae must be exposed to PTU before this stage (Karlsson et al., 2001). Survival, hatch, deformity and transparency rates were assessed from 1 to 5 days post fertilization. Preliminary trials found that a dose of 100 μM PTU resulted in lower death rates and fewer deformities than the more commonly used higher dose of 200 μM PTU, but with comparable suppression of pigment formation. Therefore, 100 μM PTU was used in all subsequent work. Two different categories of mercury compound were tested (mercuric chloride and methylmercury chloride), based on the differential toxicology previously reported (Korbas et al., 2012). In these previous studies, the highest mercury concentrations in zebrafish exposed to mercuric chloride were found in the olfactory epithelial cells (Korbas et al., 2012). In contrast, methylmercury chloride preferentially targeted the developing lens (Korbas et al., 2008; Korbas et al., 2010b; Korbas et al., 2012; Korbas et al., 2013). While zebrafish exposed to mercuric chloride accumulated mercury in the ventricular region of the brain, zebrafish exposed to methylmercury chloride accumulated mercury in the muscle tissue (Korbas et al., 2012). As one would expect, mercury accumulated in the detoxification organs, the pronephros and liver, following exposure to both forms of mercury (Korbas et al., 2012).

Zebrafish were raised to 3 dpf in either system water or in 100 μM PTU solution. Treatment solutions were replaced with fresh solution every 24 h. Fish were examined for deformities and deaths after 24, 48 and 72 h following initial exposure, with deformities being defined as fin malformations, edema, and moribund behaviour. The results of toxicological screening with mercuric chloride and methylmercury chloride are shown in Figures 4.2 and 4.3, respectively.

At 3 dpf, zebrafish larvae were exposed to 0 (control), 2 and 4 μM $HgCl_2$ in system water in the presence and absence of 100 μM PTU (n = 100 larvae per treatment). Two-way analysis of variance (ANOVA) was utilized to determine whether statistically significant differences existed for cumulative mortality between $HgCl_2$ and PTU + $HgCl_2$ treatment groups at 24, 48, and 72 h post-exposure. The PTU + $HgCl_2$ treatment group showed very significant decreases in mortalities compared to $HgCl_2$ alone (Figure 4.2), with all P values being $<10^{-3}$ or lower (see supplementary material Table S4.1). Although at first sight the data seem to suggest that there may be more deformities in the fish exposed to both $HgCl_2$ and PTU when compared to $HgCl_2$

alone, this is actually due to the fact that there are significantly more dead larvae in the latter case (Figure 4.2). Hence, the data indicate that PTU reduces the toxicity of $HgCl_2$.

Methylmercury species can be considerably more toxic than inorganic mercury compounds (Korbas et al., 2012) and can also have a very steep dose-response curve. To account for this, correspondingly lower levels of methylmercury chloride (CH_3HgCl) were used: 0.05, 0.1 and 0.5 μM CH_3HgCl in system water, in the presence and absence of 100 μM PTU. In contrast to $HgCl_2$, which had decreased toxicity in the presence of PTU, CH_3HgCl showed enhanced toxicity in the presence of PTU (Figure 4.3). While the trends were not as striking as for mercuric chloride, the increase in deaths of fish exposed to 0.5 μM CH_3HgCl + 100 μM PTU, was statistically significant at 48 and 72 h post-exposure compared to fish exposed to 0.5 μM CH_3HgCl in absence of PTU, with $P < 0.0001$ for both (see supplementary material Table S4.2). The small differences between control and 100 μM PTU in Figs. 4.2 and 4.3 are primarily a reflection of the fact that the tests for Figs. 4.2 and 4.3 were done at different times. Such variations are not uncommon and are not considered statistically significant.

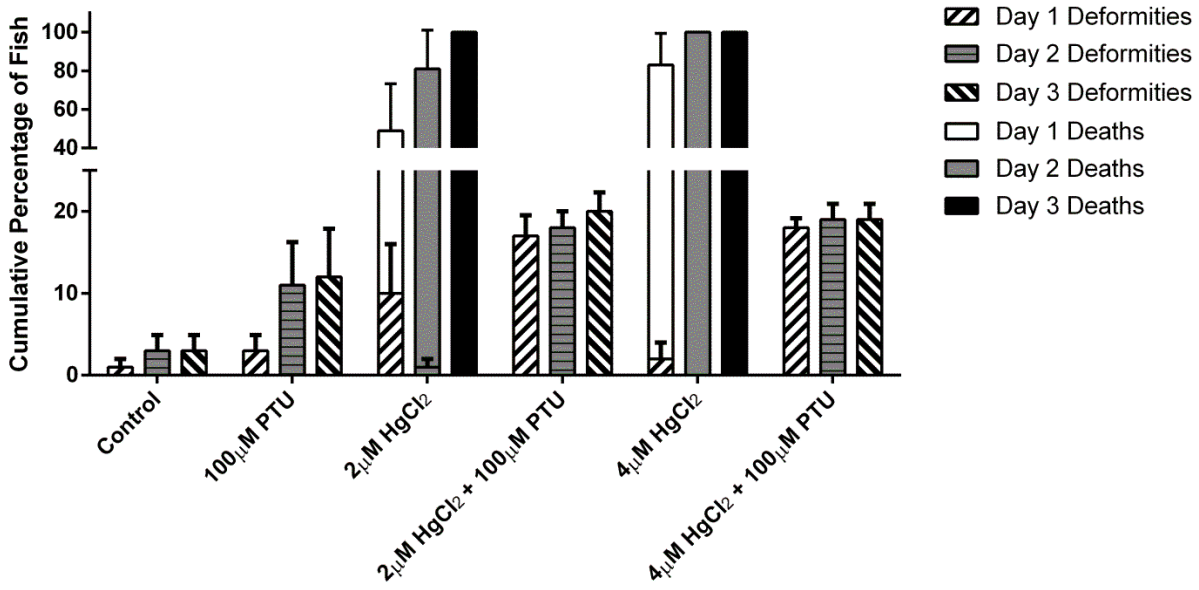

Figure 4.2 Cumulative mortality (%) stacked on top of cumulative deformity (%) (+ SE) of zebrafish larvae over 3 days of exposure to various $HgCl_2$ treatments, with and without PTU. Note the absence of deaths following PTU addition, showing that PTU *decreases* the toxicity of $HgCl_2$. The control was system water from the fish facility.

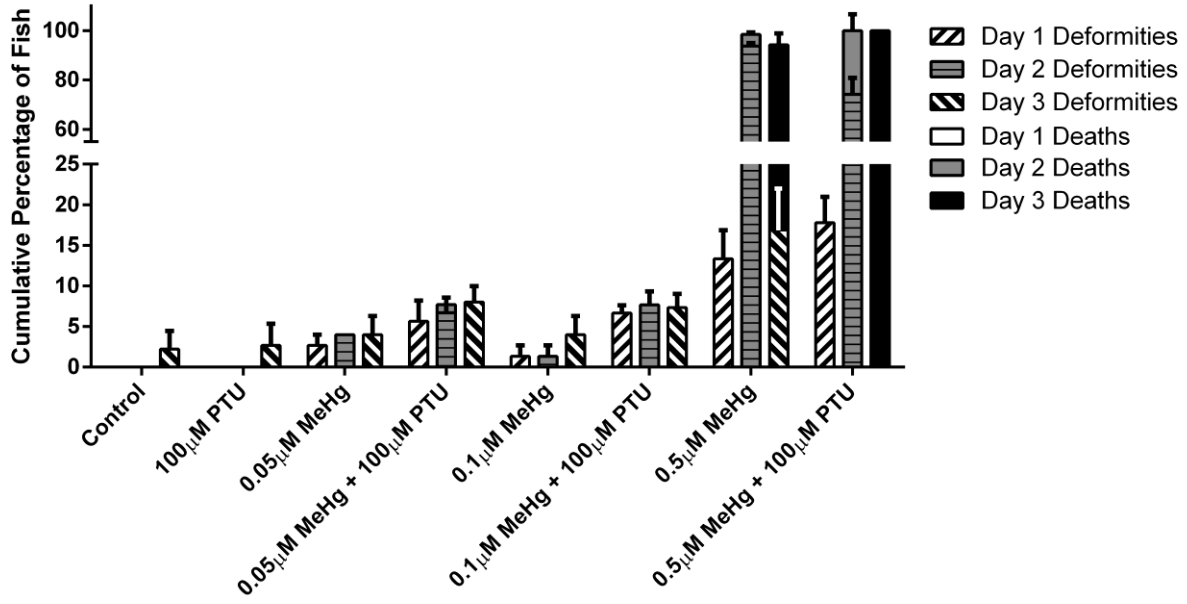

Figure 4.3 Cumulative mortality (%, blue) stacked on top of cumulative deformity (%, red) (+SE) of zebrafish larvae over 3 days of exposure to various CH_3HgCl (MeHg) treatments with and without PTU. The control was system water from the fish facility.

4.7.2. X-ray Fluorescence Imaging (XFI)

XFI (Pushie et al., 2014) was used to map Hg accumulation in representative fish from each treatment group and to quantify Hg in regions of interest. The results are shown in Figures 4.4-4.7, together with the corresponding histological images. Zinc, which is mapped simultaneously with mercury, is also shown for all sections; it is common practice to use the Zn image to ensure that the correct region is scanned (Korbas et al., 2012). Zinc is normally abundant in essentially all tissues but is present at notably high levels in pigment cells of zebrafish. Because PTU blocks pigment formation in the zebrafish, pigment levels in PTU treated fish were low and as expected, zinc levels were often correspondingly lower.

Figures 4.4-4.5 show sections from zebrafish treated with $HgCl_2$ solutions in the absence and presence of PTU. The olfactory pits have previously been shown to be a target organ for $HgCl_2$ (Korbas et al., 2012); Figure 4.4 shows XFI of sections of this region. The comparative absence of mercury in the PTU-exposed larva is striking and is consistent with the protective effect of PTU observed in the toxicological profile. Figure 4.5 shows XFI of sections through the liver, gut, muscle, and pronephros. Here, the pigment spots in the absence of PTU treatment are observed to be larger and to have higher zinc levels (Figure 4.5A & 4.5C) than the pigmented areas in the presence of PTU treatment (Figure 4.5B & 4.5D). As with olfactory pits in Figure 4.4, the levels of mercury in the trunk region are substantially lower in PTU exposed fish, relative to fish exposed to $HgCl_2$ alone. Mercury concentrations in the livers of three separate fish from the 48-hour 4 μM exposure group were quantified and averaged. A Student's two-tailed *t*-test determined the mean mercury concentrations to be significantly greater in the $HgCl_2$ treatment compared to the PTU + $HgCl_2$ treatment with $P < 0.001$ for all, and the mercury concentrations in the fish treated with solutions of PTU + $HgCl_2$ were 60-fold lower than in fish exposed to $HgCl_2$ solutions alone.

Figure 4.6 shows zebrafish head sections from larvae exposed to 0.2 μM CH_3HgCl in absence and presence of PTU. Cells in the lens and retina are known to be primary targets of methylmercury compounds (Korbas et al., 2008; Korbas et al., 2010b; Korbas et al., 2012; Korbas et al., 2013). The differences in pigment levels in the retinal pigmented epithelia in the optical micrographs can be clearly seen as a loss of black coloration in Figure 4.6B compared with Figure 4.6A, and this is paralleled by the decrease in Zn levels in those regions (Figure 4.6D compared with Figure 4.6C). Figure 4.7 shows XFI of the trunk region for the CH_3HgCl

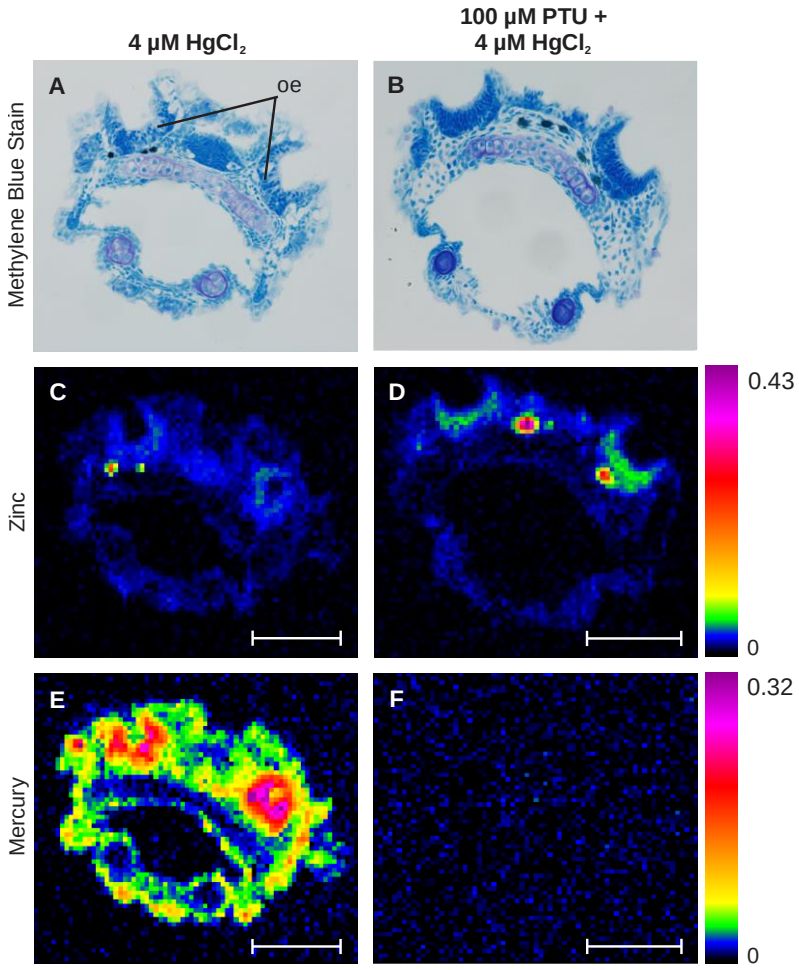

Figure 4.4 Transverse sections through the olfactory region of zebrafish treated with 4 µM $HgCl_2$ in absence (A, C and E) or presence (B, D and F) of 100 µM PTU. In each column the section stained with methylene blue for the optical image (A or B) was serial (immediately adjacent) to the unstained section used for X-ray fluorescence imaging of zinc (C or D) and mercury (E or F). White scale bars represent 100 µm. The colour bars show the quantification of zinc (C, D) and mercury (E, F) in µg/cm^2. oe= olfactory epithelium.

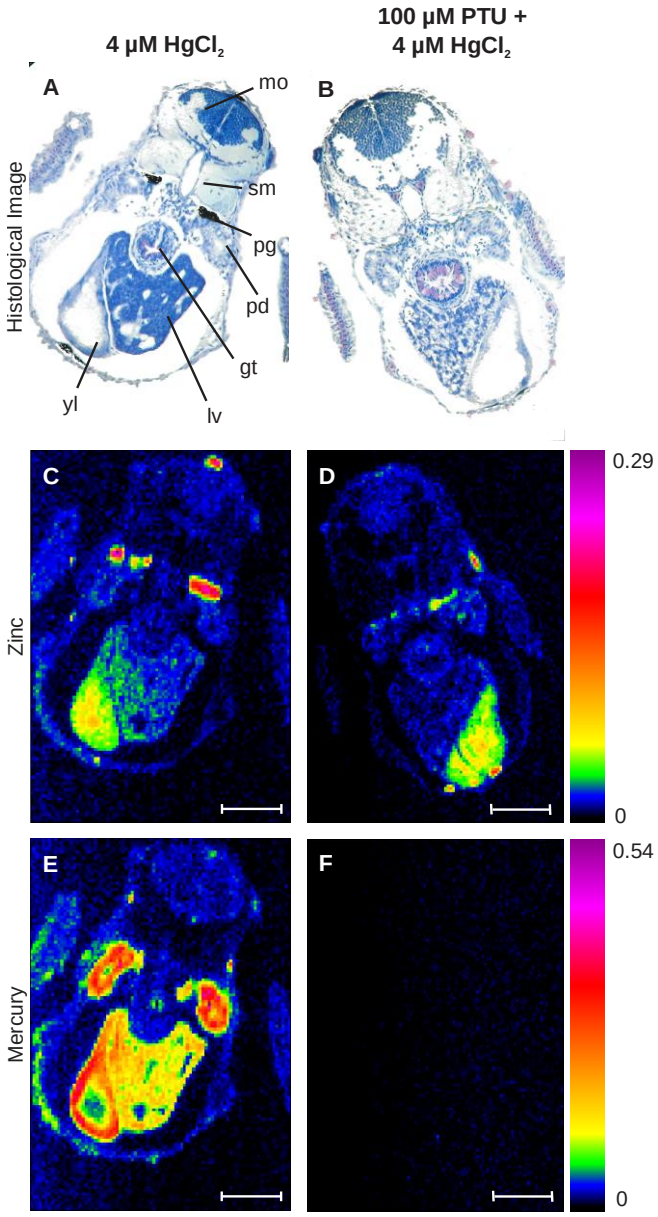

Figure 4.5 Transverse sections through the trunk region of zebrafish treated with 4 µM $HgCl_2$ in absence (A, C and E) or presence (B, D and F) of 100 µM PTU. White scale bars represent 100 µm. mo= medulla oblongata, sm= somitic muscle, pd= pronephric duct, gt= gut tube, lv= liver, yl= yolk. Additional details as for Figure 4.4.

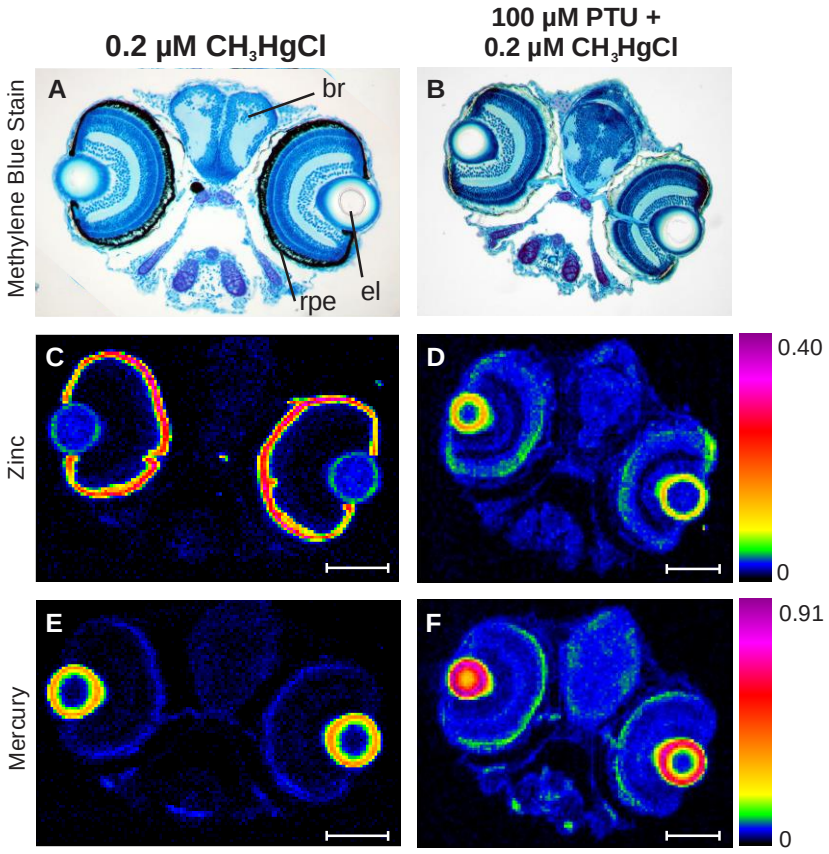

Figure 4.6 Transverse sections through the eye region of zebrafish treated with 0.2 µM CH_3HgCl in absence (A, C and E) or presence (B, D and F) of 100 µM PTU. White scale bars represent 100 µm. br= brain, el= eye lens, rpe= retinal pigmented epithelium. Additional details as for Figure 4.4.

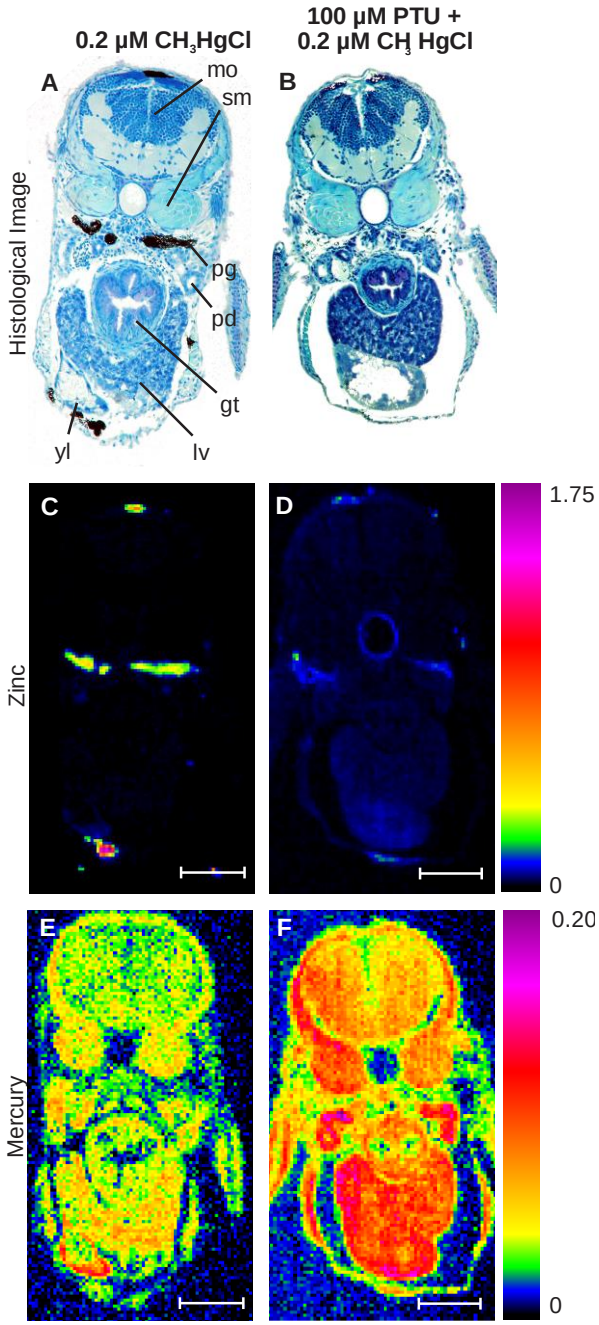

Figure 4.7 Transverse sections through the trunk region of zebrafish treated with 0.2 µM CH_3HgCl in absence (A, C and E) or presence (B, D and F) of 100 µM PTU. White scale bars represent 100 µm. mo= medulla oblongata, sm= somitic muscle, pd= pronephric duct, gt= gut tube, lv= liver, yl= yolk. Additional details as for Figure 4.4.

exposures; here also lower Zn levels in discrete regions that are normally pigmented are seen in the PTU-treated fish. In marked contrast to the $HgCl_2$ data, both head and trunk sections of the larvae treated with CH_3HgCl and PTU are visually higher in Hg than those treated with CH_3HgCl alone. This again is consistent with the increase in CH_3HgCl toxicity observed in PTU treated fish. Similar to the $HgCl_2$ treatment, a two-tailed Student's *t*-test with equal variance was conducted on average mercury levels in each liver of three fish per treatment group and showed $P < 0.05$. Zebrafish exposed to CH_3HgCl and PTU had approximately two fold higher mercury levels than those exposed to CH_3HgCl only.

The XFI results together with the observations of deformity and mortality show that PTU has opposite effects on the toxicology of the two different chemical forms of mercury, being antagonistic for inorganic mercury and synergistic with methylmercury. This suggests not only that PTU is interacting chemically with the mercury species, but also that it interacts differently with the two types of mercury species. We therefore investigated the possible solution chemistry of PTU and the mercury species using X-ray absorption spectroscopy and density functional theory (DFT).

4.7.3. Extended X-ray Absorption Fine Structure (EXAFS) and Density Functional Theory (DFT)

We examined the EXAFS portion of the X-ray absorption spectrum, which can be used with quantitative analysis to obtain a radial structure (Cotelesage et al., 2012). EXAFS spectra of methylmercury and inorganic mercury in the presence of PTU, together with the associated Fourier transforms, are shown in Figure 4.8. The results of EXAFS curve-fitting analysis are also shown in Figure 4.8, with the derived structural parameters summarized in Table 4.1. Because EXAFS currently lacks the sensitivity to the micromolar levels used in the zebrafish exposures, we employed higher concentrations of both Hg and PTU, but maintaining an excess of PTU as in the fish exposures. In the case of methylmercury we used methylmercury hydroxide (CH_3HgOH) rather than the chloride because methylmercury chloride was insufficiently soluble; this species will in any case be the dominant form in dilute solution when the chloride is used (Korbas et al., 2012). Mercury typically forms compounds with either two-coordinate linear digonal coordination, three-coordinate trigonal planar coordination, or four-coordinate pseudo tetrahedral coordination (George et al., 2008a). The bond-lengths to Hg change systematically with

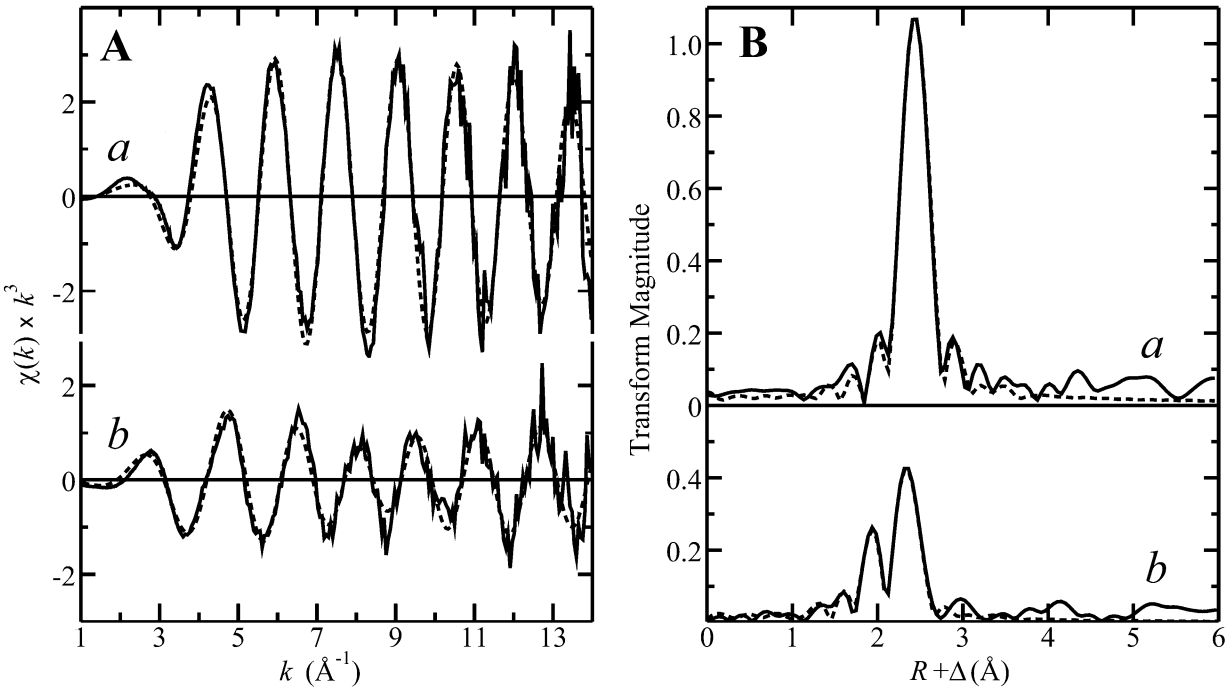

Figure 4.8 Mercury LIII-edge extended X-ray absorption fine structure (EXAFS) for phenylthiourea complexes with $HgCl_2$ and MeHgOH at a stoichiometry of 10:1. **Left:** the EXAFS oscillations. **Right:** corresponding Fourier transform phase-corrected for Hg—S backscattering. Experimental data are shown as solid lines, with the results from curve-fitting analyses (parameters from Table 4.1) shown as broken lines.

Table 4.1 Extended X-ray absorption fine structure (EXAFS) parameters[a] and curve-fitting results of phenylthiourea with mercury compounds at stoichiometry of 10:1.

aqueous complex	bond	N	R	σ2	ΔE0	F
PTU: MeHgOH	Hg-C	1	2.063(3)	0.0025(3)	-15.0(5)	0.3785
	Hg-S	1	2.374(2)	0.0038(2)		
PTU: $HgCl_2$	Hg-N	2	2.430(2)	0.0026(3)	-10.3(3)	0.2497
	Hg-S	2	2.493(1)	0.0030(1)		

a. Coordination number *N*, interatomic distances *R* (Å), Debye-Waller factors σ^2 (Å^2), and threshold energy shift ΔE_0 (eV). Values in parentheses represent the standard uncertainties between the curve fitting parameters and spectroscopy data. Goodness of fit function *F* is defined as $[\Sigma k^6(\chi(k)_{calc} - \chi(k)_{expt})^2/\Sigma k^6\chi(k)^2_{expt}]^{½}$, where $\chi(k)_{calc}$ and $\chi(k)_{expt}$ are the calculated and experimental EXAFS, respectively, with *k* being the photoelectron wavevector.

coordination type; for example for Hg—S coordination environments, two, three and four coordinate species have bond lengths of 2.35, 2.46 and 2.54 Å, respectively (Allen 2002).

The EXAFS of PTU with inorganic Hg^{2+} indicated a 4-coordinate complex, with 2 Hg—S donors at 2.49 Å and 2 Hg—N or Hg—O at 2.43 Å (Figure 4.8, Table 4.1). In support of this examination of the Cambridge Structural Database (CSD; Allen, 2002) shows a marked predominance of four-coordinate Hg^{2+} compounds when coordination with thione (C=S) sulfur donors is present, with 190 database hits for 4-coordinate species, 5 hits for 3-coordinate species, and only 3 hits for 2-coordinate species. Although EXAFS cannot normally distinguish between Hg—O and Hg—N due to the similarity in ligand atomic number, the bond-lengths of four-coordinate Hg^{2+} species in CSD strongly support the assignment of an Hg—N coordination. Thus, while the average bond-length for four-coordinate species containing Hg—O bonds is 2.61 Å, that for four-coordinate species containing Hg—N bonds is 2.42 Å, which is in good agreement with our EXAFS-derived bond-length of 2.43 Å. Similarly, while there are no examples in the CSD of Hg^{2+} bound by two thione ligands with two additional nitrogen donors, the average Hg—S bond-length for thione-coordinate species is 2.52 Å (Allen, 2002), also in good agreement with our EXAFS derived Hg—S bond-length of 2.49 Å.

The thiourea moiety in PTU contains amide and thione groups, both of which potentially can coordinate mercury. DFT calculations indicate that monomercury four-coordinate species with two PTU bound to one Hg^{2+} each as a bi-functional chelator through both –NH and =S (Figure 4.9A) will be unstable, because the bite angle of the (N–C=S) moiety is too acute to accommodate the Hg and DFT geometry optimizations yield two-coordinate species with Hg coordinated only through the thione sulfurs of the two PTU ligands. Coordination of a single Hg^{2+} by four PTU ligands is possible, with two PTUs bound through their thione sulfurs, and two PTUs contributing bound through their amide nitrogens. However, DFT indicates that such 4-coordinate S_2N_2 mononuclear entities are energetically unfavorable relative to the S_4 complex in which four thione sulfurs are bound, by some 40 kJ/mol. Thus, in order to explain the four-coordinate model with mixed N and S donors to Hg^{2+}, we need to postulate the formation of a polymeric entity in solution. While there are no crystal structures of polymeric or oligomeric thiourea or phenylthiourea Hg^{2+} structures, examples do exist of polymeric Cd^{2+} structures containing bridging thione ligands derived from phenylthiourea (Yang et al., 2001). Furthermore, while the samples of Figure 4.8 were all solutions made by slow addition with stirring of Hg^{2+} to

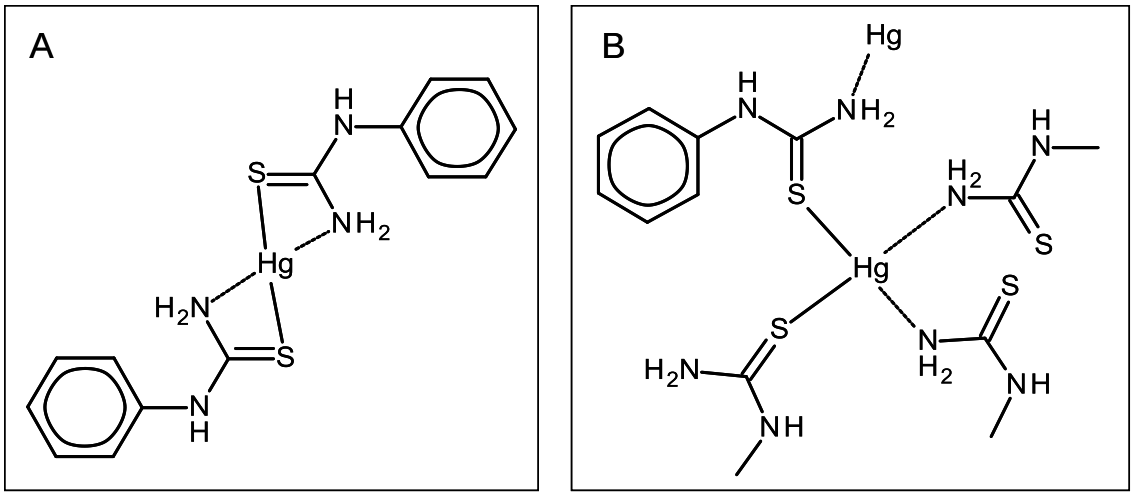

Figure 4.9 Schematic structures of four-coordinate complexes involving PTU and Hg^{2+}. (A) Hg^{2+} coordinated by two bidentate PTU ligands. As discussed in the text, density functional theory calculations indicate that A is unstable. (B) Fragment of one possible oligomeric species. See the discussion in the text for additional details.

PTU solutions, it was observed that simple mixing of PTU with Hg^{2+} in solution created an amorphous precipitate, strongly suggesting the formation of some kind of polymer. A schematic fragment of one example of the very large number of possible structures for such oligomeric or polymeric species is shown in Figure 4.9B. With our postulated N_2S_2 coordination, the nitrogen donors can be either protonated or deprotonated, corresponding to cationic or neutral oligomers, respectively. DFT calculations indicate expected Hg—N bond-lengths of protonated nitrogen donors (Hg ←:NH_2—C) to be 2.47 Å, some 0.25Å longer than the bond-length of a deprotonated nitrogen donor (Hg—NH—C) and a good match for the EXAFS derived bond-length of 2.43 Å, arguing for protonated nitrogen donors and thus a cationic oligomer. We consider the nitrogen coordinated by the phenyl group a less likely metal ligand than the amino nitrogen due to crowding by the phenyl ring. The energy minimized geometry optimized structure of one possible oligomeric fragment is shown in Figure 4.10A. Both Hg—S and Hg—N bond lengths of 2.55 and 2.47 Å, respectively, agree well with the EXAFS-derived values of 2.53 and 2.43 Å. A number of different coordination environments might be considered plausible, including S_4, N_1S_3, N_2S_2, N_3S_1 and possibly even N_4, which might combine to give an overall average coordination of N_2S_2. However, each of the above coordination environments will have significantly different and characteristic Hg—N and Hg—S bond-lengths, so that a distribution in coordination environments would inevitably result in a spread of Hg—N and Hg—S bond-lengths. This in turn would substantially increase the Debye-Waller factor of the EXAFS (Cotelesage et al., 2012). This is quantified by σ^2, the mean square deviation from the average bond-length *R* (Table 4.1). The σ^2 value has both static and vibrational components such that $\sigma^2 = \sigma^2_{vib} + \sigma^2_{stat}$ where σ^2_{vib} is the vibrational component and σ^2_{stat} is the static component resulting from heterogeneity of the individual bond-lengths *R* which is not directly resolved in the EXAFS (Cotelesage et al., 2012). Because the values obtained for σ^2 (Table 4.1) are close to the expected σ^2_{vib} values (Cotelesage et al., 2012) the aforementioned heterogeneity cannot be very pronounced, and we conclude that the bulk of the Hg is actually bound with N_2S_2 coordination. The observed lack of distinct mercury-mercury interactions in the EXAFS (Figure 4.8) means that well-defined relatively rigid bridged structures, such as rhombs with two Hg separated by bridging sulfurs and/or nitrogens, cannot be uniformly present. Investigation of this possibility with DFT indicates that such structures tend to be sterically crowded in any case because of phenyl groups on the PTU ligands.

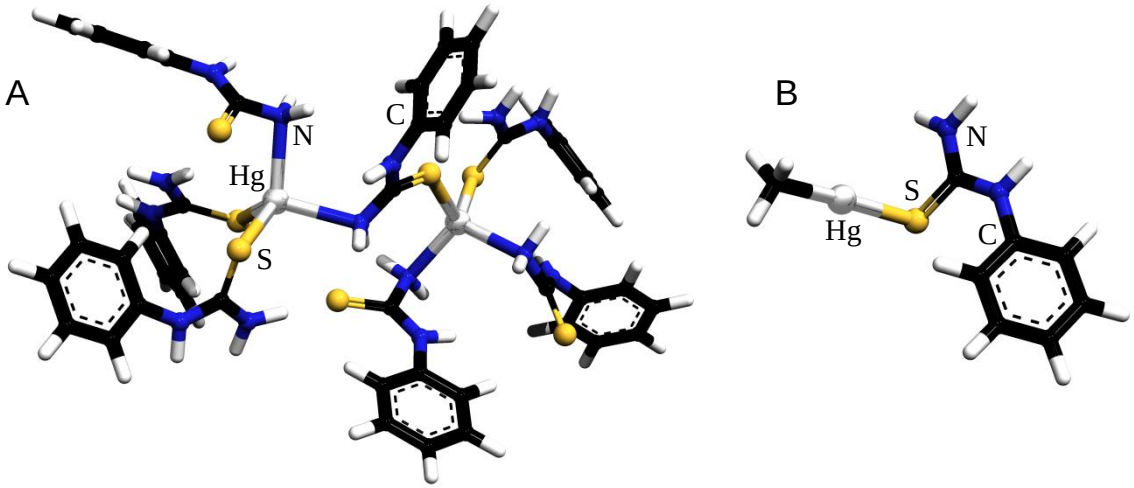

Figure 4.10 Density functional theory energy-minimized geometry-optimized structures of the products resulting from reacting phenylthiourea with (A) $HgCl_2$ or (B) CH_3HgOH in aqueous solution.

The EXAFS data of methylmercury plus excess PTU clearly indicate the formation of a 2-coordinate species, with Hg—C and Hg—S bond lengths of 2.06 and 2.37 Å, respectively (Table 4.1). The CSD (Allen, 2002) contains a number of structures in which a thione group (C=S) is coordinated to an aliphatic organo-Hg entity in a 2-coordinate complex, with mean Hg—C and Hg—S bond-lengths of 2.08 and 2.39 Å, respectively, which agree very well with the EXAFS derived bond-lengths. The presence of a two-coordinate compound with PTU is in accord both with the known stability of Hg—S complexes, and with the known predilection of CH_3—Hg species to form two-coordinate complexes; the CSD contains 178, 23 and 17 entries with two-, three- and four-coordinate CH_3Hg, respectively (Allen, 2002). The energy-minimized geometry-optimized density functional theory (DFT) model of a solution structure is shown in Figure 4.10B, for which the computed bond-lengths of 2.05 and 2.39 Å are in excellent agreement with the EXAFS derived values (Table 4.1).

Our results clearly show that oft-assumed innocuous additive PTU significantly modifies the toxicology of both inorganic mercuric and methylmercury species. In the case of inorganic mercury the toxicity is remarkably decreased, whereas with methylmercury it is substantially increased. XFI reveals that this can be attributed to differences in mercury uptake by the zebrafish larvae, with PTU treatment causing substantially decreased Hg levels for inorganic mercury and causing increased Hg levels for methylmercury. We hypothesize that inorganic Hg^{2+} forms oligomeric or polymeric species with PTU which, due to their relatively large size, would not readily cross cellular membranes and would thus be unable to enter the zebrafish. In the case of methylmercury, XAS and DFT indicate that a molecular entity $[CH_3Hg(PTU)]^+$ is generated in solution through formation of an Hg—S bond with the PTU thione sulfur. Since such a complex would bear a single positive charge, one possible explanation for its increased toxicity may lie in the surface chemistry of cells. It is well known that glycoproteins and polysaccharide chains on cell membranes contribute a negative charge to the cell surface (van den Berg et al. 2006). Electrostatic attraction between positively charged CH_3HgPTU and the cell surface might increase the local availability of $[CH_3Hg(PTU)]^+$, which might then enter the cell and exert its lethal effects.

At the time of writing there is widespread use of PTU for generating transparent zebrafish larvae. However, other methods of obtaining essentially transparent zebrafish larvae are available as alternatives to using PTU and wild-type fish. The *roy orbison* mutant zebrafish

lacks iridophores, has few melanocytes and thus has translucent skin and uniformly pigmented eyes (White et al., 2008), while Lister et al. (1999) have reported a mutant named *nacre* that lacks melanophores but has increased numbers of iridophores. White et al. (2008) subsequently created the *casper* strain that is doubly mutant for *roy orbison* and *nacre*, thus lacking both melanocytes and iridophores from embryogenesis to adulthood (White et al., 2008).

In conclusion, while PTU is used very widely in studies of larval phase zebrafish, our results indicate that it can interfere remarkably with the toxicology of mercury compounds. Our study was initiated following control experiments when we sought to use PTU together with conventional microscopy to study aspects of mercury toxicology, but our findings have broad implications that extend outside mercury toxicology. Even though the coordination chemistry of PTU itself has only been studied in few cases, a search of the CSD (Allen, 2002) indicates that PTU forms structurally characterized complexes with Cu, Zn, Ag and Cd. PTU would be expected to coordinate a wide variety of metals, and a CSD search for thiourea-related ligands to metals returns some 1,636 hits. Transition metal complexes account for 1,504 of these, including pharmacologically-relavent platinum and ruthenium species, with the remainder including complexes with toxic metals such as indium, tin, antimony, lead and bismuth. The fact that many of these metals have been studied using the larval stage zebrafish model expands the implications of our work, and we suggest that extreme caution should be exercised when employing PTU in toxicological studies of metal ions using zebrafish larvae.

CHAPTER 5. EFFECTS OF INORGANIC MERCURY ON THE OLFACTORY PITS OF ZEBRAFISH LARVAE

5.1. Preface

Following the discovery of preferential accumulation of mercury in the olfactory pits of zebrafish larvae exposed to mercuric chloride, further analysis on the role of mercury in the olfactory system was initiated. Chapter 3 utilized XFI to image whole sections of zebrafish with 5 μm resolution. Here we present XFI of olfactory epithelial cells using 500 nm resolution which demonstrates the accumulation of mercury in individual cells. Immunohistochemistry was also conducted to stain the primary neurons that innervate the cells in the olfactory pits. Anti-acetylated tubulin staining reveals damage to the primary neurons in the olfactory epithelia suggesting that proper functioning of these cells may also be affected.

5.2. Author Contributions

This chapter will be reformatted for submission as a communication.

T.C. MacDonald conducted fish trials with mercuric chloride, collected and analyzed XFI data, and drafted the manuscript.

N.J. Sylvain optimized the immunohistochemistry protocol and assisted with fluorescence imaging.

A.K. James assisted with XFI data collection.

I.J. Pickering, P.H. Krone, and G.N. George provided scientific input and guidance, commented on and edited the manuscript, and provided funding for the research.

5.3. Acknowledgements

This research used resources of the Advanced Photon Source (APS), a U.S. Department of Energy (DOE) Office of Science User Facility operated for the DOE Office of Science by Argonne National Laboratory under Contract No. DE-AC02-06CH11357. Data for this chapter were collected from beamlines 2-ID-E and 20-ID-B. Sector 20 facilities at the APS, and research

at these facilities, are supported by the U.S. DOE, Office of Basic Energy Sciences (OBES), the Canadian Light Source and its funding partners, the University of Washington, and the APS.

5.4. Abstract

Mercury compounds are highly toxic; due to the rising levels of mercury pollution, human exposure to mercury is increasing. Occupational exposure to inhaled mercury can be high, causing adverse effects not only in the lungs, but in the olfactory system as well. Although olfactory damage in humans is not a primary focus of most research, impaired olfaction can impact the overall quality of human life. In comparison, olfaction plays a critical role in the survival of fish and other animals. We present a study of the effects of mercury exposure in the olfactory pits of zebrafish larvae, using a combination of X-ray fluorescence imaging and immunohistochemistry, where mercury not only accumulates, but damages the primary neurons innervating the olfactory pits.

5.5. Introduction

Mercury compounds can be more toxic than those of any non-radioactive heavy metal (Clarkson and Magos, 2006); however, environmental mercury contamination is increasing. This increase in mercury exposure poses substantial risks to both human and environmental health. Anthropogenic mercury emissions include contributions from artisanal and small-scale gold mining, fossil fuel combustion, and a number of other sources, totaling nearly 2,000 metric tons per annum (Pacyna et al., 2010). In particular, the extraction of gold by heating a gold and mercury amalgam releases toxic mercury vapour into the air (Bose-O'Reilley et al., 2003; 2008). Other occupational exposures in industries such as cement production, chlor-alkali plants, and coal power plants release mercury into the atmosphere. All of these emissions could result in olfactory impairment; therefore, there is a substantial interest in understanding the mechanisms of the toxic action of mercury compounds.

Olfactory systems are vital for fish with regards to their abilities to reproduce, locate prey, avoid predators, and navigate. For example, salmon are well-known for their ability to return accurately to natal streams during spawning migrations. This navigational ability is due to a combination of senses (Putman et al., 2014), but namely with stream identity derived from olfactory cues (Quinn and Dittman, 1990; Johnson and Banks, 2009). In fish, olfactory

information is gathered from sensory neurons in their olfactory pits. These neurons are essentially in direct contact with the aquatic environment in an olfactory pit, maximizing the possible interaction of odorant molecules, pollutants, and toxic species. In previous work (Korbas et al., 2012), we have used the larval stage zebrafish model with X-ray fluorescence imaging (XFI) (Pushie et al., 2014) to develop an understanding of the effects of mercury compounds on developing vertebrate. Inorganic mercury administered in the form of mercuric chloride was found to show a distinct accumulation pattern compared with mercury(II)-*bis*-L-cysteinate, methylmercury-L-cysteineate, and methylmercury chloride; this distinction is based on the fact that, with mercuric chloride treatment, mercury specifically accumulated in the olfactory pits (Korbas et al., 2012). Here we build upon these observations. Through the combined use of high resolution XFI and confocal immunofluorescence microscopy, we demonstrate that inorganic mercury specifically accumulates in the sensory cells of the olfactory pits, and this may mean mercury is depleting the immunoreactive tubulin in these cells.

5.6. Experimental

5.6.1. Zebrafish

All procedures were approved by the University of Saskatchewan Ethics Board. Embryos were collected, rinsed, and raised to 72 hours post-fertilization (hpf), as previously described (Korbas et al., 2012; MacDonald et al., 2015a; MacDonald et al., 2015b). Larvae were then exposed either to system water (control) or to 2 μM $HgCl_2$ for an additional 72 hours. As previously discussed (Korbas et al., 2012), the fish culture water employed is slightly basic (pH 7.8) with low chloride (~0.3 mM). As a result, we expect quite complex water chemistry so that 90% of the mercury present was dissolved $Hg(OH)_2$ with 9.5% Hg(OH)Cl, 0.3% $HgCO_3$ and 0.2% $HgCl_2$ (Korbas et al., 2012). All forms are expected to be dissolved in water, as their concentrations are well below their aqueous solubilities (Korbas et al., 2012). Thus, the addition of $HgCl_2$ solution to the culture water actually presents the fish larvae with a complex mixture of species, and the description of $HgCl_2$ exposure refers to what was initially added, rather than the form to which the fish were exposed. Following exposure, the zebrafish were then rinsed three times with water, and embedded in JB-4 methacrylate. Zebrafish were sectioned, as previously described (Korbas et al., 2012; MacDonald et al., 2015a; MacDonald et al., 2015b), either to 6

μm thickness and mounted on Thermanox plastic coverslips (Gibco BRL), or to 3 μm thickness and mounted on 500 nm thick silicon nitride windows (Silson Ltd., Northampton, England).

5.6.2. X-ray Fluorescence Imaging (XFI)

XFI data was collected at the APS with the storage ring containing 102 mA at 7 GeV in top-up mode on beamline 20-ID-B or 2-ID-E. Beamlines used Si(111) double crystal monochromators with Rh-coated mirrors employed for focusing and harmonic rejection at the APS. An incident X-ray energy, 13.45 keV, was selected so as to be above the Hg L_{III} edge, but below the Br K-edge and to avoid unwanted Br fluorescence from plastic components of the experimental setup. X-ray fluorescence was monitored using silicon-drift Vortex detectors (Hitachi High-Technologies Science America Inc., Northridge, CA, USA). Data reduction and analysis were carried out as previously described (Korbas et al., 2012; MacDonald et al., 2015a; MacDonald et al., 2015b). Following established practices (Pushie et al., 2014), we quantify mercury and other elements as areal densities, expressed in units of $\mu g/cm^2$.

5.6.3. Tubulin Visualization

The protocol used for tubulin staining to visualize primary neurons was adapted from Sylvain et al. (2010). Larvae were fixed in Dents fixative (80% methanol, 20% DMSO) overnight at 4ºC. Samples were rehydrated in 75%, 50%, and 25% methanol for 30 minutes per step. Once rehydrated, zebrafish were washed in PBST (phosphate buffered saline with 0.1% Tween) for 2 hours, followed by a 1-hour incubation in a blocking buffer containing 2% bovine serum albumin (BSA) and 10% natural goat serum (NGS). Larvae were incubated in anti-acetylated tubulin monoclonal antibody (1:500; Sigma-Aldrich, St.Louis, MO) overnight at 4ºC. Zebrafish were then washed in PBST every 15 minutes for the next 2-3 hours, and then blocked again for an additional hour. Larvae were incubated in a goat anti-mouse IgG coupled to Alexa Fluor 488 (1:1000; Molecular Probes) at 4ºC overnight, followed by 7 hours of rinsing in PBST. The fish were then mounted in 5% methylcellulose (Sigma-Aldrich) in Ringer's solution (116 mM NaCl, 2.9 mM KCl, 1.8 mM $CaCl_2$, 5 mM HEPES) to obtain images (Westerfield, 1995).

5.6.4. Optical Microscopy

Larvae were imaged using a Zeiss Axio Imager apotome microscope with a AxioCam MRm. Apotome images were compiled using AxioVision 4.8 and shown as z-stacks of the whole thickness of the fish. Tissue sections were imaged using a Nikon Eclipse E600 photomicroscope (Nikon, Tokyo, Japan).

5.7. Results and Discussion

Figure 5.1 shows a 5 μm resolution Hg XFI of a section of a larval-stage zebrafish, taken through the olfactory region through the front part of the larval head, together with a histologically-stained section immediately adjacent to the section examined by XFI. Mercury accumulation can be seen in the olfactory pits and in the adjacent neuromasts, which are sensory structures that detect localized water motion displacement of mechanosensory hair cells (Ghysen and Dambly-Chaudière, 2004; Olt et al., 2014). Figure 5.2 shows high resolution XFI of the olfactory epithelium in an olfactory pit in order to determine if mercury is also accumulating in the olfactory sensory epithelium. The olfactory epithelial cell nuclei are visible through their high phosphorus content; whereas, other elements, such as sulfur, are distributed more evenly throughout the cells. The Hg is observed to be distributed independently of the cell nuclei, with loci of higher concentration that do not seem to be associated with cellular structures recognizable at the 500 nm resolution of the XFI data.

Figure 5.3 shows a comparison of tubulin immunofluorescence for the head region of control and $HgCl_2$ treated zebrafish larvae. The control fish show bright and distinctive tubulin staining from the olfactory pits, the various neuromasts in the region examined (two of which are indicated in Figure 5.3), and the axons that can be seen tracing their characteristic paths around the head region in Figure 5.3. The dark patches in Figure 5.3 are pigment spots on the skin surface of the fish. According to standard practice (Karlsson et al., 2001), larvae may be rendered mostly transparent by treatment with the tyrosinase inhibitor 1-phenyl-2-thiourea (PTU) to suppress pigment formation and allow improved visualization. This procedure was not

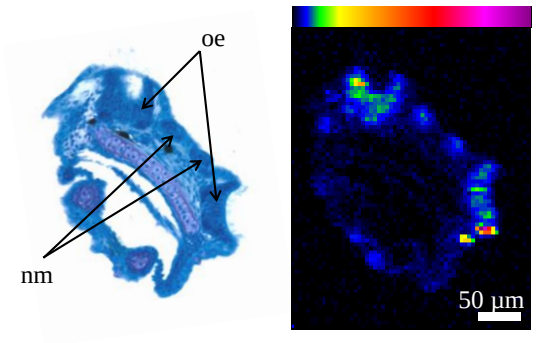

Figure 5.1 Olfactory epithelium of a zebrafish larva exposed to 1 µM $HgCl_2$ for 24 hours. The methylene blue stained histological image (left) shows both the olfactory epithelia (oe) and neuromasts (nm). The XFI image (right) collected at APS 20-ID-B shows mercury accumulation in the region of the olfactory epithelial cells and the neuromasts.

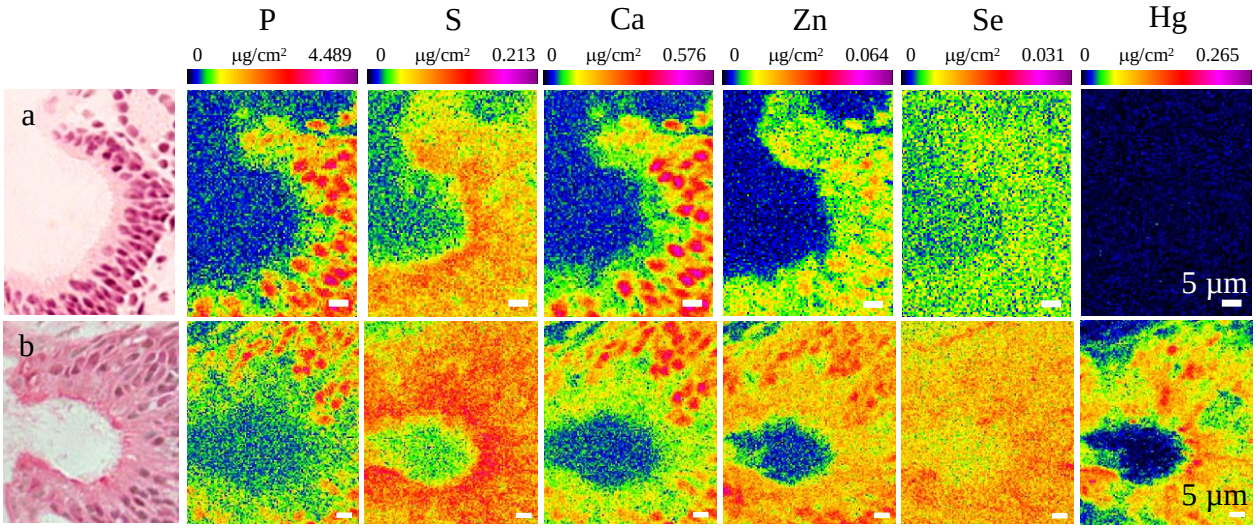

Figure 5.2 High resolution (500 nm) XFI images of olfactory epithelium in zebrafish raised to 3 dpf then exposed to a) system water (control) or b) 2 µM $HgCl_2$ for 72 hours.

adopted here, as our previous findings demonstrate that PTU interferes with the toxicology of mercury compounds (MacDonald et al., 2015a). Figure 5.3 shows marked differences between the tubulin fluorescence of the control and $HgCl_2$ treated fish. In the treated fish, the tubulin fluorescence from olfactory pits show substantially diminished fluorescence, and the neuromasts are only faintly visible. The specific effects of mercury on neuromasts will be addressed in a future publication and will not be considered further in this paper. This indicates that the immunoreactive tubulin in these areas is substantially decreased in the treated fish possibly due to cell death in these areas. Moreover, the axonal processes in the treated fish also appear to be subtly diminished in intensity, although more work is needed to establish this definitively. Mercury is known to interfere with tubulin polymerization through binding to the β-tubulin guanosine triphosphate (GTP) binding region (Pendergrass et al., 1997), probably through formation of a highly covalent and stable Hg—S bond with a cysteinyl thiol group in the active site (Pendergrass et al., 1997). Microtubules are vital components of cellular cytoskeletons (Alberts et al., 2014). In a typical cell, microtubules extend through the cytoplasm, supporting the cell and acting as tracks for the motor proteins kinesin and dynein (Alberts et al., 2014); these motor proteins affect translocation of cellular components, such as vesicles. In neurons, microtubules extend the length of the axon and facilitate transport to and from the periphery of the cell. In the cell, cytoskeletal microtubules are in a state of dynamic instability, constantly forming and dissociating. This process is controlled by GTP binding to β-tubulin (Alberts et al., 2014). Free tubulin αβ-dimers have GTP bound, and these dimers can add to growing microtubules. In the microtubule, GTP to guanosine diphosphate (GDP) conversion causes the αβ-tubulin dimer to bend and can seed or contribute to microtubule disassembly, a process that can be reversed by binding of GTP αβ-tubulin dimers to the end of the microtubule. Mercury-based inhibition of microtubule formation would profoundly disrupt the cytoskeleton and a large number of essential cellular processes. Our tubulin immunofluorescence studies, together with the XFI data, indicate that mercury in $HgCl_2$ treated zebrafish larvae is targeting tubulin-rich cells. The XFI data indicates that the Hg is primarily localized in cells, but not with any resolved structure, which would be in agreement with its association with tubulin. We note that some sensory cells specifically employ copper metal ions to detect certain categories of compounds (Crabtree, 1978; Duan et al., 2012). Cu(I) and Hg(II) have somewhat similar coordination chemistries; both metals have an affinity for thiol ligands, and it seems plausible

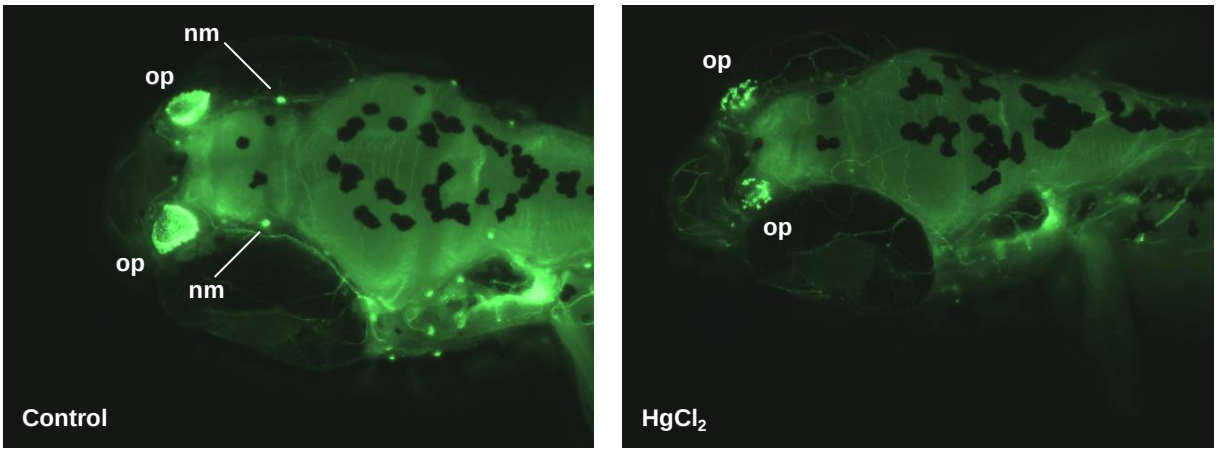

Figure 5.3 Anti-acetylated tubulin staining of zebrafish exposed to a) system water (control) or b) 4 μM $HgCl_2$ for 24h.

that, in addition to profound disruption of the sensory cells, mercury might also interfere directly with such receptors.

CHAPTER 6. DIFFERENTIAL LOCALIZATION OF MERCURY IN THE PRESENCE OF THE PUTATIVE SEQUESTRATION AGENTS DIMERCAPTOSUCCINIC ACID AND α-LIPOIC ACID

6.1. Preface

People are exposed to various levels of different chemical forms of mercury from both natural and anthropogenic sources. For example, over one billion people worldwide depend on marine fish as their primary source of protein, and large, predatory fish often have high levels of methyl mercury compounds in muscle tissue. In cases of acute high dose exposure to mercury the current clinical treatments include chelation therapy. This chapter focuses on possible sequestration agents for mercury including alpha lipoic acid (ALA) and dimercaptosuccinic acid (DMSA). Zebrafish larvae were treated with one of two chemical forms of mercury then subsequently treated with a sequestration agent. XFI was used to determine if mercury accumulation levels or patterns were altered. The results of this study suggest that ALA and DMSA are not ideal treatments for mercury exposure. A custom chelating agent that binds with at least two sites and has optimized bond lengths and angles may be the most effective treatment.

6.2. Manuscript Author Contributions

This chapter will be reformatted and submitted as a manuscript.

MacDonald, T.C.,[¶] Korbas, M.,[¶] Pickering, I.J., Krone, P.H. and George, G.N. Differential localization of mercury in the presence of the putative sequestration agents dimercaptosuccinic acid and α-lipoic acid. [¶] These authors contributed equally to this work.

T.C. MacDonald conducted fish trials with $HgCl_2$, collected and analyzed XFI data, worked on statistical analysis, and drafted the manuscript.

M. Korbas conducted fish trials for organic mercury collected and analyzed XFI data, worked on statistical analysis, and edited the manuscript.

I.J. Pickering, G.N. George, and P.H. Krone provided scientific input and guidance, commented on and edited the manuscript, and provided funding for the research.

6.3. Acknowledgements

This research used resources of the Advanced Photon Source (APS), a U.S. Department of Energy (DOE) Office of Science User Facility operated for the DOE Office of Science by Argonne National Laboratory under Contract No. DE-AC02-06CH11357. Data for this chapter were collected from beamline 20-ID-B. Sector 20 facilities at the APS, and research at these facilities, are supported by the U.S. DOE, Office of Basic Energy Sciences (OBES), the Canadian Light Source and its funding partners, the University of Washington, and the APS.

6.4. Abstract

Clinical management of heavy metal poisoning generally involves chelation therapy, which uses one or more chelators to sequester and promote excretion of heavy metal ions. A chelator is a molecule that binds a metal ion by two or more functional groups to form a stable ring-complex known as a chelate. Treatment of mercury intoxication typically combines chelation therapy with elimination of the source of exposure, together with symptomatic medication in patients with neuropsychiatric sequelae. Mercury chelation therapy typically employs vicinal dithiols such as dimercaptosuccinic acid (DMSA), although these are not true chelators because these vicinal dithiols do not form true chelate complexes with mercury, acting instead as monofunctional sequestration agents. Moreover their use is associated with adverse side-effects. The reduced form of α-lipoic acid (ALA) [(6R)-6,8-bis(sulfanyl)octanoic acid] is one of a very few naturally occurring dithiols; it has been postulated that ALA might be more effective as a chelating agent than current treatments. Here we present a quantitative comparative study of ALA and DMSA on mercury localization and levels in zebrafish larvae following exposure to mercuric mercury and methylmercury. We show that while there are suggestions that ALA may decrease brain mercury in methylmercury-exposed fish and that DMSA may increase liver mercury in mercuric mercury-exposed fish, neither DMSA nor ALA show statistically significant effects. We conclude that neither compound is an effective therapeutic under the conditions of the study.

6.5. Introduction

Treatment of heavy metal poisoning generally involves chelation therapy, a well-established clinical practice which uses one or more chelators to sequester and promote excretion of heavy metal ions (Aposhian et al., 1995; Campbell et al., 1986). A chelator is a molecule that binds a metal ion by two or more functional groups to form a stable ring-complex known as a chelate (Greenwood and Earnshaw, 1984). True chelators thus show a high affinity for their target metal ion relative to species having a sole binding group, which is the origin of the term "chelate effect" and the chemical basis for chelation therapy (Greenwood and Earnshaw, 1984). Intoxication by mercury, one of the potentially most problematic heavy metals to which human populations are exposed, has been treated by "chelation therapy" (Aposhian et al., 1995; Wang et al., 2007) typically employing drugs with thiolate ligands to take advantage of the well-known affinity of mercury for chalcogenide donors. Among these drugs, *meso*-dimercaptosuccinic acid (DMSA) [(2R,3S)-2,3-*bis*(sulfanyl)butanedioic acid] and dimercaptopropanesulfonic acid (DMPS) [2,3-*bis*(sulfanyl)propane-1-sulfonic acid] are the most prominent; these are sold commercially under their respective drug names Chemet® and Dimaval®, although a number of alternative drug names are also used (e.g. succimer for DMSA and unithiol for DMPS). We have previously shown that neither DMSA nor DMPS form true chelate complexes with Hg^{2+} (George et al., 2004; George et al., 2008a), and moreover that none of the current so-called mercury chelation therapy drugs are likely to be true chelators for Hg^{2+} (Fu et al., 2011). More recently we have shown that mercury's lighter group 12 counterpart cadmium can, in the form of Cd^{2+}, form genuine chelate complexes with DMSA and DMPS (Jahromi et al., 2014). The reported clinical benefits of these drugs on mercury (Wang et al., 2007) and their abilities to promote urinary mercury excretion (Zalups and Bridges, 2012) are thus more likely to be due to mono-functional sequestration typical of thiols in general, rather than to the formation of specific chelate complexes (George et al., 2004; Fu et al., 2011). A number of other agents have been used in the clinical treatment of mercury intoxication, including α-lipoic acid (ALA; Rooney, 2007) [(R)-5-(1,2-dithiolan-3-yl)pentanoic acid] which is required for aerobic metabolism. ALA is a *bona-fide* nutritional supplement, and in its reduced form is one of a very few naturally occurring dithiol species; for these reasons α-lipoic acid is gaining in popularity for "chelation therapy" (Rooney, 2007). As we have noted previously (Fu et al., 2011), chelation therapy is

frequently abused in fringe medicine as an agent for “mercury detox” sometimes with severe iatrogenic health consequences, including some deaths (Risher and Amler, 2005).

We have previously used larval zebrafish (*Danio rerio*), a well characterized model vertebrate organism, together with X-ray fluorescence imaging to understand the uptake, transport and redistribution of different inorganic and organic chemical forms of mercury in developing larvae (Korbas et al., 2008; Korbas et al., 2010b; Korbas et al., 2012). Here we present a study of the effects of two putative sequestration agents, DMSA and R-(+)-ALA, upon zebrafish larvae exposed to inorganic mercury or organometallic mercury compounds. ALA exists in oxidized or reduced forms (Figure 6.1); the latter is a dithiol, often called dihydro-α-lipoic acid (DHLA) [(6R)-6,8-bis(sulfanyl)octanoic acid], and is expected to be present *in vivo* and to be the active form for mercury sequestration. We show that under the conditions of exposure employed there is no large-scale depletion or redistribution of tissue mercury levels induced by exposure to either DMSA or ALA. Small changes do appear to be present for both agents, with ALA showing a decrease in brain mercury for fish treated with methylmercury L-cysteineate (CH_3HgS-L-Cys).

6.6. Materials and methods

6.6.1. Animal Care and Embryo Collection

Adult wild type zebrafish were kept at 28°C in fish culture water (carbon-filtered municipal potable water) with a photo-period of 14 hours. Adult zebrafish were mated using the marble technique in 10 L tanks (Westerfield, 1995). Fertilized embryos were collected within 2 hours of spawning and staged following standard procedures; following collection, embryos and larvae were reared in culture water with methylene blue (1 mL per L of culture water) to prevent fungal growth until zebrafish were 3 days post fertilization. At 3 dpf zebrafish having hatched

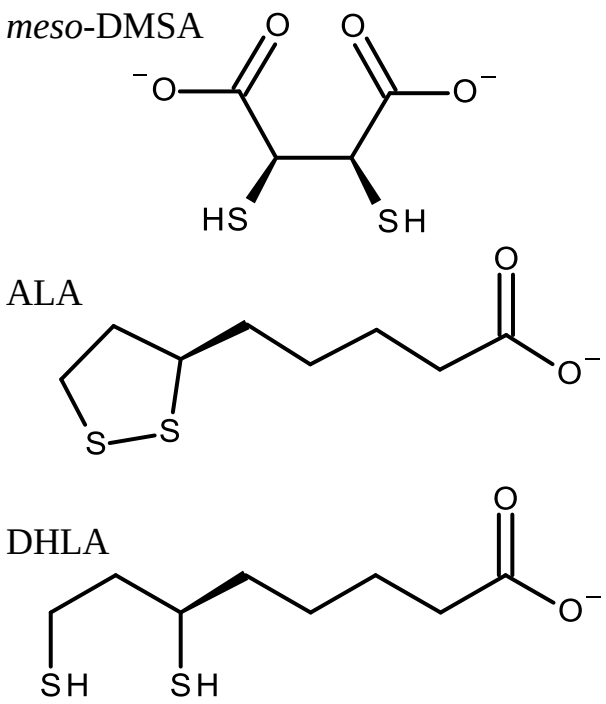

Figure 6.1 Schematic structures for meso-dimercaptosuccinic acid (meso-DMSA) and R-(+) α-lipoic acid (ALA) and R-(+) dihydro α-lipoic acid (DHLA).

from their chorions were then rinsed and raised without methylene blue in 25-mL Petri dishes. Regardless of treatment all solutions were changed daily. All procedures were approved by the University of Saskatchewan's Animal Research Ethics Board, with full adherence to the Canadian Council on Animal Care in science guidelines (http://www.ccac.ca).

6.6.2. Mercury Treatment Solutions

Mercury solutions for treatment of zebrafish were prepared by adding triple distilled water to mercuric chloride ($HgCl_2$) powder (Sigma Aldrich, Oakville, ON) to create a 5 mM stock solution. A 2 μM solution was prepared by dilution in fish culture water. A 1 mM stock solution of methylmercury L- cysteineate (CH_3HgL-cys) was prepared by mixing suitable aliquots of 4 mM methylmercury hydroxide aqueous solution (Strem Chemicals Inc., Newburyport, MA) and 4 mM L-cysteine (Sigma Aldrich) solution (in 30 mM phosphate buffered saline-PBS) to give a 20% molar excess of L- cysteine (*i.e.*, a molar ratio of 1:1.2) with addition of 30 mM PBS. Because organomercury compounds are much more toxic than inorganic mercury compounds, a 0.5 or 1 μM solution was prepared by diluting the 1 mM CH_3HgL-cys solution with fish culture water. ALA and DMSA were purchased from Sigma Aldrich. A 10 mM stock solution of ALA was prepared and later diluted with culture water to 10 μM for treatments. A DMSA stock solution was prepared by adding culture water to DMSA powder to reach a concentration of 1 mM before diluting with culture water to create a final treatment concentration of 100 μM. All stock solutions were prepared on the first day of exposure while treatment solutions were made daily prior to each exposure. The first experiments involved a 24 h mercury exposure (2 μM $HgCl_2$ or 1 μM CH_3HgL-cys) followed by 20 h exposure to 100 μM DMSA, 10 μM ALA or water. It was then determined which chelating agent looked most promising for each mercury compound. The second experiment involved a 24 h exposure to mercury (2 μM $HgCl_2$ or 0.5 μM CH_3HgL-cys), followed by up to 72 h in water or 100 μM DMSA in the case of $HgCl_2$ or 72 h in water or 10 μM ALA in the case of CH_3HgL-cys.

6.6.3. Preparation of Sections

At the cessation of the experiment zebrafish larvae were thoroughly washed in fresh culture water and then fixed in 4% paraformaldehyde for two hours at room temperature. After

removing the paraformaldehyde the fixed larvae were dehydrated in a graded series (0%, 25%, 50%, 75% and 100%) of ethanol in PBST buffer (30 mM PBS, 0.01% Tween 20) for 5 minutes each, and stored in 100% ethanol at -20°C until needed. For sectioning, the fixed and dehydrated larvae were rehydrated into PBST by 5 minute washes in the reversed ethanol gradient. Approximately 10 randomly selected larvae from each treatment group were properly oriented and embedded in 1% agarose gel. The blocks of gel containing the fish were cut out and dehydrated in 100% ethanol by gentle shaking for 5-8 hours at 4°C. Following dehydration the blocks were infiltrated overnight on a rotating shaker at 4°C with JB-4 infiltration solution (10 mL solution A: 0.125 g catalyst; Polysciences Inc., Warrington, PA, USA). The infiltration process with fresh infiltration solution continued on the following day for 5-6 hours. The infiltrated samples were placed in embedding moulds, filled with a mixture of JB-4 solution B and fresh infiltration solution (1 ml solution B: 25 mL infiltration solution), wrapped in plastic wrap to decrease air exposure and left overnight on ice chips at 4°C to polymerize. Sections of 6 μm thickness were cut on a microtome using glass knives. Of two adjacent sections, one was mounted on a glass slide and stained with hematoxylin and eosin (H&E; Polysciences Inc.), while the other, intended for synchrotron X-ray fluorescence imaging, was fixed on a Thermanox plastic coverslip (Gibco BRL) without any further processing.

6.6.4. X-ray Fluorescence Imaging (XFI)

X-ray fluorescence images were collected at the Advanced Photon Source (Argonne, IL, USA) using beamline 20-ID-B (PNC/XOR) with the storage ring operating in continuous top-up mode at 102 mA and 7.0 GeV. With the incident X-ray energy set to 13.45 keV, the Hg $L\alpha_{1,2}$ fluorescence lines, as well as the intensity of the total scattered X-rays, were monitored using a four element silicon-drift Vortex ME4 array detector (SII NanoTechnology USA Inc.). Incident and transmitted X-ray intensities were measured with nitrogen-filled gas ionization detectors. Experiments used a Si(111) double crystal monochromator with Rh-coated silicon mirrors for focusing and harmonic rejection. The microfocused beam of 5 μm diameter was generated by Kirkpatrick-Baez (K-B) Rh-coated focusing mirrors. Samples were mounted at 45° to the incident X-ray beam and were spatially rastered in the microbeam with a step size of 5 μm. Beam exposure was 0.6 sec per step.

6.6.5. X-ray Fluorescence Imaging Data Analysis

The XFI data were processed using the SMAK MicroAnalysis Toolkit (http://ssrl.slac.stanford.edu/~swebb/). Windowed fluorescence counts were normalized by the dead-time corrected incident X-ray intensity and background-corrected by subtracting the average intensity obtained of pixels outside the tissue. Quantities of mercury per pixel were calibrated using two certified highly uniform thin film standards on 6.3 μm-thick mylar substrates (Micromatter, Vancouver, BC, Canada) containing 16.3 and 17.1 $\mu g/cm^2$ Au and TlCl, respectively. Using standards of gold and thallium, adjacent to mercury in the periodic table, was preferable to employing a mercury amalgam standard because the latter decreased in mercury content slowly over time, presumably due to loss of elemental mercury vapor. Average background intensities for windowed fluorescence from the standards were estimated from the X-ray fluorescence image of the 6.3 μm-thick Mylar film. The background-corrected Au and Tl $L\alpha_{1,2}$ fluorescence intensities were used to interpolate a Hg $L\alpha_{1,2}$ fluorescence intensity, which was applied to the background-corrected Hg distribution maps to obtain the quantities of Hg per pixel in $\mu g/cm^2$. The use of this unit is widespread in the XFI literature because it directly relates to what is being measured. These units can be simply related to effective mercury concentration in mM by assuming that the sections are uniformly 6 μm thick and by multiplying the areal Hg densities (in $\mu g/cm^2$) by 8.3.

6.7. Results and Discussion

We initially examined larval sections in the vicinity of the liver (Korbas et al., 2012), since these typically include a number of different tissues such as liver, gut, skeletal (somitic) muscle, pronephric duct, and hind-brain. Figure 6.2A shows the X-ray fluorescence imaging results following exposure to inorganic mercury by addition of 2 μM $HgCl_2$ to the culture water for 24 hours. As we have previously noted (Korbas et al., 2012), inorganic forms such as $HgCl_2$ are subject to quite complex water chemistry so that in culture water 2 μM Hg^{2+} will be present as only about 0.2% as $HgCl_2$, with the remainder as $Hg(OH)_2$ (90.0%), HgClOH (9.5%) and $HgCO_3$ (0.3%). The pattern of Hg accumulation after 24 hours exposure is very similar to that previously reported, with accumulation in the pronephric ducts and the liver, but little in the gut, somitic muscles and brain (Korbas et al., 2012). Following exposure, fish were removed from the mercury-containing solutions, washed three times, and then exposed either to culture water alone

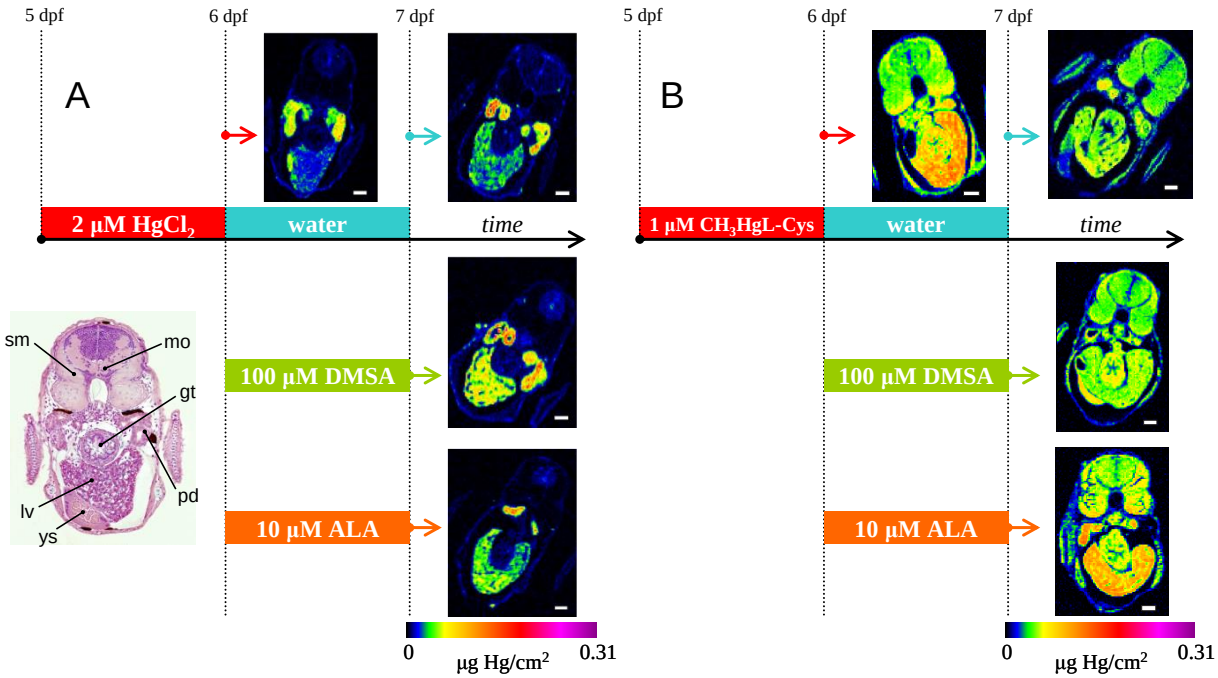

Figure 6.2 Effects of 20 hour exposure to water (control), 100 µM DMSA and 10 µM ALA on larval stage zebrafish previously exposed for 24 hours to A $HgCl_2$ solutions in fish culture water (2 µM, final Hg) or B 1 µM CH_3HgL-Cys in fish culture water. The axes indicate exposure time protocols (in days post fertilization, dpf) as colored bars. Images of sections show areal concentrations of mercury derived from X-ray fluorescence imaging. Scale bars indicate 50 µm. A characteristic histological section is shown for comparison, indicating the somitic muscle (sm), the medulla oblongata (mo), the pronephric duct (pd), the liver (lv), the yolk (yl), and the gut (gt).

(as control), to 100 μM *meso*-DMSA or to 10 μM ALA in culture water. These concentrations of DMSA and ALA were found not to adversely affect the health of zebrafish larvae in separate experiments, and in previous work by others (Francis et al., 2012). Parng et al. (2006) tested a variety of neuroprotectants and found that a dose of 10 μM ALA significantly decreased the percentage of apoptosis in the brains of zebrafish. A dose of 10 μM ALA was selected based on previous research showing that doses greater than 15 μM resulted in higher mortality rates than those in the control group and the lethality threshold is at 12 μM (Francis et al., 2012; Tilton et al., 2008). While no substantial changes were observed with ALA (Figure 6.2A), increased liver Hg levels in the 20 hours following exposure were observed with the DMSA exposure, suggesting increased Hg mobilization in the presence of DMSA causing Hg to be re-localized to the liver from other tissues. Figure 6.2B shows the results of a similar experiment using 1 μM methylmercury L-cysteineate (CH_3HgL-Cys). In this case neither 100 μM DMSA nor 10 μM ALA caused obvious changes to Hg levels relative to the water control, although ALA may have caused a subtle decrease in the brain (Figure 6.2B). We therefore examined the effects of longer exposure times to DMSA for $HgCl_2$ and to ALA for CH_3HgL-Cys. The results of these experiments are shown in Figure 6.3 A and B, respectively. With $HgCl_2$ more prolonged exposure of fish to culture water alone shows a progressive decrease in Hg in all tissues in the section over time, whereas with DMSA the Hg levels in the liver and brain ventricle appear to increase slightly but no large scale changes are observed (Figure 6.3B). With CH_3HgL-Cys a lower concentration of 0.5 μM was chosen for the longer time experiments in order to help ensure fish survival. In this case the liver levels also appear to increase with time, for both control and ALA exposed fish, but following a 3 day treatment with ALA, the observed Hg levels in the hind-brain appeared decreased in comparison with the control fish (Figure 6.3B).

Because this finding may have significance for human use of ALA as a mercury sequestration agent, we then studied the effects of a 3 day treatment with ALA following exposure to CH_3HgL-Cys in brain sections, for which the results are shown in Figure 6.4. An apparent decrease in brain Hg was again observed for the ALA treated sample. Although replicates are often neglected in XFI experiments because sufficient synchrotron beamtime to collect them is difficult to obtain, in this case replicates were considered essential because the changes are at best subtle. The average Hg level in the brain section can be estimated by simply summing the areal density from the quantitative maps (e.g. Figure 6.3) and dividing by the total

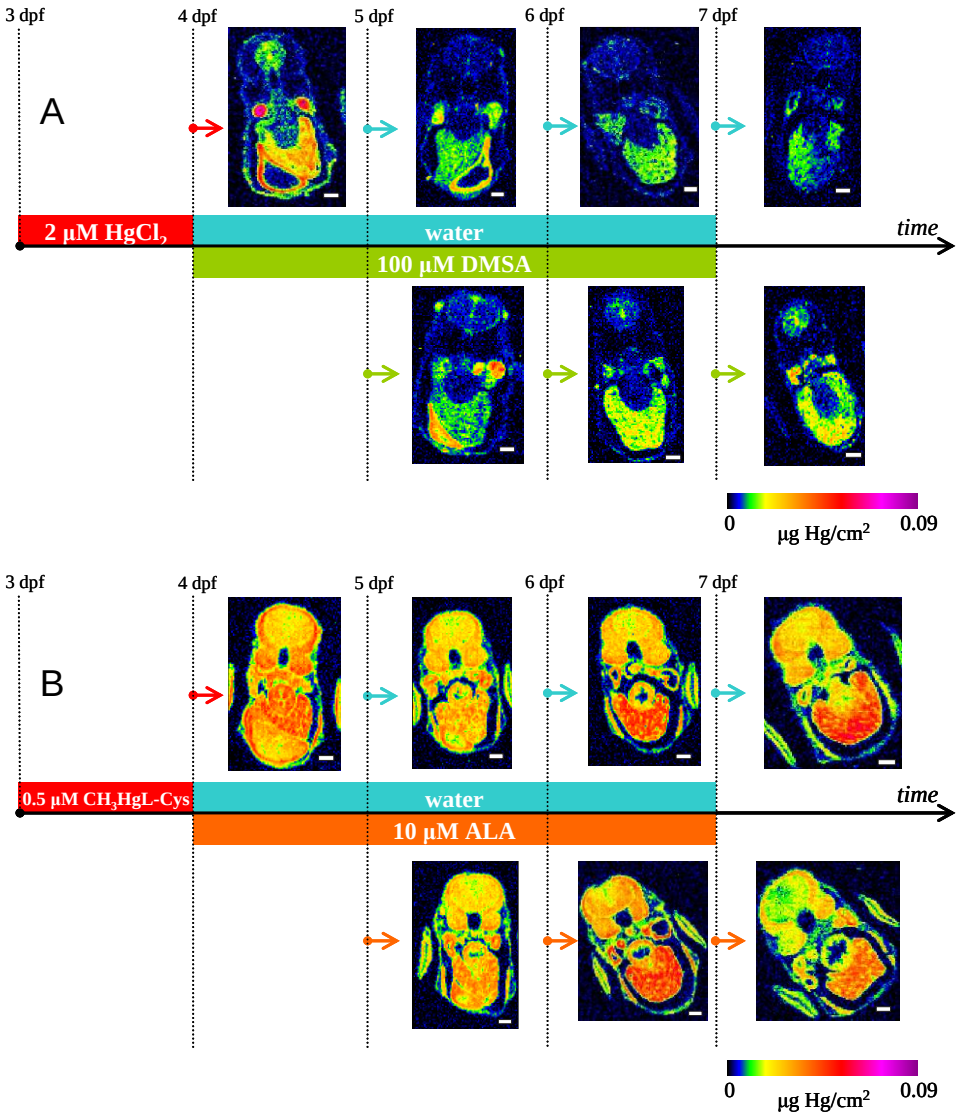

Figure 6.3 Effects of extended exposure (up to 72 hours) to A 100 µM DMSA on larval stage zebrafish exposed to $HgCl_2$ solutions in fish culture water (2 µM, final Hg), or B to 10 µM ALA on larval stage zebrafish exposed to 0.5 µM CH_3HgL-Cys in fish culture water.

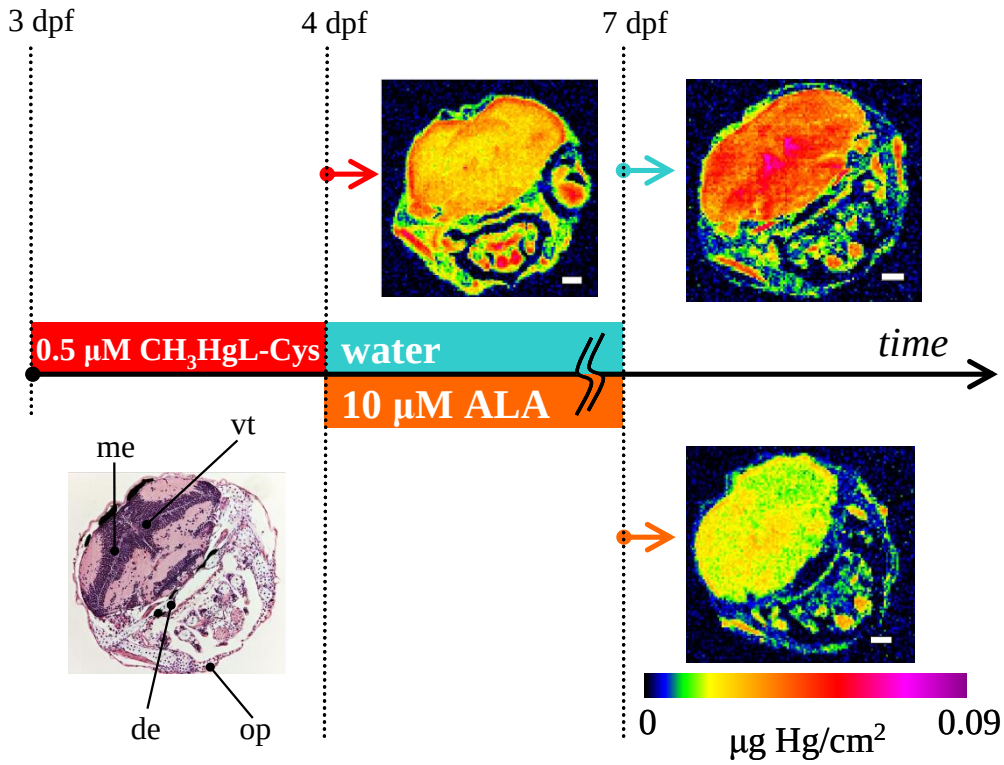

Figure 6.4 Effects of extended ALA exposure (72 hours) on brains of larval stage zebrafish exposed to 0.5 µM CH_3HgL-Cys in fish culture water. Scale bars indicate 50 µm. A characteristic histological section is shown for comparison, indicating the ventricle (vt), the mesencephalon (me), the operculum (op), and the diencephalon (de).

pixels. A two-tailed Student's t-test was used to calculate statistical significance. After calculating the average Hg level for CH_3HgL-Cys and ALA exposed fish (n=4) the mercury level in brain was not significantly different than CH_3HgL-Cys alone (n=4; $p<0.06$). A significant difference was not detected between the fish exposed to CH_3HgL-Cys followed by 3 days in culture water (n=5) compared to CH_3HgL-Cys alone (n=4; $p<0.22$). Thus, we conclude that observed changes are within statistical variation from sample to sample, and that no significant changes were observed. Previous work has shown that in rodents DMSA can substantially assist in clearing a renal mercury burden following administration of inorganic mercury as $HgCl_2$ (Zalups and Bridges, 2012) that the multidrug resistance protein-2 (MRP-2) is important in this process (Zalups and Bridges, 2010; Bridges et al., 2013; Zalups et al., 2014), and that animal age is an important factor in disposition of Hg (Bridges et al., 2014). Our results show that DMSA does not substantially impact inorganic Hg levels in the larval zebrafish model over the timescales investigated, aside from possibly increasing the levels in liver and brain ventricle. Only limited clinical data is available for DMSA as a mercury sequestration agent; for example, McFee and Caraccio (2001) have reported upon a patient who, while hospitalized, had both swallowed and intravenously injected himself with elemental mercury taken from a wall-mounted sphygmomanometer. While the patient improved significantly after administration of DMSA, the authors conclude that it is unclear whether there was a causal relationship between the clinical improvement and the administration of DMSA (McFee and Caraccio, 2001). Alhamad et al. (2012) have reported upon a fatal case of inorganic mercury intoxication arising from elemental mercury vapor inhalation and possible injection. Despite treatment with DMSA a dramatic increase in blood mercury occurred (Alhamad et al., 2012), and the patient subsequently died. Alhamad et al. (2012) also document a number of apparent side-effects of DMSA treatment including nausea, generalized pain, elevated liver transaminases and mild to moderate neutropenia.

As we have noted, methylmercury is highly toxic and previously treatment with DMSA has been recommended in management of methylmercury exposure (Aaseth et al., 1995). Similarly to inorganic mercury, animal work suggests that DMSA may have beneficial effects following administration of methylmercury, although the clinical data is less clear. Cao et al. (2011) have reported a study of the effects of DMSA on blood methylmercury levels in young children that were treated with DMSA for lead exposure, finding that the mean methylmercury

levels fell only slightly after three courses of DMSA treatment. These researchers concluded that such modest decreases might be related to an organ-to-blood redistribution, and that DMSA had limited efficacy for treatment of organic mercury exposure in children. Perhaps the best known case is that of a researcher exposed to dimethylmercury (CH_3HgCH_3) through skin absorption (Nierenberg et al., 1998; Korbas et al., 2010a). Much of any ingested dimethylmercury is expected to be exhaled (Östlund, 1969), while the remainder will not be particularly stable in aqueous media and would be expected to rapidly undergo protonolysis to yield mono-methylmercury derivatives and methane (Ni et al., 2006). The victim in this case was treated with DMSA from close to the onset of poisoning symptoms until just before her death, and while there were indications of initial mercury clearance in urine (Nierenberg et al., 1998) the failure of the treatment caused the attendant clinicians to question the usefulness of DMSA in treatment of methylmercury intoxication (Nierenberg et al., 1998). In agreement with this, treatment of methylmercury intoxication victims in a widespread mass-poisoning in Iraq in the early 1970's failed to show measurable clinical benefits (Clarkson et al., 1981). Our data show no significant effects of DMSA upon mercury distributions in the zebrafish model system over the timescales investigated.

While the clinical data on DMSA and mercury is admittedly quite sparse, no analogous clinical data on ALA and mercury has been reported; however ALA has been considered as a promising possibly therapeutic alternative for a number of reasons. Unlike DMSA, ALA is a natural product and in its reduced form, DHLA, is one of only a few naturally-occurring dithiols. It is part of important enzyme systems such as the pyruvate dehydrogenase complex, and can be synthesized by humans. It is essential for both prokaria and eukaria, and also for at least some of the archaea (Jolley et al., 2000). The ALA/DHLA thiol-disulfide redox couple is approximately -290 mV (Krishnan et al., 2011) so that when administered as the ALA disulfide form, it is expected to be reduced inside cells to the dithiol form, DHLA, which is the form that might potentially chelate mercury. Moreover, unlike DMSA, ALA will cross the blood-brain barrier (Gilgun-Sherki et al., 2001) and therefore has access to the central nervous system. Reaction products of DHLA with both inorganic (Brown and Edwards, 1970; Bonomi et al., 1995) and organo-mercury species (Strasdeit et al., 2000) have been reported. In the case of inorganic Hg^{2+}, and unlike DMSA (George et al. 2004), DHLA may act as a true chelator, although no structural information has yet been reported (Brown and Edwards, 1970; Bonomi et al., 1995). DHLA

reacts with the organo-mercury species diphenylmercury and dimethylmercury in organic solvents (1,4-dioxane) to form inorganic complexes, although it does so extremely slowly with the latter to form mono-methylmercury species. With diphenyl mercury mixed 2:1 phenyl-mercury ($[C_6H_5Hg]^+$) and inorganic Hg^{2+} species result, with the two sulfurs of the dithiol groups being bound to different mercury atoms, and not as a chelate (Strasdeit et al., 2000).

In summary, we find no evidence that DMSA causes any beneficial changes in Hg distributions in the larval zebrafish model over the timescales investigated, apart from a possible increase in liver Hg with inorganic mercury exposure, which may be part of a detoxification mechanism. ALA, however, initially appeared to shows signs of affecting Hg levels in the brains of zebrafish larvae exposed to methylmercury, but examination of replicates indicated that this was within the statistical variation observed from sample to sample. We conclude that under the conditions of our study neither DMSA nor ALA show any evidence of being potentially effective therapeutics for either methylmercury or inorganic mercury.

CHAPTER 7. INTERACTION OF MERCURY AND SELENIUM IN THE LARVAL STAGE ZEBRAFISH VERTEBRATE MODEL

7.1. Preface

Research has suggested that an antagonistic relationship between mercury and selenium may be an effective treatment or prevention measure in mercury toxicity. While analyzing the data presented in Chapter 3 of zebrafish exposed to mercuric chloride, mercury appeared to co-localize with selenium. This chapter examines where mercury and selenium accumulate in zebrafish exposed to inorganic or organometallic mercury as well as where natural selenium stores appear to be located in zebrafish larvae. Zebrafish were exposed to one of two forms of mercury but were not supplemented with selenium (i.e. the selenium in all treatments was from maternal transfer only or the external environment). The findings suggest that mercuric selenide particles may be formed in the zebrafish exposed to mercuric chloride and this compound has an extremely low solubility thus rendering the mercury benign. However, this may lead to a depletion of available selenium and could be the cause of some of the detrimental effects observed with mercury exposure.

7.2. Manuscript Author Contributions

This chapter was published in *Metallomics* and was reformatted to follow the guidelines for a manuscript style thesis.

MacDonald, T.C., Korbas, M., James, A.K., Sylvain, N.J., Hackett, M.J., Nehzati, S., Krone, P. H., George G.N., Pickering, I J. (2015a). Interaction of mercury and selenium in the larval stage zebrafish vertebrate model. *Metallomics*, 7, 1247-1255.

T.C. MacDonald conducted fish trials with inorganic mercury, collected and analyzed XFI data, and drafted the manuscript.

M. Korbas conducted fish trials with organic mercury, collected and analyzed XFI data, and edited the manuscript.

A.K. James, N.J. Sylvain, M.J. Hacket, and S. Nehzati assisted with XFI and μ–XAS data collection and edited the manuscript.

P.H. Krone provided scientific input and guidance, commented on and edited the manuscript, and provided funding for the research.

G.N. George and I.J. Pickering wrote a custom computer program to calculate XFI correlation plots by minimizing the sum of the squares of the perpendicular (closest) distance from each point to the line. They also analyzed the μ–XAS data, provided scientific input and guidance, commented on and edited the manuscript, and provided funding for the research.

7.3. Acknowledgements

This research used resources of the Advanced Photon Source (APS), a U.S. Department of Energy (DOE) Office of Science User Facility operated for the DOE Office of Science by Argonne National Laboratory under Contract No. DE-AC02-06CH11357. Data for this chapter were collected from APS beamlines 2-ID-D, 2-ID-E and 20-ID-B and SSRL beamline 2-3. Sector 20 facilities at the APS, and research at these facilities, are supported by the U.S. DOE, Office of Basic Energy Sciences (OBES), the Canadian Light Source and its funding partners, the University of Washington, and the APS. Use of the Stanford Synchrotron Radiation Lightsource (SSRL), SLAC National Accelerator Laboratory, is supported by the U.S. DOE, Office of Science, OBES under Contract No. DE-AC02-76SF00515. The SSRL Structural Molecular Biology Program is supported by the DOE Office of Biological and Environmental Research, and by the National Institutes of Health (NIH), National Institute of General Medical Sciences (NIGMS) (including P41GM103393). The contents of this publication are solely the responsibility of the authors and do not necessarily represent the official views of NIGMS or NIH.

7.4. Abstract

The compounds of mercury can be more toxic than those of any other non-radioactive heavy element. Despite this, environmental mercury pollution and human exposure to mercury are widespread, and are increasing. While the unusual ability of selenium to cancel the toxicity

of mercury compounds has been known for nearly five decades, only recently have some aspects of the molecular mechanisms begun to be understood. We report herein a study of the interaction of mercury and selenium in the larval stage zebrafish, a model vertebrate system, using X-ray fluorescence imaging. Exposure of larval zebrafish to inorganic mercury shows nano-scale structures containing co-localized mercury and selenium. No such co-localization is seen with methylmercury exposure under similar conditions. Micro X-ray absorption spectra support the hypothesis that the co-localized deposits are most likely comprised of highly insoluble mixed chalcogenide $HgS_xSe_{(1-x)}$ where x is 0.4–0.9, probably with the cubic zincblende structure.

7.5. Introduction

The compounds of mercury are more toxic than any other nonradioactive element (Clarkson and Magos, 2006), but despite its toxicity mercury exposure of humans is surprisingly widespread. Mercury in the environment can be divided based upon its chemistry into inorganic forms, comprising elemental Hg and Hg^{2+} compounds, and organometallic forms, comprising methylmercury $CH_3Hg–$ and related compounds. Sources of exposure to inorganic mercury include the burning of fossil fuels, the use of mercury-containing dental restoratives, and the practice of artisanal gold mining procedures in parts of the developing world (Liang et al., 2015; Driscoll et al., 2013). Sources of methylmercury exposure are primarily through consumption of marine fish (Driscoll et al., 2013; Harris et al., 2003), particularly large predatory species such as swordfish or shark, which have high methylmercury contents.

Both inorganic and organometallic forms of mercury are highly toxic, but with quite distinct toxicologies (Clarkson and Magos, 2006; Korbas et al., 2012). Inorganic mercury is neurotoxic, and can also give rise to kidney damage, digestive tract problems, increased blood pressure, altered heart rate, and acrodynia (Clarkson and Magos, 2006). Organic mercury compounds are also neurotoxic, but are typically more potent in this regard than inorganic mercury, targeting the central nervous system. While adults can be severely affected by organic mercury, infants are especially sensitive, particularly when exposed *in utero* (Clarkson and Magos, 2006). Despite its toxicity, and its potential to adversely impact human health, many unanswered questions remain about the mechanisms of mercury's toxicity and the extent of human health risk from exposure.

The toxicology of mercury has been known to be linked to the biochemistry of selenium for nearly five decades (Parízek and Ostádalová, 1967). Since the initial reports, the protective effects of selenium administration have since been studied extensively, both in animal models (Gailer et al., 2000; Gailer, 2007) and more recently in human brain (Korbas et al., 2010a). In all previous animal studies of the interaction of mercury and selenium, organisms were dosed both with compounds of mercury and with compounds of selenium (Gailer, 2007), whereas in the study of human exposure only endogenous selenium is implicated (Korbas et al. 2010a).

Larval stage zebrafish (*Danio rerio*) are increasingly used as a model vertebrate in toxicology. Their advantages include high fecundity, well characterized developmental stages, and genomic characterization (Westerfield, 1995). Previously we have used the larval zebrafish model in combination with X-ray fluorescence imaging (XFI) (Pushie et al., 2014) in the study of mercury toxicology for both organic and inorganic forms (Korbas et al., 2012; Korbas et al., 2008; Korbas et al., 2010b; Korbas et al. 2013). We present herein an XFI and micro-X-ray absorption spectroscopy (μ-XAS) study of the interaction of both inorganic and organic forms of mercury with endogenous selenium in the zebrafish model.

7.6. Methods

7.6.1. Zebrafish

All procedures were approved by the University of Saskatchewan Ethics Board. Embryos were collected, rinsed, and raised to 72 hours post fertilization (hpf) in methylene blue (to prevent fungal growth) with system water (1 mL methylene blue: 1 L system water) in a 28 ºC incubator with a 14:10 hour (h) light: dark cycle. By 72 hpf zebrafish larvae had hatched from their chorions and were exposed to either system water (control), 2 μM $HgCl_2$, or 0.5 or 1 μM CH_3HgCl. Preliminary studies on 20-ID-D used 24-36 h exposures to 2 μM $HgCl_2$ and 1 μM CH_3HgCl. Subsequent studies used 48 h exposures, but with a lower CH3HgCl dose of 0.5 μM in order to prevent morbidity. In all cases doses were chosen based on our previously reported studies (Korbas et al., 2012) so as to prevent larval morbidity and mortality.

Zebrafish were rinsed three times then embedded in JB-4 methacrylate as previously described (Korbas et al., 2012). Zebrafish larvae to be imaged at Advanced Photon Source (APS) beamline 20-ID-B and at the Stanford Synchrotron Radiation Lightsource (SSRL) beamline 2-3 were sectioned to 6 μm thick and mounted on Thermanox plastic coverslips (Gibco BRL). For

imaging at APS beamlines 2-ID-D and 2-ID-E, 3 µm thick sections were collected and mounted on 500 nm thick silicon nitride windows (Silson Ltd, Northampton, England). In most cases, trunk sections (Figure 7.1) were scanned to interrogate a variety of tissues and organs in a single section.

7.6.2. X-ray Fluorescence Imaging (XFI)

XFI data were collected at the APS with the storage ring containing 102 mA at 7 GeV in top-up mode on beamlines 20-ID-B, 2-ID-D and 2-ID-E. Additional XFI data collection and X-ray absorption spectroscopy were carried out at SSRL with the storage ring operating at 500 mA at 3 GeV on beamline 2-3. All beamlines employed Si(111) double crystal monochromators with Rh-coated mirrors employed for focusing and harmonic rejection at the APS. On APS 20-ID and SSRL 2-3, micro-focus X-ray beams of respective approximate diameters of 5 and 2 µm were obtained by using Rh-coated Kirkpatrick-Baez mirrors, with samples mounted at 45º to the incident X-ray beam. The high-resolution micro-focused beams on 2-ID-D and 2-ID-E were generated by Fresnel zone plates (X-radia, Pleasanton, CA). In all cases an incident X-ray energy of 13.45 keV was selected to be above both the Se K-edge and the Hg L_{III} edge, but below the Br K-edge to avoid unwanted Br fluorescence from plastic components of the experimental setup. X-ray fluorescence was monitored using silicon-drift Vortex detectors (Hitachi High-Technologies Science America Inc., Northridge, CA, USA). Data reduction and analysis were carried out as previously described (Korbas et al., 2012; Korbas et al., 2010a; Korbas et al., 2008; Korbas et al., 2010b; Korbas et al., 2013; MacDonald et al., 2015b). Following established practices (Pushie et al. 2014), we quantify mercury, selenium, and other elements as areal densities *a*, which are normally expressed in units of µg/cm^2. A conversion to equivalent concentration in mM can be accomplished by computing $a \times 10^4/(t\mathrm{M})$ where *t* is the sample thickness in µm and M is the molecular weight.

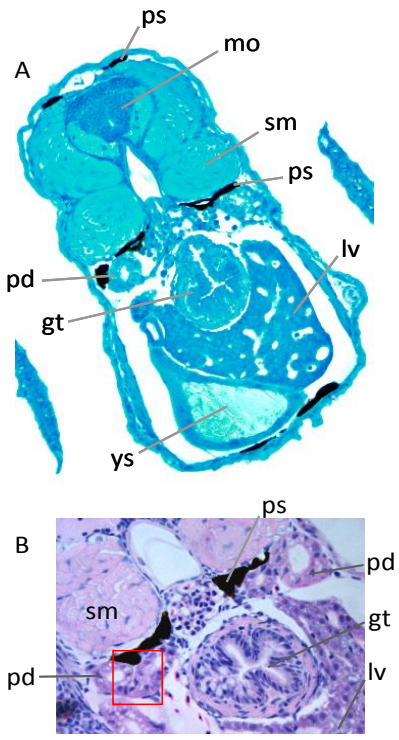

Figure 7.1 Typical larval zebrafish trunk sections, stained with methylene blue (A) and hematoxylin and eosin (H&E) (B). A shows the whole section indicating hindbrain (medulla oblongata; mo), somitic muscle (sm), pronephric ducts (pd), liver (lv), gut tube (gt), pigment spots (ps), and yolk sac (ys). (B) shows a higher resolution micrograph with a typical region of a kidney sections studied at high resolution indicated by the red rectangle, which included both the midline pigment spot and the pronephric ducts.

7.6.3. Micro X-ray Absorption Spectroscopy (μ-XAS)

Micro-XAS data were recorded on SSRL beamline 2-3 using the setup as described for XFI. Following XFI, the beam was positioned on the cells of the pronephric duct. To obtain data approaching adequate signal to noise, 28 spectra of 20 minutes each were averaged. Spectra were calibrated with reference to a Hg-Sn amalgam, assuming the lowest energy inflection of the L_{III}-edge to be 12.285 keV. Data were analyzed using the EXAFSPAK suite of programs (http://ssrl.slac.stanford.edu/exafspak.html.).

7.6.4. Correlation Plots

With correlation plots of XFI data, errors are present in both abscissa and ordinate. Contrary to common practice, the use of standard linear regression is not appropriate for analysis of XFI correlation plots as standard linear regression considers only a single dependent variable, typically graphed on the ordinate, with no presumed errors in abscissa. The resulting line differs depending on whether Hg or Se (for example) is plotted on the abscissa. A valid method for XFI correlation plots is to minimize the sum of the squares of the perpendicular (closest) distance from each point to the line, the slope of which estimates the ratio of the two elements for the data set. A custom computer program was written for this purpose.

7.7. Results and Discussion

7.7.1. X-ray Fluorescence Imaging (XFI)

Figure 7.2 shows selenium and mercury XFI data for trunk sections of zebrafish larvae treated with mercuric chloride and with methylmercury chloride, together with a section from a control fish with no exogenous mercury. The locations of the sections were chosen to show a range of important anatomical features, including the liver, somitic muscle, the hind-brain (medulla oblongata), the pronephric duct (kidney), the yolk sac, and the gut (Figure 7.1). The mercury XFI data show the previously described differences in tissue-specific localization as a function of administered mercury chemical form (Korbas et al., 2012). The inorganic mercury treated section shows localization to the kidney and to a lesser extent the liver, whereas the organic mercury treatment shows concentration in organs including the kidney, liver, somitic muscle, gut and brain, as well as some accumulation in the yolk sac, especially at the periphery. As expected the control shows no detectible mercury.

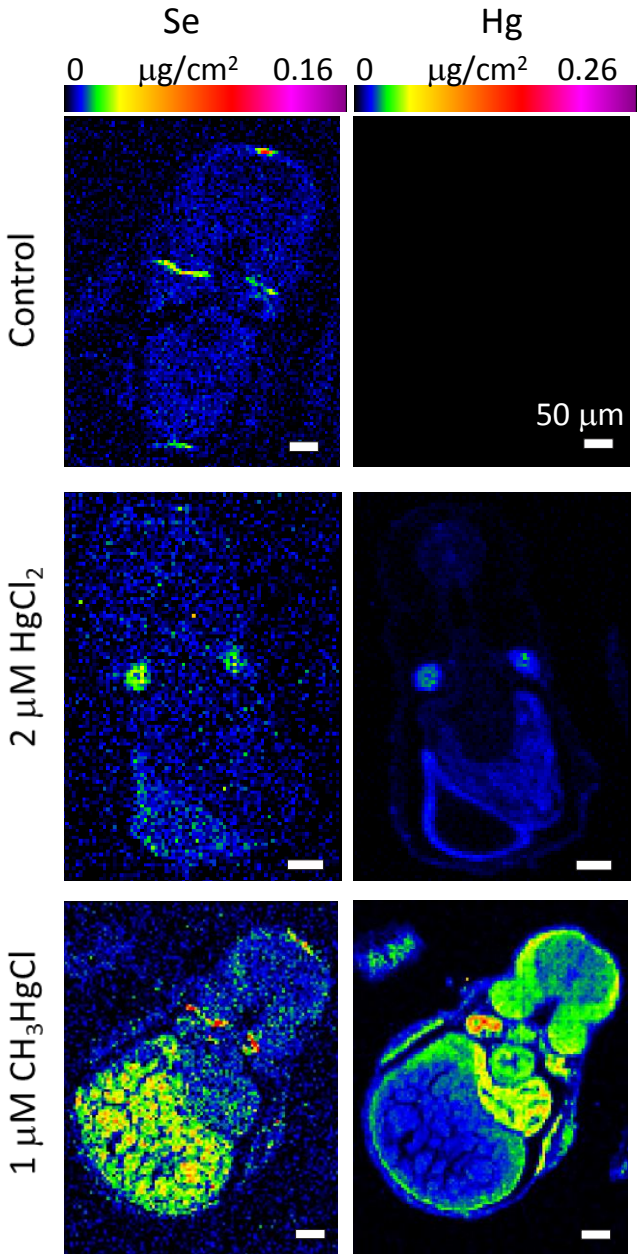

Figure 7.2 Localization of selenium and mercury in trunk sections of larval zebrafish exposed to system water (control), 2 µM $HgCl_2$, or 1 µM CH_3HgCl. Each section was imaged using a step size of 5 µm and a dwell time of 0.6 s on beamline 20-ID. The levels of Se and Hg are shown as areal density ranges, which correspond to concentration ranges of 0–0.36 mM and 0–2.2 mM for Se and Hg, respectively.

The fish in the present study were not supplemented with selenium in any way. The fish larvae at this developmental stage are not yet feeding so that all of their nutrition, including the selenium observed by XFI, is derived from maternal transfer through the yolk sac. The actual amount of selenium in the yolk sac has been observed to vary from fish to fish, presumably because of variations in maternal transfer (Choudhury et al., 2015). This can be observed in Figure 7.2 which shows high Se levels in the yolk sac for the CH_3HgCl exposed larva, but lower amounts in the other sections. Moreover, the other sections in Figure 7.2 happen to have less prominent yolk sacs. Selenium in the control section (Figure 7.2), without exogenous mercury, is observed to be localized predominantly in pigmented tissues, which occur most prominently along the midline pigmentation lying between the kidney and somatic muscle (Figure 7.1). We have observed previously that pigment spots show high levels of localized zinc (MacDonald et al., 2015b). The black pigment of zebrafish is predominantly comprised of melanin and related pigments, synthesized in melanophores. While the association of zinc with melanin has been known for more than six decades (Bowness and Morton, 1953), the chemistry of this association remains unexplored. It seems likely that the zinc is coordinated through the oxygen donors of the catechols that are integral to the polymeric melanin, although whether the zinc is adventitious or has some specific function is unknown. Unlike zinc, the association of selenium with pigment has not been reported previously for zebrafish, although we have consistently observed it in the course of previous studies. In contrast, the association of selenium and neuromelanin in human brain has been reported (Zecca et al., 1994), although the chemical nature of this selenium also remains unknown.

When fish were treated with methylmercury compounds, the selenium distribution appeared similar to the controls which were not treated with exogenous mercury compounds, showing selenium localized most strongly to pigmented areas (Figure 7.2). There was no apparent co-localization of selenium with mercury in the fish tissues. In marked contrast, when fish were treated with inorganic mercury ($HgCl_2$), clear co-localization of exogenously administered mercury with endogenously derived selenium can be seen in the pronephric ducts. In addition, selenium levels in the pigment spots are negligible, suggesting that selenium in these regions may have been depleted in favor of co-localization with mercury in the pronephric ducts. In our XFI data the selenium is present at lower levels than that of mercury, with maximum levels, in the case of kidney, that are about 10% of the observed mercury maxima (Figure 7.2).

The low levels accumulated can be gauged from the average concentrations over the zebrafish tissues in this section which we compute as 0.084 and 0.33 mM, for Se and Hg, respectively. Since at the spatial resolution of Figure 7.2 (5 μm) the strong co-localization within the pronephros is in intense spots that appear smaller than one pixel, we examined sections at higher spatial resolutions. XFI results using a 500 nm resolution X-ray beam are shown in Figure 7.3. As before, the mercury-selenium co-localized areas were only observed with inorganic mercury, and were less than one pixel across. The selenium levels in the pigmented areas, as clearly demarked by the zinc localization in the XFI data, were observed to be depleted (Figure 7.3), reinforcing the suggestion that the selenium that is co-localized with mercury originated in the pigmented areas. Figure 7.4 shows a region scanned at the still higher XFI resolution of 250 nm. Here also the spots were less than one pixel in size, indicating the presence of nano-sized structures less than 250 nm across containing both Hg and Se. However, a single bright spot of mercury in the sample showed much lower accumulation of selenium, indicating chemical heterogeneity. Moreover, the levels of selenium off the co-localized regions were relatively higher than those of mercury indicating either a background tissue level of selenium or an incomplete removal of scattered radiation.

Figure 7.5 shows a section taken through the eye and brain of a zebrafish larva treated with 2 μM $HgCl_2$. In this case the eye lens contains large quantities of selenium, which we have previously observed using confocal methods in selenium supplemented fish (Choudhury et al., 2015), but with the rest of the section showing selenium levels that are more typical of those observed in the trunk section. In particular, pigmented areas of the retina show high relative selenium levels, consistent with those observed in the pigmented areas of the trunk section. Within the brain co-localization of mercury and selenium in small regions is again observed in the fish exposed to inorganic mercury. As with the kidney, mercury is consistently higher than selenium. Figure 7.6 shows a higher resolution data set of part of the dorsal brain from a larval zebrafish eye section. The epiphysis, the dorsal thalumus, habenula (which plays a role in olfactory perception (Krishnan et al., 2014) can all be seen in the figure and these, together with surrounding tissues, are peppered with nano-sized deposits of Hg and Se with, in this case, an Hg:Se molar ratio of about 2-3:1.

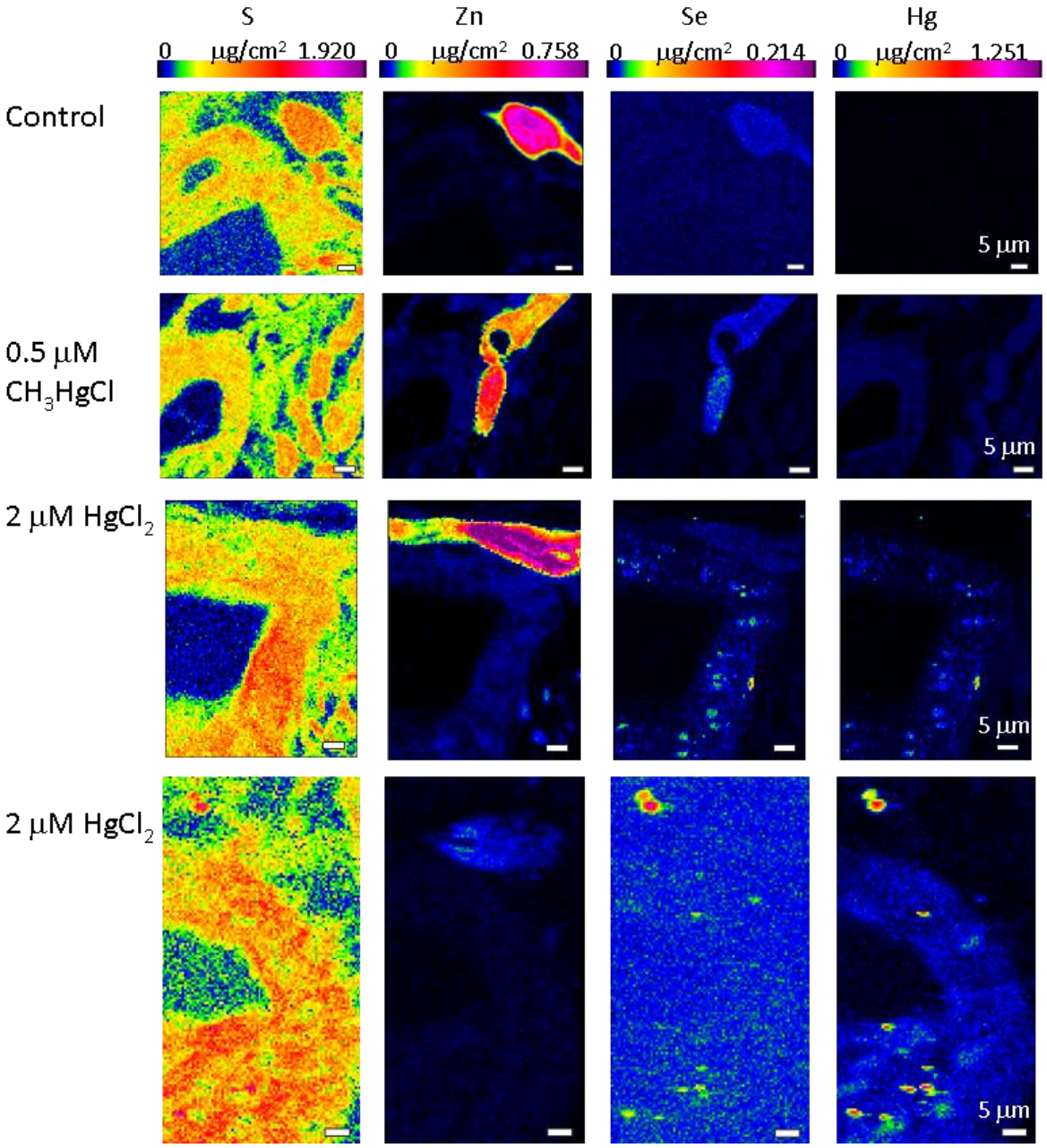

Figure 7.3 Localization of sulfur, zinc, selenium, and mercury in pronephros of larval zebrafish exposed to system water (control), 0.5 µM CH_3HgCl, or 2 µM $HgCl_2$. Sections were imaged at beamline 2-ID-D and 2-ID-E. A typical section of this region is indicated in Figure 7.1. The pigment spots can be located by their high zinc content.

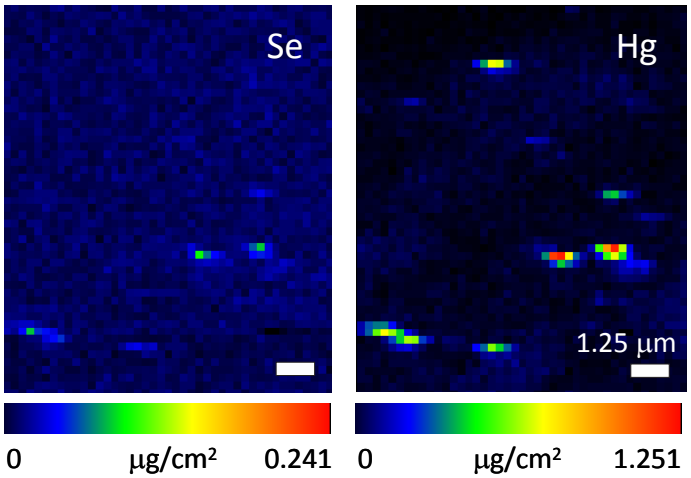

Figure 7.4 High resolution XFI of selenium and mercury in zebrafish pronephric duct of the zebrafish exposed to 2 µM $HgCl_2$ shown in Figure 7.3. Image collected using a step size of 250 nm and a dwell time of 1 s per pixel on beamline APS 2-ID-E.

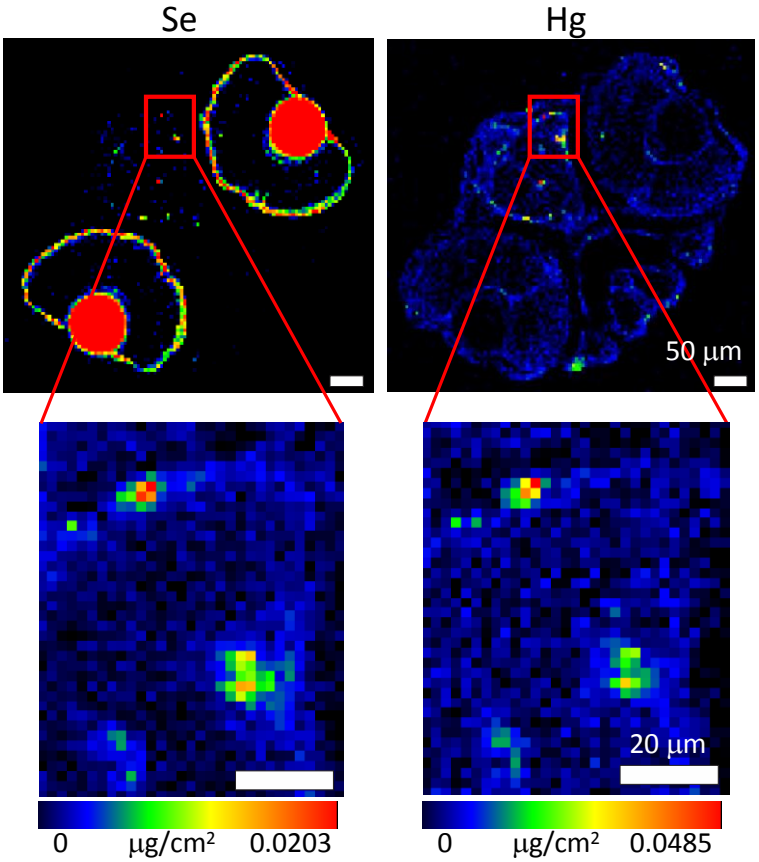

Figure 7.5 Mercury selenium co-localization in zebrafish brain of fish exposed to 2 µM $HgCl_2$. The upper image of the entire section was imaged on APS 20-ID using a step size of 5 µm and a dwell time of 0.6 s per pixel. The higher resolution image region (indicated with the red box) was collected subsequently using a step size of 2 µm and a count time of 0.6 s per pixel.

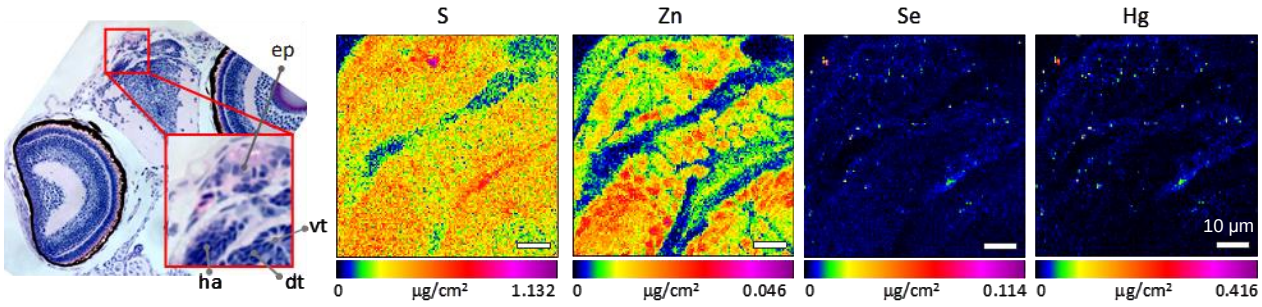

Figure 7.6 High-resolution (500 nm) XFI of larval zebrafish brain imaged at APS beamline 2-ID-D. The H&E stained histology of the adjacent section to that scanned with XFI is shown on the left of the figure, with the area scanned outlined as a red rectangle. The epiphysis (ep), habenula (ha), dorsal thalamus (dt), and ventricle (vt) are indicated.

7.7.2. Correlations Plots

Correlation plots of the levels of Hg and Se for four higher resolution images (Figure 7.3, 7.5, and 7.6) are shown in Figure 7.7. In all cases for $HgCl_2$ treated larvae, there is excellent correlation between the levels of Hg and Se in the regions of the images with elevated levels. This is best illustrated when data are limited to include only the top 90% of Hg and Se levels, which excludes the pixels with almost no Hg and Se that are close to the axes origin. Using the top 90%, correlation coefficients for all images from $HgCl_2$ treated larvae are in the vicinity of 0.9 (Figure 7.7). For the data from $HgCl_2$-treated larvae shown in Figure 7.7, the slopes of the lines give the Hg:Se mass ratios, in most cases being close to 4:1, corresponding to molar ratios of 1.6:1. In contrast, with the data from methylmercury chloride-treated larvae no correlation is seen between Hg and Se, with an R^2 (90%) value of only 0.24.

The other kidney section from a $HgCl_2$ treated larva (Figure 7.3, lower panels) shows a different type of relationship, the correlation plot for which is shown in Figure 7.8. Here there are two distinct correlation domains, and subjecting the data to a domain sorting algorithm with regression analysis indicates that two linear relationships exist with slopes of 19 and 4.5, respectively, with respective R^2 (90%) values of 0.89 and 0.97. The respective Hg:Se molar ratios of the two domains correspond to 7.5:1 and 1.8:1. The images corresponding to the domain-sorted data are also shown in Figure 7.8. The higher Hg content domain (the red line in Figure 7.8) lies predominantly within the cells of the wall of the pronephric duct itself, whereas the lower Hg domain (the blue line in Figure 7.8) lies mostly exterior to the duct. This clearly indicates that the observed Hg:Se ratio is variable and is tissue specific.

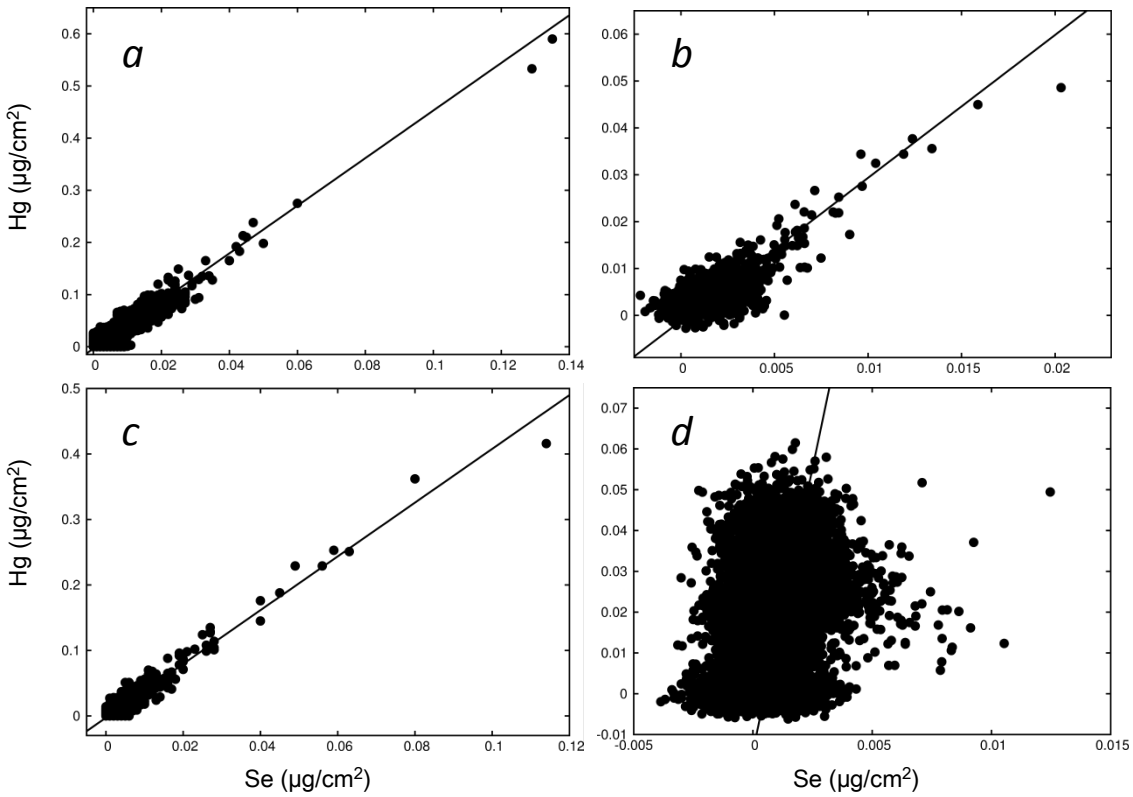

Figure 7.7 Correlation plots of Hg *vs.* Se for selected data sets. (a) shows the kidney section from Figure. 7.3 with $HgCl_2$ treatment, b, and c the brain sections with $HgCl_2$ treatment from Figure 7.5 and 7.6, respectively, and d shows the kidney section from CH_3HgCl-treated larvae from Figure 7.3. The straight lines are derived from regression analysis, as described in the methods section, and give slopes (mass ratios) of 4.6, 3.1, and 4.1 for a, b, and c, respectively, with intercepts within 0.005 of the origin in all cases. Correlation coefficients, R^2, are 0.76 (0.98), 0.53 (0.84), and 0.70 (0.98) for the data from $HgCl_2$-treated larvae a, b, and c, respectively, where the values in parentheses are the R^2 excluding points with less than 10% of maximum. The data from CH_3HgCl-treated larvae give R^2 values of 0.12 (0.24) indicating that there is no correlation between Hg and Se in this sample.

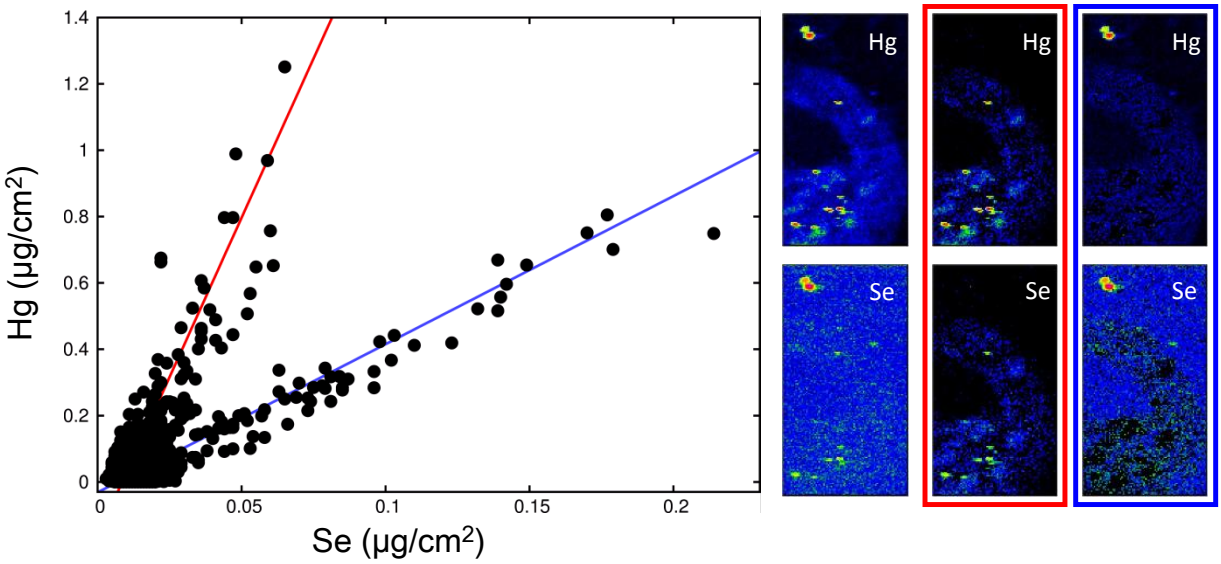

Figure 7.8 Correlation plot of Hg *vs.* Se for a kidney section from a $HgCl_2$-treated zebrafish showing two distinct correlation domains. The red line shows the domain 1 correlation and the blue line shows the domain 2 correlation. The images display the Hg and Se images with (left to right) total, domain 1 (red outline), and domain 2 (blue outline). The slopes for domain 1 and domain 2 were 19.2 and 4.5, respectively. The correlation coefficients, R^2, were 0.79 (0.89) and 0.53 (0.97), where the values in parentheses are the R^2 excluding points with less than 10% of maximum.

In mammals, injection of solutions of sodium selenite and mercuric chloride causes a mutual detoxification through formation of nano-particulate HgSe in blood plasma (Gailer et al., 2000). Similar protective effects for different Se compounds with Hg intoxication have also been demonstrated (Sakamoto et al., 2013), including with larval stage zebrafish (Yamashita et al., 2013). These particles have an approximate size of 100-200 atoms (Gailer et al., 2000; Yoneda and Suzuki, 1997) and may be sequestered by selenoprotein P (Yoneda and Suzuki, 1997). Selenoprotein P is the most abundant extracellular selenoprotein and is now known to be important in selenium homeostasis, especially in brain (Nakayama et al., 2007; Hill et al., 2012). It seems probable that the reported binding of nano-particulate HgSe (Yoneda and Suzuki, 1997) is adventitious, rather than a genuine function of selenoprotein P, and that the sequestration by this essential selenium transporter may indeed be detrimental through diversion of the transporter from its proper function. Indeed, previous work has shown that gluthathione can fulfil a similar function by acting as an external ligand to the HgSe nano-particles (Gailer et al., 2000). The HgSe nano-particles forming in blood give XAS spectra that are consistent with the zincblende structure (Gailer et al., 2000), in which both Se and Hg are bound to each other in approximately tetrahedral geometries, in agreement with the crystal structure of the bulk HgSe mineral tiemannite (de Jong, 1926; Earley, 1950). Compounds related to HgSe, such as CdSe, can exist in either zincblende or wurtzite structures, especially when in nanoparticulate form, and as previously discussed these structures cannot be rigorously distinguished using XAS (Gailer et al., 2000). Bulk mercuric sulfide (HgS) exists in two stable forms at room temperature. The familiar red form, α-HgS, is thermodynamically favored at ambient conditions and has a structure named for its mineral form, cinnabar, with chains of two-coordinate mercury and sulfur (Buckley and Vernon, 1925). The black form, β-HgS, known mineralogically as metacinnabar, is kinetically favored being quite close in energy to α-HgS, and is isostructural with bulk HgSe having the zincblende structure with four-coordinate tetrahedral Hg and S. In mineral formations tiemannite often contains substitution of sulfur for selenium in its structure as the mixed chalcogenide $HgS_xSe_{(1-x)}$ with almost the whole range of HgSe to HgS compositions having been observed (Boctor and Brady, 1980). Synthetic colloidal clusters of $HgS_xSe_{(1-x)}$, varying in size between 2 and 3 nm, were also shown to have the cubic zincblende structure of the bulk (Kuno et al., 2003).

7.7.3. Micro-X-ray Absorption Spectroscopy (μ-XAS)

In the zebrafish model we have described co-localizations of Hg and Se that occur with Hg:Se molar stoichiometries that vary from 7.5:1 to 1.6:1. Sulfur is present at high levels throughout the samples (Figure 7.3), consistent with its various and diverse biological roles. We note that sample regions containing co-localized Hg and Se also contain elevated levels of sulfur (Figure 7.3 and 7.6). Our data are therefore consistent with the presence of nano-sized particles of the mixed chalcogenide $HgS_xSe_{(1-x)}$. In order to investigate this possibility further we used μ-XAS to examine the chemical form of mercury *in situ*. The results of this for zebrafish pronephric duct are shown in Figure 7.9, together with selected model compounds. The mercury L_{III} near-edge spectra show only subtle variation with chemical form, and because of the relatively low overall levels of Hg, the XAS spectra reported here have poorer signal to noise than that normally required for unambiguous speciation (George et al., 2008b). Moreover, the even lower levels of selenium meant that collection of Se K-edge spectra with usable signal to noise ratios was not practical for these samples. Nevertheless, comparison of the Hg L_{III} near-edge spectrum with those of standard compounds indicates that the fish spectrum most resembles that of β-HgS, supporting the hypothesis that mercury is sequestered as a mixed chalcogenide $HgS_xSe_{(1-x)}$ where *x* is 0.44-0.87 most probably with the cubic zincblende structure typical of these materials (Kuno et al., 2003). Both β-HgS and HgSe are highly insoluble compounds, with extremely low molar solubility products (Drott et al., 2013). They can be regarded as essentially chemically inert under biological conditions, with the mercury effectively sequestered and potentially benign. Fish with mercury sequestered in this way lack the typical selenium co-localization in the pigment spots, suggesting that the source of the selenium bound in $HgS_xSe_{(1-x)}$ is that associated with the pigment spots in the control. As we have already discussed, this selenium must originate in the yolk sac, but whether it is diverted from its transport from the yolk to the pigment spots and other tissues, or is remobilized from that already in pigment spots and other tissues, remains unknown. Selenium is an essential element for all kingdoms of life, with a number of roles in vertebrates including redox homeostasis (Weekley and Harris, 2013). Irrespective of whether the selenium involved in mercury sequestration is depleted from tissues directly or comes from the yolk, localized depletion of essential selenium in the fish tissues may be in part responsible for the toxic effects of inorganic mercury (Ralston et al., 2007). Indeed,

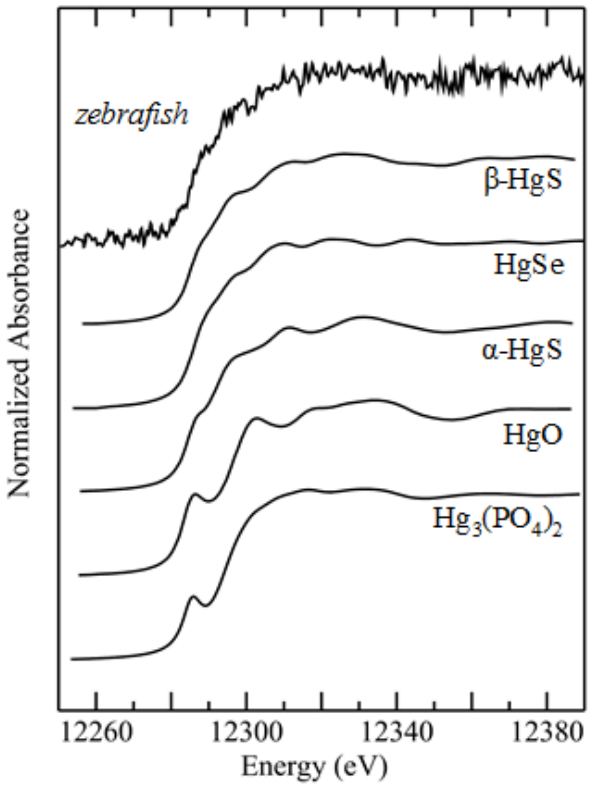

Figure 7.9 Hg L_{III} micro X-ray absorption near-edge spectra of zebrafish pronephric duct, compared with spectra of selected model compounds. Data were measured on SSRL 2–3. Best fit comparison between the fish spectrum and individual model spectra gave fit indices ($\times 10^{-3}$) of 1.04 for β-HgS, 1.38 for $Hg(SG)_2$, 1.42 for HgSe, 1.42 for α-HgS, 1.48 for $[Hg(SR)_4]^{2-}$, 4.44 for HgO, and 5.27 for $Hg_3(PO_4)_2$, indicating that the data are consistent with chalcogenide coordination, and in particular with a substance resembling β-HgS. $Hg(SG)_2$ and $[Hg(SR)_4]^{2-}$ are aqueous solutions of mercury(II)-bis-S-glutathione and mercury(II)-tetrakis-dimercaptoproanesulfonic acid (George et al. 2004), respectively, both in 50 mM HEPES buffer pH 7.0. The fit index is defined as $F = \frac{1}{N-1}\sum_{i-1}^{N}(d_i - s_i)^2$ where *d* corresponds to the fish data and *s* to the standard data, and the summation is over all *N* data points within the data range of 12,260 to 12,370 eV.

depletion of essential selenium through inhibition of essential seleno-enzymes has been suggested as a primary source of mercury's toxicity in what is known as the selenium depletion hypothesis (Ralston et al., 2007).

7.8. Conclusions

Here we show that endogenous selenium can play a role in vertebrates by sequestering inorganic mercury, probably as the insoluble mixed chalcogenide $HgS_xSe_{(1-x)}$. Such sequestration has been suggested to be part of detoxification mechanisms in other vertebrates, including humans, subsequent to *in situ* demethylation of methylmercury compounds (Korbas et al., 2010a). Our observations are on a much shorter time scale following mercury exposure than previous work (Korbas et al., 2010a), and under our conditions the rapid formation of mixed chalcogenides $HgS_xSe_{(1-x)}$ suggests that inorganic mercury, whether this is the form of initial exposure or from demethylation of methylmercury species, might be sequestered very rapidly in exposed humans. An open question is whether selenium supplementation might also play a prophylactic role in populations exposed to high mercury.

CHAPTER 8. DISCUSSION, CONCLUSIONS, AND FUTURE DIRECTIONS

A significant amount of research has been conducted on organic forms of mercury, especially methylmercury chloride. It is important to note that the predominant chemical form in fish is a species with methylmercury and an aliphatic sulfur, most likely methylmercury cysteine (Harris et al., 2003). Most research on inorganic mercury focuses on mercuric chloride; however, once in solution it can also form a number of other compounds depending on pH, chloride concentration, and other components in the system water (Morel et al., 1998). To better elucidate the effects that specific chemical forms of mercury have on the developing zebrafish we exposed larvae to four different treatments, two organic (methylmercury chloride, methylmercury L-cysteineate) and two inorganic (mercuric chloride, mercury bis-L-cysteineate).

In our study, we discovered that the predominant form in the system water was $Hg(OH)_2$ following exposure to mercuric chloride but other chemical forms exist as well. This serves as a reminder that understanding mercury exposure in the environment is highly complex compared to in a laboratory setting because there is often a combination of forms present and it is difficult to understand exactly which form causes which effects. Initial tests demonstrated that different chemical forms of mercury have different toxicities. Methylmercury chloride was more toxic than all other forms tested including methylmercury cysteineate. Mercuric chloride was much more toxic than mercury bis-L-cysteineate. By using synchrotron XFI to collect mercury localization maps of zebrafish larvae, we were also able to demonstrate that unique accumulation patterns occur depending on the specific chemical form. Both forms of methylmercury accumulated in the muscle tissue, the entire yolk sac, and the eyes, where we now know that mercury specifically accumulates in the secondary fiber cells underlying the lens epithelial cells as well as in the photoreceptor cells of the retina (Korbas et al., 2013). Larvae exposed to mercury bis-L-cysteineate accumulated mercury to a much lesser extent than those exposed to mercuric chloride. Inorganic forms of mercury were found to accumulate in the ventricular region of the brain as well as on the periphery of the yolk sac. Mercury accumulation was also noted in the liver, the pronephros, the gut tube, the olfactory epithelium, and the neuromasts in the lateral line of fish exposed to all forms of mercury. As previously mentioned, the lateral line is a mechano-sensory system in fish that detects vibrational changes in the water around the fish. This system is critical for schooling, shoaling, predator avoidance, prey detection and mating

rituals (Alexandre and Ghysen, 1999; Collazo et al., 1994; Dambly-Claudière et al., 2003). Neuromasts are similar to mammalian inner ear hair cells and zebrafish have been used to investigate how certain drugs cause hearing loss (Ou et al., 2010). Visual, olfactory, and auditory deficits following mercury exposure may be due to mercury accumulation directly in these cells as opposed to only via damage to the brain.

Following the discovery of mercury accumulation in several sensory cell types, it was logical to examine the extent of damage caused by the mercury accumulation using immunohistochemistry and/or vital stains. Although zebrafish embryos are transparent they rapidly begin to develop pigment spots starting at 24 hpf. It is common practice in the zebrafish community to use PTU to block the formation of pigment spots by blocking tyrosinase in melanogenesis (Thanigaimalai et al., 2011). Suprisingly, a protective effect in the form of decreased mortality was found in zebrafish exposed to PTU and $HgCl_2$ compared to those exposed to $HgCl_2$ alone. In contrast, zebrafish exposed to PTU and CH_3HgCl exhibited increased mortality rates. XFI supported the hypothesis that mercury levels were lower in fish exposed to PTU and $HgCl_2$ and higher in fish exposed to PTU and CH_3HgCl. Perhaps not surprisingly, EXAFS and DFT showed that PTU binds to mercury in solution. Methylmercury chloride appears to bind to PTU to form a positively charged $[CH_3Hg(PTU)]^+$ compound that may easily cross membranes and cause detrimental effects in the cells. In contrast, PTU and $HgCl_2$ in solution appear to form a large oligomeric structure that would not readily cross cell membranes and therefore would not be expected to exert toxic effects. Because different chemical forms of mercury in combination with PTU cause different alterations in toxicity we discontinued the use of PTU in our studies and recommend that others carefully consider the potential effects PTU could cause when added to other compounds prior to use. The *casper* strain of zebrafish lacks both melanophores and iridophores and presents a viable option for those concerned with impaired visualization due to pigmentation (White et al., 2008). Subsequent experiments utilized wild-type zebrafish because we did not find that the pigment spots in the larvae severely inhibited our ability to visualize fluorescence from the immunohistochemistry protocol used.

High resolution XFI was conducted to determine if inorganic mercury was localized in a particular cell type; however, no specific localization within the olfactory epithelial cells was observed. Understanding the effects of mercury accumulation in the olfactory epithelium of zebrafish larvae was attempted using immunohistochemistry. Anti-acetylated tubulin stains all

primary neurons including those innervating the olfactory system and the lateral line system (Sylvain et al., 2010). Images of the zebrafish exposed to $HgCl_2$ show damage to primary neurons in both the olfactory pits and the lateral line.

Other metals have been shown to affect olfactory function in fish (Blechinger et al., 2002; 2007; McPherson et al., 2004; Meyer et al., 2010; Dew et al., 2014). To determine if mercury causes impaired olfaction we attempted to conduct a behavioural test using a known odorant. This test specifically measures the aversion of zebrafish larvae to noxious olfactory stimuli, and has been used successfully to examine the reduced olfactory response in cadmium-exposed larvae (Matz and Krone, 2007). Unfortunately, the test could not be optimized for mercury-exposed fish in my experiments. Future research could include using a specialized swim-chamber with known attractants and repellent odorants to determine behavioural effects of mercury. Dew et al. (2014) designed a simple rectangular swim chamber with a bottomless acclimation chamber in the middle and blank and stimulus zones on either side. The acclimation chamber can be raised allowing fish access to both the blank and stimulus zones for behavioural analysis (Dew et al., 2014). Blechinger et al. (2007) found that even after a recovery period zebrafish larvae exposed to cadmium still had lingering effects on olfaction. Tests on zebrafish exposed to mercury could thus include a recovery period to examine long-term behavioural effects. TUNEL assays have also been used to detect cell death in zebrafish exposed to cadmium chloride (Blechinger et al., 2007), and could determine if cell death caused by mercury exposure during olfactory system development could lead to permanent olfactory deficits.

A common theme in this work is the accumulation of mercury in sensory cells of zebrafish larvae. Understanding the effects of mercury on neuromasts in lateral lines can aid in understanding both how mercury can affect normal fish behaviour as well as understanding how mercury causes auditory deficits in humans. Although not included in this thesis, we have conducted tests on the localization of mercury in neuromasts and on the effects mercury has on active hair cells in neuromasts. The original data presented in Chapter 3 shows that mercury accumulates in the region of neuromasts. However, it was unclear whether mercury was on the periderm or if it was accumulating in cells within the neuromasts. High resolution XFI demonstrates that zebrafish larvae exposed to $HgCl_2$ and CH_3HgCl accumulate mercury in the cells of the neuromast. A vital stain, 4-(4-diethylaminostyryl)-*N*-methylpyridinium iodide (4-Di-2-Asp) was used to stain active hair cells within neuromasts. Statistical analysis has not yet been

completed; however, a visual assessment of the number of active hair cells appears to show a trend of fewer active hair cells in zebrafish exposed to $HgCl_2$ and CH_3HgCl compared to control fish. A disadvantage of 4-Di-2-Asp is that inactive hair cells cannot be easily viewed therefore it is unclear if the cells are absent or inactive. Additional studies should use both 4-Di-2-Asp and a stain to label the inactive cells to help determine the number of active hair cells and the total number of cells present.

XFI images presented in Chapter 3 show mercury accumulation in the livers of fish exposed to all forms of mercury. Zebrafish larvae exposed to $HgCl_2$ were found to exhibit large spaces in the liver tissue compared to control larvae. Perhaps mercury targets a particular type of cell in the liver, mercury may cause non-specific cell death to a large number of cells, or mercury could be expanding a specific structure in the liver such as sinusoids. Studying the type of damage causing spaces in liver tissue will help elucidate the mechanisms of liver damage that $HgCl_2$ exposure can cause.

Mercury compounds can be extremely toxic and can exert many adverse effects on a number of systems in the body. Currently, mercury poisoning in humans can be treated with dimercaptosuccinic acid (DMSA), a so-called chelator. However, true chelators form stable ring complexes by binding a metal or metalloid with a minimum of two functional groups (Fu et al., 2011). DMSA is poorly optimized for use as a chelator of mercury as it requires more than one molecule of DMSA to bind one atom of mercury. Alpha lipoic acid (ALA) is a naturally occurring dithiol compound that has also been used in clinical studies (Rooney, 2007). We endeavored to better understand the efficacy of DMSA and ALA in decreasing mercury burdens in zebrafish larvae exposed to organic and inorganic forms of mercury. Our preliminary study found that zebrafish treated with ALA following CH_3HgCl exposure had slightly higher levels of mercury. Larvae exposed to $HgCl_2$ and then treated with DMSA had slightly higher levels of mercury in the liver tissue compared to those treated with system water (control). The result suggested that DMSA and ALA may help remobilize mercury to the liver for detoxification. No changes were found in larvae exposed to CH_3HgCl and DMSA or in larvae exposed to $HgCl_2$ and ALA. In light of these findings, subsequent studies were conducted using longer treatment with ALA for CH_3HgCl exposed zebrafish and DMSA for $HgCl_2$ exposed zebrafish. Overall, DMSA was not found to significantly increase or decrease the mercury concentrations compared to those treated with system water. The mercury levels in the methylmercury experiments with

ALA treated fish were also not statistically significant (P<0.06); however, this may in part be due to the data analysis. We averaged the total amounts of mercury in the liver and in the brain. Upon closer inspection, one can see a ring of higher mercury levels on the periphery of the brain compared to the centre in the larvae exposed to CH_3HgCl. After a recovery in water, larvae exposed to CH_3HgCl had higher levels of mercury in the whole brain. In comparison, larvae treated with ALA had lower mercury levels in the brain. Further studies should focus on examining specific regions of the brain to better understand the changing mercury levels following different treatments. Different doses or longer exposure to the sequestration agents may alter efficacy as well. Our research group has also designed a custom chelator (Fu et al., 2011) to bind to both organic and inorganic forms of mercury. Once synthesized and purified, trials should be conducted on zebrafish to determine the efficacy and safety of the chelator.

The antagonistic relationship between mercury and selenium has been known for decades yet the exact relationship between mercury and selenium in living systems is not completely understood. Research suggests that eating fish with naturally higher levels of selenium may counteract some of the adverse effects of mercury (Clarkson and Magos, 2006). However, fish also contain other important nutrients that could be confounding the research by conferring other health benefits (Clarkson and Magos, 2006). Prior research in our laboratory found evidence of mercuric selenide formation in human brain samples (Korbas et al., 2010), and suggested that mercuric selenide formation may play a role in detoxification of methylmercury (Korbas et al., 2010). While analyzing the data from a number of studies conducted throughout this thesis, we noticed colocalization of mercury and selenium zebrafish larvae exposed to $HgCl_2$. The colocalization pattern was evident in the pronephros but was also discovered in the brain of zebrafish larvae. Higher resolution images were collected in control zebrafish larvae as well as those exposed to CH_3HgCl and $HgCl_2$. Colocalization of mercury and selenium was not observed in larvae exposed to CH_3HgCl. Larvae were not supplemented with selenium therefore the selenium present is assumed to be the result of maternal transfer through the yolk sac. The selenium localization patterns in CH_3HgCl exposed fish matched that of the control fish; selenium stores were colocalized with zinc in the melanophores. In contrast, larvae exposed to $HgCl_2$ exhibited decreased levels of selenium in the melanophores suggesting that selenium may have been remobilized from the pigment spots to the pronephros and other areas where inorganic mercury was accumulating. It is also possible that the selenium found in areas of colocalization

may be all or partly from other sources in the organism. Although detoxification of mercury through the formation of highly insoluble mercuric selenide (Drott et al., 2013) formation is beneficial, selenium is an essential trace element (Weekley and Harris, 2013). Depleting selenium to aid in mercury detoxification may result in adverse effects if selenium deficiency occurs (Ralston et al., 2007). Microinjection of selenium into zebrafish embryos provides an elegant method of controlling the amount of selenium embryos contain. Future work utilizing microinjection of selenium could further our understanding of the role of endogenous selenium in mercury detoxification.

Mercury exposure is a global issue that affects people to varying degrees. Although people in North America are less likely than people in other regions of the world to experience mercury poisoning, the general public is exposed to mercury through dental amalgams and fish. Certain sensitive subpopulations including pregnant mothers, fetuses, infants and children also need to be protected. Health Canada (2007) estimates that 50% of the mercury exposure to the average Canadian is through dental amalgams. A serious issue in developed countries is antibacterial resistance (Nue, 1992). Interestingly, a growing number of studies are demonstrating that mercury from dental amalgams correlates with antibiotic resistance (Ready et al., 2007). When mercury dental amalgams are installed a small amount of mercury can be ingested, additionally, the grinding of teeth on the amalgam, drinking hot fluids, and chewing gum can all lead to ingestion of mercury (Lorscheider et al., 1995). Summers et al. (1993) discovered that mercury and antibiotic resistance of many bacterial strains could be transferred to other bacterial recipients in the laboratory which suggested a genetic linkage. It appears that strains carrying plasmids with both antibiotic and mercury resistance were selected for due to mercury released from dental amalgams and has resulted in a higher incidence of multiple antibiotic resistant strains of bacteria (Summers et al. 1993). Aktas and co-workers (2015) investigated the incidence of *H. pylori* in people with dental amalgams and noticed a decreased incidence of infection. However, those with dental amalgams demonstrated higher levels of antibiotic resistance (Aktas et al. 2015). Despite the fact that dental associations maintain the stance that mercury dental amalgams are safe (Lorscheider et al. 1995; ADA 2010), mercury in dental amalgams appears to be contributing to the issue of antibiotic resistance and this may be another reason to limit the installation of new mercury dental amalgams.

With mercury deposition in the arctic being higher than lower latitudes people living in the arctic are consequently exposed to higher levels of mercury. For example, people living in the Faroe Islands depend on food sources in the arctic, including fish and whale, as their primary source of protein and the fish and mammals living in the arctic are likely to accumulate higher levels of mercury (Clarkson and Magos, 2006; WHO, 2003). Mercury can travel long distances from the point source in the atmosphere. Because emissions in China and India are expected to continue to rise, people around the world will be exposed to higher amounts of mercury. It is critical to understand how mercury can affect people near the point sources as well as how mercury may affect people in other locations following long-range transport.

Knowing that methylmercury in fish is the primary source of organic mercury to humans has prompted governments to set guidelines or recommendations on fish consumption (FAO/WHO, 2011). While recommendations are intended to protect people, it is important to remember that a significant portion of the global population depends on fish as their primary source of protein (FAO/WHO, 2011; UNEP, 2013) and that fish also contain many important nutrients including omega-3 fatty acids, vitamin D, selenium, iodine, magnesium, iron and copper (Health Canada, 2007). Because avoidance of fish consumption could result in worse health outcomes in terms of fetal development and cardiovascular health, determining the mercury: selenium ratios in seafood is of great importance (Raymond and Ralston, 2009). To protect the developing fetus the Joint WHO/FAO Expert Committee on Food Additives (JECFA) suggested a provisional tolerable weekly intake of 1.6 μg of methylmercury per kg of body weight per week (WHO, 2003).

Studies on cohort in the Faroe Islands demonstrate a correlation between prenatal mercury exposure and adverse neurological outcomes (Clarkson and Magos, 2006). The studies on the Seychellois found no associations between mercury levels in maternal hair and neurodevelopmental tests and no evidence demonstrating negative effects on development of children exposed to mercury prenatally (Clarkson and Magos, 2006). Developmental outcomes may have stronger correlations with other population characteristics or other factors such as maternal smoking habits and alcohol intake, maternal diet, or concomitant exposure to other pollutants (Clarkson and Magos, 2006). Budtz-Jorgenson et al. (2007) reported that ocean fish consumption protected against adverse effects of high mercury exposures. In conclusion, it is unclear whether intake of methylmercury in fish causes developmental delays and the general

recommendations are that people continue to eat fish as the dietary benefits appear to outweigh the risks (Clarkson and Magos, 2006). Health Canada (2007) recommends two fish meals per week and suggests eating smaller fish rather than large, predatory fish such as swordfish. Clarkson and Magos (2006) suggest that frequent low mercury fish meals are less damaging than infrequent high mercury meals.

Ultimately, the ideal solution to protect people from mercury exposure is to eliminate the release of mercury. The burning of fossil fuels, particularly coal, is a significant source of mercury emissions, therefore methods to decrease mercury emissions from the burning of coal should be explored. As previously discussed, artisanal and small-scale gold mining is the primary contributor of mercury to atmospheric emissions (UNEP, 2013). Children have been forced to work in these conditions due to extreme poverty (Bose-O'Reilly et al., 2003). Even if children are not performing the gold extraction, families often bring the amalgam home and extract the gold inside their home in order to help protect against thievery (Bose-O'Reilly et al., 2008). It is critical to investigate other options of gold extraction that would provide safer alternatives to protect the health of everyone exposed to the mercury vapour especially developing infants and children. Decreasing the use of mercury in gold extraction would also decrease overall global emissions of mercury to the atmosphere. Although it is unrealistic to complete block all mercury emissions we should aim to reduce emissions as much as possible. It is estimated that if mercury emissions were reduced now a noticeable change in mercury levels in the environment and in fish would take decades to occur (UNEP, 2013). In the meantime, we should also continue research to elucidate the mechanisms by which different forms of mercury exert their toxic effects. By understanding these mechanisms it may aid in the development of true chelators or other antidotes.

We have shown that inorganic mercury, although not as toxic as methylmercury, can cause many adverse effects. We used mercury doses higher than environmentally relevant levels in order to understand the potential accumulation patterns and effects resulting from inorganic mercury exposure. From here a logical progression would involve similar studies with low dose, chronic exposures. The research presented here contributes to the body of knowledge on mercury and demonstrates the importance of chemical form in understanding mercury toxicity, particularly in sensory cells.

REFERENCES

Aaseth J., Jacobsen, D., Andersen, O., and Wickstrom, E. (1995) Treatment of mercury and lead poisoning with dimercaptosuccinic acid and sodium dimercaptopropanesulfonate. *Analyst*, 120, 853–854.

Aktaş, B., Başyiğit, S., Yüksel, O., Akkan, T., Atbaş, S.T., Uzman, M., Yılmaz, B., Şimşek, G. and Nazlıgül, Y. (2015) The impact of amalgam dental fillings on the frequency of Helicobacter pylori infection and *H. pylori* eradication rates in patients treated with concomitant, quadruple, and levofloxacin-based therapies. *Eur J Gastroen Hepat*, 27(7), 769–775.

Alberts, B., Johnson, A., Lewis, J., Morgan, D., Raff, M., Roberts, K., and Walter, P. (2015) Molecule biology of the cell, 6th edition. New York: Garland Press.

Alexandre, D. and Ghysen, A. (1999) Somatotopy of the lateral line projection in larval zebrafish. *Proc Natl Acad Sci*, 96, 7558–7562.

Alhamad, T., Rooney, J., Nwosu, A., MacCombs, J., Kim, Y-S., and Shukla, V. (2012) Lessons learned from a fatal case of mercury intoxication. *Int Urol Nephrol*, 44, 647–651.

Allen, F.H. (2002) The Cambridge Structural Database: a quarter of a million crystal structures and rising. *Acta Cryst B*, 58, 380–388.

American Dental Association (ADA) (2010). Literature review: dental amalgam fillings and health effects. ADA Council on Scientific Affairs.

Amlund, H., Lundebye, A.-K., Boyle, D., and Ellingsen, S. (2015) Dietary selenomethionine influences the accumulation and depuration of dietary methylmercury in zebrafish (*Danio rerio*). *Aquat Toxicol*, 158, 211–217.

Aposhian, H.V., Maiorino, R.M., Gonzalez-Ramirez, D., Zuniga-Charles, M., Xu, Z., Hurlbut, K.M., Junco-Munoz, P., Dart, R.C., and Aposhian, M.M. (1995) Mobilization of heavy metals by newer, therapeutically useful chelating agents. *Toxicology*, 97, 23–38.

Bassnett, S., Wilmarth, P.A., and David, L.L. (2009) The membrane proteome of the mouse lens fiber cell. *Mol Vis*, 15, 2448–2463.

Berntssen, M.H.G.,Hylland, K., Lundebye, A.-K., Julshamn, K. (2004) Higher faecal excretion and lower tissue accumulation of mercury in Wistar rats from contaminated fish than from methylmercury chloride added to fish. *Food Chem Toxicol*, 42, 1359–1366.

Bewer, B. (2015) Quantification estimate methods for synchrotron radiation X-ray fluorescence spectroscopy. *Nucl Instr Meth Phys Res B*, 347, 1–6.

Blechinger, S.R., Kusch, R.C., Haugo, K., Matz, C., Chivers, D.P., and Krone, P.H. (2007). Brief embryonic cadmium exposure induces a stress response and cell death in the developing

olfactory system followed by long-term olfactory deficits in juvenile zebrafish. *Toxicol Appl Pharm*, 224, 72–80.

Blechinger, S.R., Warren, J.T., Kuwada, J.Y., and Krone, P.H. (2002) Developmental toxicology of cadmium in living embryos of a stable transgenic zebrafish line. *Environ Health Persp*, 110, 1041–1046.

Boctor, N.Z., and Brady, J.B. (1980). Interdiffusion of sulfur and selenium in tiemannite. *Amer Mineral*, 65, 797–799.

Bohnsack, B.L., Gallina, D., and Kahana, A. (2011) Phenylthiourea sensitizes zebrafish cranial neural crest and extraocular muscle development to changes in retinoic acid and IGF signaling. *PLoS ONE*, 6, e22991.

Bonomi, F., Pagani, S., Cariati, F., Pozzi, A., Crisponi, G., Cristiani, F., Diaz A., and Zanoni, R. (1995) Synthesis and characterization of metal derivatives of dihydrolipoic acid and dihydrolipoamide. *Inorg Chim Acta*, 192, 237–242.

Bose-O'Reilly, S., Drasch, G., Beinhoff, C., Maydl, S., Vosko, M.R., Roider, G., and Dzaja, D. (2003) The Mt. Diwata study on the Philippines, 2000-treatment of mercury intoxicated inhabitants of a gold mining area with DMPS (2,3-dimercapto-1-propane-sulfonic acid, Dimaval). *Sci Total Environ*, 307, 71–82.

Bose-O'Reilly, S., Lettmeier, B., Gothe, R.M., Beinhoff, C., Siebert, U., and Drasch, G. (2008) Mercury as a serious health hazard for children in gold mining areas. *Environ Res*, 107(1), 89–97.

Bowness, J.M. and Morton, R.A. (1953) The association of zinc and other metals with melanin and a melanin-protein complex. *Biochem J*, 53, 620–626.

Bravo, A.G., Loizeau, J.L., Bouchet, S., Richard, A., Rubin, J.F., Ungureanu, V.G., Amouroux, D., and Dominik, J. (2010) Mercury human exposure through fish consumption in a reservoir contaminated by a chlor-alkali plant: Babeni reservoir (Romania). *J Environ Sci Pollut Res Int*, 17, 1422–1432.

Bridges, C.C., Joshee, L., van den Heuvel, J.J.M.W., Russel, F.G.M., and Zalups, R.K. (2013) Glutathione status and the renal elimination of inorganic mercury in the Mrp2-/- mouse. *PLoS One*, 8, e73559.

Bridges, C.C., Joshee, L., and Zalups, R.K. (2014) Aging and the disposition and toxicity of mercury in rats. *Exp Geront*, 53, 31–39.

Bridges, C.C., and Zalups, R.K. (2010) Transport of inorganic mercury and methylmercury in target tissues and organs. *J Toxicol Environ Health B Crit Rev*, 13, 385–410.

Brown, P.R., and Edwards, J.O. (1970) Reactions of 1,3-dimercaptopropane, lipoic acid, and dihydrolipoic acid with metal ions. *J Inorg Nucl Chem*, 32, 2671–2675.

Buckley, H.E., and Vernon, W.S. (1925) The crystal structures of the sulfides of mercury. *Mineral Mag J M Soc*, 20, 382–392.

Budtz-Jorgensen, E., Grandjean, P., and Weihe, P. (2007) Separation of risks and benefits of seafood intake. *Environ Health Persp*, 115, 323–327.

Burk, R.F., and Hill, K.E. (2005) Selenoprotein P: an extracellular protein with unique physical characteristics and a role in selenium homeostasis. *Annu Rev Nutr*, 25, 215–235.

Campbell, J.R., Clarkson, T.W., and Omar, M.D. (1986) The therapeutic use of 2,3-dimercaptopropane-1-sulfonate in two cases of inorganic mercury poisoning. *J Am Med Assoc*, 256, 3127–3130.

Cao, Y., Chen, A., Jones, R.L., Radcliffe, J., Dietrich, K.N., Caldwell, K.L., Peddada, S., and Rogan, W.J. (2011) Efficacy of succimer chelation of mercury background exposures in toddlers: a randomized trial. *J Pediatrics*, 158, 480–485.

Carvalho, C.M.L., Chew, E.-H., Hashemy, S.I., Lu, J., and Holmgren, A. (2008) Inhibition of the human thioredoxin system: A molecular mechanism of mercury toxicity. *J Biol Chem*, 283(13), 11913–11923.

Chen, J., and Berry, M.J. (2003). Selenium and selenoproteins in the brain and brain tissues. *J Neurochem*, 86, 1–12.

Cheng, J., Gao, L., Zhao, W., Liu, X., Sakamoto, M., and Wang, W. (2009) Mercury levels in fisherman and their household members in Zhoushan, China: impact of public health. *Sci Total Environ*, 407, 2625–2630.

Choudhury, S., Thomas, J.K., Sylvain, N.J., Ponomarenko, O., Gordon, R.A., Heald, S.M., Janz, D.M., Krone, P.H., Coulthard, I., George, G.N. and Pickering, I.J. (2015) Selenium preferentially accumulates in the eye lens following embryonic exposure: a confocal X-ray fluorescence imaging study. *Environ Sci Technol*, 49, 2255–2261.

Clarkson T.W., and Magos, L. (2006) The toxicology of mercury and its chemical compounds. *Crit Rev Toxicol*, 36, 609–662.

Clarkson, T.W., Magos, L., Cox, C., Greenwood, M.R., Amin-Zaki, L., Majeed, M.A., and Al-Damluji, S.F. (1981) Tests of efficacy of antidotes for removal of methylmercury in human poisoning during the Iraq outbreak. *J Pharmacol Exp Ther*, 218, 74–83.

Collazo, A., Fraser, S.E., and Mabee, P.M. (1994) A dual embryonic origin for vertebrate mechanoreceptors. *Science*, 264, 426–430.

Cotelesage, J.J.H., Pushie, M.J., Grochulski, P., Pickering, I.J., and George, G.N. (2012) Metalloprotein active site structure determination: Synergy between X-ray absorption spectroscopy and X-ray crystallography. *J Inorg Biochem*, 115, 127–137.

Crabtree, R.H. (1978) Copper (I): A possible olfactory binding site. *J Inorg Nucl Chem*, 40, 1453.

Craig, M.P., Gilday, S.D., and Hove, J.R. (2006) Dose-dependent effects of chemical immobilization on the heart rate of embryonic zebrafish. *Lab Animal*, 35, 41–47.

Cramer, S.P., Tench, O., Yocum, M., and George, G.N. (1988) A 13-element Ge detector for fluorescence EXAFS. *Nucl Instrum Meth A*, 266, 586–591.

Dai, Y.-J., Jia, Y.-J., Chen, N., Bian, W.-P., Li, Q.-K., Ma, Y.-M., Chen, Y.-L., and Pei, D.-S. (2014) Zebrafish as a model system to study toxicology. *Environ Toxicol Chem*, 33(1), 11–17.

Dambly-Chaudière, C., Sapède, D., Soubiran, F., Decorde, K., Gompel, N. and Ghysen, A. (2003) The lateral line of zebrafish: a model system for the analysis of morphogenesis and neural development in vertebrates. *Biol Cell*, 95, 579–587.

Dave, G., and Xiu, R. (1991) Toxicity of mercury, copper, nickel, lead, and cobalt to embryos and larvae of zebrafish, Brachydanio rerio. *Arch Environ Contam Toxicol*, 21, 126–134.

de Jong, W.F. (1926) Die struktur des tiemannit und koloradoit. *Z Kristallogr*, 63, 466–472.

Delley, B.J. (1990) An all-electron numerical method for solving the local density functional for polyatomic molecules. *Chem Phys*, 92, 508–517.

Delley, B J. (2000) From molecules to solids with the $DMol^3$ approach. *Chem Phys*, 113, 7756–7764.

Delnomdedieu, M., Boudou, A., Georgescauld, D., and Dufourc, E.J. (1992) Specific interactions of mercury chloride with membranes and other ligands as revealed by mercury-NMR. *Chem Biol Interact*, 81, 243–269.

de Oliveira Ribeiro, C.A., Belger, L., Pelletier, E., and Rouleau, C. (2002) Histopathological evidence of inorganic mercury and methyl mercury toxicity in the arctic charr (Salvelinus alpinus). *Environ Res*, 90, 217–225.

Dew, W.A., Azizishirazi, A., and Pyle, G.G. (2014) Contaminant-specific targeting of olfactory sensory neuron classes: connecting neuron class impairment with behavioural deficits. *Chemosphere*, 112, 519–525.

Douglas, T.A., Loseto, L.L., Macdonald, R.W., Outridge, P., Dommergue, A., Poulain, A., Amyot, M., Barkay, T., Berg, T., Chételat, J., Constant, P., Evans, M., Ferrari, C.,

Gantner, N., Johnson,m M.S., Kirk, J., Kroer, N., arose, C., Lean, D., Muir, D., Nielsen, T.G., Poissant, L., Rognerud, S., Skov, H., Sørensen, S., Wang, F., and Zdanowicz, C.M. (2012) The fate of mercury in the Arctic terrestrial and aquatic ecosystems, a review. *Environ Chem*, 9, 321–55.

Driscoll, C.T., Mason, R.P., Chan, H.M., Jacob, D.J. and Pirrone, N. (2013) Mercury as a global pollutant: Sources, pathways, and effects. *Environ Sci Technol*, 47, 4967–4983.

Drott, A., Björn, E., Bouchet, S., and Skyllberg, U. (2013) Refining thermodynamic constants for mercury(II)-sulfides in equilibrium with metacinnabar at sub-micromolar aqueous sulfide concentrations. *Environ Sci Technol*, 47, 4197–4203.

Duan, X., Block, E., Li, Z., Connelly, T., Zhang, J., Huang, Z., Su, X., Pan, Y., Wu, L., Chi, Q., Thomas, S., Zhang, S., Ma, M., Matsunami, H., Chen, G.Q., Zhuang, H. (2012) Crucial role of copper in detection of metal-coordinating odorants. *Proc Natl Acad Sci*, 109, 3492–3497.

Dyrssen, D., and Wedborg, M. (1991) The sulphur-mercury(II) system in natural waters. *Water Air Soil Poll*, 56, 507–519.

Earley, J.W. (1950) Description and syntheses of the selenide minerals. *Am Mineral*, 35, 337–364.

Elsalini, O.A., and Rohr, K.B. (2003) Phenylthiourea disrupts thyroid function in developing zebrafish. *Dev Genes Evol*, 212, 593–598.

Falnoga, I., Tusek-Znidaric, M., Horvat, M., and Stegnar, P. (2000) Mercury, selenium, and cadmium in human autopsy samples from Idrija residents and mercury mine workers. *Environ Res*, 84, 211–218.

FAO/WHO (2011). Report of the Joint FAO/WHO Expert Consultation on the Risks and Benefits of Fish Consumption. Rome, Food and Agriculture Organization of the United Nations; Geneva, World Health Organization, 50 pp.

Francis, S., Delgoda, R., and Young, R. (2012) Effects of embryonic exposure to α-lipoic acid or ascorbic acid on hatching rate and development of zebrafish (*Danio rerio*). *Aquacult Res*, 43, 777–788.

Frisk, P., Yaqob A., Nilsson K., Carlsson J, and Lindh, U. (2001) Influence of selenium on mercuric chloride cellular uptake and toxicity indicating protection. *Biol Trace Elem Res*, 81, 229–244.

Froehlicher, M., Liedtke, A., Groh, K.J., Neuhauss, S.C., Segner, H., and Eggen, R.I. (2009) Zebrafish (Danio rerio) neuromast: Promising biological endpoint linking developmental and toxicological studies. *Aquat Toxicol*, 95, 307–319.

Fu, J., Hoffmeyer, R.E., Pushie, M.J., Singh, S.P., Pickering, I.J., and George, G.N. (2011) Towards a custom chelator for mercury - evaluation of coordination environments by molecular modeling. *J Biol Inorg Chem*, 16, 15–24.

Gailer, J. (2007) Arsenic-selenium and mercury-selenium bonds in biology. *Coord Chem Rev*, 251, 234–254.

Gailer, J., George, G.N., Pickering, I.J., Madden, S., Prince, R.C., Yu, E.Y., Denton, M.B., Younis, H.S., and Aposhian, H.V. (2000) Structural basis of the antagonism between inorganic mercury and selenium in mammals. *Chem Res Toxicol*, 13, 1135–1142.

Gailer, J., George, G.N., Pickering, I.J., Prince R.C., Younis, H.S., Winzerling, J.J. (2002). Biliary excretion of $[(GS)_2AsSe]^-$ after intravenous injection of rabbits with arsenite and selenate. *Chem Res Toxicol*, 15 (11), 1466-1471.

George, G.N. (2000) http://ssrl.slac.stanford.edu/exafpak.html

George, G.N., Garrett, R.M., Prince, R.C., and Rajagopalan, K.V. (1996) The molybdenum site of sulfite oxidase: A comparison of wild-type and the cysteine 207 to serine mutant using X-ray absorption spectroscopy. *J Am Chem Soc*, 118, 8588–8592.

George, G.N., and Pickering, I.J. (2007) X-ray Absorption Spectroscopy in Biology and Chemistry. Brilliant Light in Life and Material Sciences. Springer. 97–119.

George, G.N., Pickering, I.J., Doonan, C.J., Korbas, M., Singh, S.P, and Hoffmeyer, R. (2008a) Inorganic molecular toxicology and chelation therapy of heavy metals and metalloids. *Adv Mol Toxicol*, 2, 125–155.

George, G.N., Prince, R.C., Gailer, J. Buttigieg, G.A., Denton, M.B., Harris, H.H., and Pickering, I.J. (2004) Mercury binding to the chelation therapy agents DMSA and DMPS, and the rational design of custom chelators for mercury. *Chem Res Toxicol*, 17, 999–1006.

George, G.N., Singh, S.P., Hoover, J., and Pickering, I.J. (2009) The chemical forms of mercury in aged and fresh dental amalgam surfaces. *Chem Res Toxicol*, 22, 1761–1764.

George, G.N., Singh, S.P., Prince, R.C., and Pickering, I.J. (2008b) The chemical forms of mercury and selenium in fish following digestion with simulated gastric fluid. *Chem Res Toxicol*, 2008, 21, 2106–2110.

Ghysen, A., and Dambly-Chaudière, C. (2004) Development of the zebrafish lateral line. *Curr Opin Neurobiol*, 14, 67–73.

Gilgun-Sherki, Y., Melamed, E., and Offen, D. (2001) Oxidative-stress induced-neurodegenerative diseases: the need for antioxidants that penetrate the blood brain barrier. *Neuropharmacology* 40, 959–975.

Greenwood, N.N., and Earnshaw, A., Chemistry of the Elements, Second Edition. Butterworth-Heinemann, Oxford, 1984.

Gustin, M.S., Lindberg, S.E., and Weisberg, P.J. (2007) An update on the natural sources and sinks of atmospheric mercury. *Applied Geochemistry*, 23, 482–493.

Hansen, A. and Zeiske, E. (1993) Development of the olfactory organ in the zebrafish, *Brachydanio rerio*. *J Comp Neurol*, 333, 289–300.

Hara, T.J. (Ed). (1982) Chemoreception in fishes. Amsterdam: Elsevier Scientific Publishing Company.

Harris, H. H., Pickering I. J., and George, G. N. (2003) The chemical form of mercury in fish. *Science*, 301, 1203.

Health Canada. (2007) Human health risk assessment of mercury in fish and health benefits of fish consumption. Ottawa, Ontario.

Henriksson, J., and Tjälve, H. (1998) Uptake of inorganic mercury in the olfactory bulbs via olfactory pathways in rats. *Environ Res*, 77, 130–140.

Hill, K.E., Wu, S., Motley, A.K., Stevenson, T.D., Winfrey, V.P., Capecchi, M.R., Atkins, J. F., and Burk, R. F. (2012) Production of selenoprotein P (Sepp1) by hepatocytes is central to selenium homeostasis. *J Biol Chem*, 287, 40414–40424.

Hill, K.E, Zhou, J., McMahan, W.J., Motley, A.K., Atkins, J.F., Gesteland, R.F., and Burk, R.F. (2003) Deletion of selenoprotein P alters distribution of selenium in the mouse. *J Biol Chem*, 278, 13640–13646.

Hoyle, I., and Handy, R.D. (2005) Dose-dependent inorganic mercury absorption by isolated perfused intestine of rainbow trout, Oncorhynchus mykiss, involves both amiloride-sensitive and energy-dependent pathways. *Aquat Toxicol*, 72, 147–159.

Huang, C-F., Liu S-H., and Lin-Shiau, S-Y. (2007) Neurotoxicological effects of cinnabar (a Chinese mineral medicine, HgS) in mice. *Toxicol Appl Pharmacol*, 224, 192–201.

Jahromi, E.Z., Gailer, J., Pickering, I.J., and George, G.N. (2014) Structural characterization of Cd^{2+} complexes in solution with DMSA and DMPS. *J Inorg Biochem*, 136, 99–106.

Jeong, J.Y., Kwon, H.B., Ahn, J.C., Kang, D., Kwon, S.H., Park, J.A., and Kim, K.W. (2008) Functional and developmental analysis of the blood-brain barrier in zebrafish. *Brain Res Bull*, 75, 619–628.

Johnson, M.A. and Banks, M.A. (2009) Interlocus variance of F(ST) provides evidence for directional selection over an olfactory receptor gene in Coho salmon (Oncorhynchus kisutch) populations. *Marine genomics*, 2(2), 127–31.

Jolley, K.A., Maddocks, D.G., Gyles, S.L., Mullan, Z., Tang, S-L., Dyall-Smith, M.L., Hough, D.W., and Danson, M.J. (2000) 2-oxoacid dehydrogenase multienzyme complexes in the halophilic Archaea? Gene sequences and protein structural predictions. *Microbiology*, 146, 1061–1069.

Kari, G., Rodeck, U., and Dicker, A.P. (2007) Zebrafish: an emerging model system for human disease and drug discovery. *Clin Pharmacol Ther*, 82, 70–80.

Karlsson, J., von Hofsten, J., and Olsson, P-E. (2001) Generating transparent zebrafish: a refined method to improve detection of gene expression during embryonic development. *Mar Biotechnol (NY)*, 3, 522–527.

Kehrig, H.A. (2011) Mercury and plankton in tropical marine ecosystems: a review. *Oecologia Australis*, 15 (4), 869–80.

Kim, C.Y., Nakai, K., Kameo, S., Kurokawa, N., Liu, Z.M., and Satoh, H. G. (2000) Protective effect of melatonin on methylmercury-Induced mortality in mice. *Tohoku J Exp Med* 191, 241–246.

Kimmel, C.B., Ballard, W.W., Kimmel, S.R., Ullman, B., and Shilling, T.F. (1995) Stages of embryonic development of the zebrafish. *Dev Dynam*, 203, 253–310.

Klaassen, C.D. (Ed.). (2001) Cassarett and Doull's Toxicology: The Basic Science of Poisons (6^{th} ed.). New York, NY: McGraw-Hill.

Klamt A., and Schüürmann, G. (1993) COSMO: a new approach to dielectric screening in solvents with explicit expressions for the screening energy and its gradient. *Chem Soc Perkin Trans*, 2, 799–805.

Kobal, A.B., and Grum, D.K. (2010) Scopoli's work in the field of mercurialism in light of today's knowledge: Past and present perspectives. *Am J Ind Med*, 53, 535–547.

Korbas, M., Blechinger, S.R., Krone, P.H., Pickering I.J., and George, G.N. (2008) Localizing organomercury uptake and accumulation in zebrafish larvae at the tissue and cellular level. *Proc Natl Acad Sci*, 105, 12108–12112.

Korbas, M., Lai, B., Vogt, S., Gleber, S.-C., Karunakaran, C., Pickering, I.J., Krone, P.H., and George, G.N. (2013) Methylmercury targets photoreceptor outer segments. *ACS Chem Biol*, 8, 2256–2263.

Korbas, M., Krone, P.H., Pickering, I.J., and George, G.N. (2010b) Dynamic accumulation and redistribution of methylmercury in the lens of developing zebrafish embryos and larvae. *J Biol Inorg Chem*, 15, 1137–1145.

Korbas, M., MacDonald, T.C., Pickering, I.J., George, G.N., and Krone, P.H. (2012) Chemical form matters: differential accumulation of mercury following inorganic and organic mercury exposures in zebrafish larvae. *ACS Chem Biol*, 7, 411–420.

Korbas, M., O'Donoghue, J.L., Watson, G.E., Pickering, I.J., Singh, S.P., Myers, G.J., Clarkson, T.W., and George, G.N. (2010a) The chemical nature of mercury in human brain following poisoning or environmental exposure. *ACS Chem. Neurosci*, 1, 810–818.

Krishnan, C.V., and Garnett, M. (2011) Electrochemical behavior of the super antioxidant, α-lipoic acid. *Int J Electrochem Sci*, 6, 3607–3630.

Krishnan, S., Mathuru, A.S., Kibat, C., Rahman, M., Lupton, C.E., Stewart, J., Claridge-Chang, A., Yen, S.C. and Jesuthasan, S. (2014) The right dorsal habenula limits attraction to an odor in zebrafish. *Curr Biol*, 24, 1167–1175.

Kuno, M., Higginson, K.A., Qadri, S.B., Yousuf, M., Lee, S.H., Davis, B.L., and Mattoussi, H. (2003) Molecular clusters of binary and ternary mercury chalcogenides: colloidal synthesis, characterization, and optical spectra. *J Phys Chem B*, 107, 5758–5767.

Laks, D.R. (2009) Assessment of chronic mercury exposure within the U.S. population, National Health and Nutrition Examination Survey, 1999–2006. *Biometals*, 22, 1103–1114.

Laporte, J-M., Andres, S., and Mason, R.P. (2002) Effect of ligands and other metals on the uptake of mercury and methylmercury across the gills and the intestine of the blue crab (Callinectes sapidus). *Comp Biochem Phys C*, 131, 185–196.

Lele, Z. and Krone, P.H. (1996) The zebrafish as a model system in developmental, toxicological and transgenic research. *Biotechnol Adv*, 14(1), 57–72.

Li, Z., Ptak, D., Zhang, L., Walls, E. K., Zhong, W. and Leung, Y. F. (2012) Phenylthiourea specifically reduces zebrafish eye size. *PLoS ONE*, 7, e40132.

Li, J., Zhang, B., Ren, Y., Gu, S., Xiang, Y., Huang, C., and Du, J. (2015) Intron targeting-mediated and endogenous gene integrity-maintaining knockin in zebrafish using the CRISPR/Cas9 system. *Cell Research*, 25, 634–637.

Liang, S., Wang, Y., Cinnirella, S., and Pirrone, N. (2015) Atmospheric mercury footprints of nations. *Environ Sci Technol*, 49, 3566–3574.

Lister, J.A., Robertson, C.P., Lepage, T., Johnson, S.L., and Raible, D.W. (1999) Nacre encodes a zebrafish microphthalmia-related protein that regulates neural-crest-derived pigment cell fate. *Development*, 126, 3757–3767.

Lobinski, R., Moulin, C., and Ortega, R. (2006) Imaging and speciation of trace elements in biological information. *Biochimie*, 88, 1591–1604.

Lorscheider, F.L., Vimy, M.J., Summers, A.O., and Zwiers, H. (1995). The dental amalgam mercury controversy – inorganic mercury and the CNS; genetic linkage of mercury and antibiotic resistances in intestinal bacteria. *Toxicology*, 97(1-3), 19–22.

Luque-Garcia, J.L., Cabezas-Sanchez, P., Anunciacão¸ D.S., and Camara, C. (2013) Analytical and bioanalytical approaches to unravel the selenium–mercury antagonism: A review. *Anal Chim Acta*, 80, 1–13.

MacDonald, T.C., Korbas, M., James, A.K., Sylvain, N.J., Hackett, M.J., Nehzati, S., Krone, P.H., George G.N., and Pickering, I.J. (2015a) Interaction of mercury and selenium in the larval stage zebrafish vertebrate model. *Metallomics*, 7, 1247–1255.

MacDonald, T.C., Nehzati, S., Sylvain, N.J., James, A.K., Korbas, M., Caine, S., Pickering, I.J., George, G.N. and Krone, P.H. (2015b) Phenylthiourea alters toxicity of mercury compounds in zebrafish larvae. *J Inorg Biochem*, 151, 10–17.

Martena, M.J., Van Der Wielen, J.C., Rietjens, I.M., Klerx, W.N., De Groot, H.N., and Konings, E.J. (2010) Monitoring of mercury, arsenic, and lead in traditional Asian herbal preparations on the Dutch market and estimation of associated risks. *Food Addit Contam Part A Chem Anal Control Expo Risk Assess*, 27, 190–205.

Mason, R.P., Reinfelder, J.R., and Morel, F.M.M. (1996) Uptake, toxicity, and trophic transfer of mercury in a coastal diatom. *Environ Sci Technol*, 30, 1835–1845.

Matz, C.J., and Krone, P.H. (2007) Cell death, stress-responsive transgene activation, and deficits in the olfactory system of larval zebrafish following cadmium exposure. *Environ Sci Technol*, 41(14), 5143–5148.

McFee, R.B., and Caraccio, T.R. (2001) Intravenous mercury injection and ingestion: clinical manifestations and management. *J Toxicol Clin Toxicol*, 39, 733–738.

McGrath, P. and Li, C.Q. (2008) Zebrafish: a predictive model for assessing drug induced toxicity. *Drug Discov Today*, 13 (9-10), 394–401.

McPherson, T.D., Mirza, R.S. and Pyle, G.G. (2004). Responses of wild fishes to alarm chemicals in pristine and metal-contaminated lakes. *Can J Zool*, 82, 694–700.

Meyer, J.S. and Adams, W.J. (2010) Relationship between biotic ligand model-based water quality criteria and avoidance and olfactory responses to copper by fish. *Environ Toxicol Chem*, 29(9); 2096–2103.

MINTEQ Program. Retrieved online September 2011 at: http://www.epa.gov/ceampubl/mmedia/minteq/

Møller-Madsen, B., and Danscher, G. (1986) Localization of mercury in the CNS of rats: Mercuric chloride per os. *Environ Res*, 41, 29–43.

Moore, K.L., Lombi, E., Zhao, F.-J., Grovenor, C.R.M. (2012) Elemental imaging at the nanoscale: nanoSIMS and complementary techniques for element localization in plants. *Anal Bioanal Chem*, 402, 3263–3273.

Morel, F.M.M., Kraepiel, A.M.L., and Amyot, M. (1998) The chemical cycle and bioaccumulation of mercury. *Annu Rev Ecol Syst*, 29, 543–66.

Mortimer, N.J., Chave T.A., and Johnston, G.A. (2003) Red tattoo reactions. *Clin Exp Dermatol*, 28, 508–510.

Nakayama, A., Hill, K.E., Austin, L.M., Motley, A.K., and Burk, R.F. (2007) All regions of mouse brain are dependent on selenoprotein P for maintenance of selenium. *J Nutr*, 137, 690–693.

Neu, H.C. (1992). The crisis in antibiotic resistance. *Science*, 257(5073), 1064–1073.

Ni, B., Kramer, J.R., Bell, R.A., and Werstiuk, N.H. (2006) Protonolysis of the Hg-C bond of chloromethylmercury and dimethylmercury. A DFT and QTAIM study. *J Phys Chem A*, 110, 9451–9458.

Nierenberg, D.W., Nordgren, R.E., Chang, M.B., Siegler, R.W., Blayney, M.B., Hochberg, F., Toribara, T.Y., Cernichiari E., and Clarkson, T.W. (1998) Delayed cerebellar disease and death after accidental exposure to dimethylmercury. *N Engl J Med*, 338, 1672–1676.

Nusslein-Volhard, C., and Dahm, R. Eds. (2002) Zebrafish. New York: Oxford Univeristy Press.

Olt, J., Johnson, S.L., Martcotti, W. (2014) In vivo and in vitro biophysical properties of hair cells from the lateral line and inner ear of developing and adult zebrafish. *J Physiol*, 592, 2041–2058.

Östlund, K. (1969) Studies on the metabolism of methyl mercury and dimethyl mercury in mice. *Acta Pharmacol Tox* 27 (Suppl. 1), 1–51.

Ou, H.C., Santos, F., Raible, D.W., Simon, J.A., and Rubel, E.W. (2010) Drug screening for hearing loss: Using the zebrafish lateral line to screen for drugs that prevent and cause hearing loss. *Drug Discov Today* 15, 265–271.

Pacyna, E.G., Pacyna, J.M., Sundseth, K., Munthe, J., Kindbom, K., Wilson, S., Steenhuisen, F., and Maxson, P. (2010) Global emission of mercury to the atmosphere from

anthropogenic sources in 2005 and projections to 2020. *Atmos Environ*, 44(20), 2487–2499.

Parízek, J. and Ostádalová, I. (1967). The protective effect of small amounts of selenite in sublimate intoxication. *Experientia*, 23, 142–143.

Parker, M.O., Brock, A.J., Millington, M.E., and Brennan, C.H. (2013) Behavioral phenotyping of Casper mutant and 1-pheny-2-thiourea treated adult zebrafish. *Zebrafish*, 10, 466–471.

Parng, C., Ton, C., Lin, Y.-X., Roy, N.M., and McGrath, P. (2006) A zebrafish assay for identifying neuroprotectants in vivo. *Neurotoxicol Teratol*, 28, 509–516.

Paunesku, T., Vogt, S., Maser, J., Lai, B., and Woloschak, G. (2006) X-ray fluorescence microprobe imaging in biology and medicine. *J Cell Biochem*, 99, 1489–1502.

Pendergrass, J.C., Haley, B.E., Vimy, M.J., Winfield, S.A., Lorscheider, F.L. (1997) Mercury vapor inhalation inhibits binding of GTP to tubulin in rat brain: Similarity to a molecular lesion in Alzheimer diseased brain. *Neurotoxicol*, 18, 315–324.

Penglase, S., Hamre, K., and Ellingsen, S. (2014a) Selenium and mecury have a synergistic negative effect on fish reproduction. *Aquat Toxicol*, 149, 16–24.

Penglase, S., Hamre, K., and Ellingsen, S. (2014b) Selenium prevents downregulation of antioxidant selenoprotein genes by methylmercury. *Free Radical Bio Med*, 75, 95–104.

Perdew, J.P., Burke, K., and Ernzerhof, M. (1996) Generalized gradient approximation made simple. *Phys Rev Lett* 77, 3865–3868; (1997) Erratum, 78, 1396.

Petibois, C., and Guidi, M.C. (2008) Bioimaging of cells and tissues using accelerator-based sources. *Anal Bioanal Chem*, 391, 1599–1608.

Pickering, I.J., Prince, R.C., Salt, D.E., and George, G.N. (2000) Quantitative, chemically specific imaging of selenium transformation in plants. *Proc Natl Acad Sci*, 97 (20), 10717–10722.

Pitcher, T.J. (Ed.). (1993) Behaviour of teleost fishes (2nd ed.). London: Chapman & Hall.

Poulin J., and Gibb, H. (2008) Mercury: Assessing the environmental burden of disease at national and local levels. World Health Organization, Geneva, WHO Environmental Burden of Disease Series, no. 16.

PubChem Database. Retrieved online September 2011 at: http://pubchem.ncbi.nlm.nih.gov/

Pushie, M.J., and George, G.N. (2011) Spectroscopic studies of molybdenum and tungsten enzymes. *Coord Chem Rev*, 255(9-10), 1055–1084.

Pushie, M.J., Pickering, I.J., Korbas, M., Hackett, M.J., and George, G.N. (2014) Elemental and chemically specific X-ray fluorescence imaging of biological systems. *Chem Rev*, 114, 8499–8541.

Pushie, M.J., Zhang, L., Pickering, I.J., and George, G.N. (2012) The fictile coordination chemistry of cuprous-thiolate sites in copper chaperones. *Biochim Biophys Acta*, 1817, 938–947.

Putman, N.F., Scanlan, M.M., Billman, E.J., O'Neil, J.P., Couture, R.B., Quinn, T.P., Lohmann, K,J., Noakes, D.L.G. (2014) An inherited magnetic map guides ocean navigation in juvenile pacific salmon. *Curr Biol*, 24(4), 446–450.

Qin, Z., Caruso, J.A., Lai, B., Matusch, A., and Becker, J.S. (2010) Trace metal imaging with high spatial resolution: Applications in biomedicine. *Metallomics*, 3, 28–37.

Quinn, T.E., and Dittman, A.H. (1990) Pacific salmon migrations and homing: mechanisms and adaptive significance. *Trends Ecol Evol*, 5, 174–177.

Ralston, N.V.C. (2008) Selenium health benefit values as seafood safety criteria. EcoHealth, 5, 442–455.

Ralston, N.V.C., Azenkeng, A., Raymond, L.J. (2012) Mercury-dependent inhibition of selenoenzymes and mercury toxicity. Current topics in neurotoxicity. London: Springer. 91–99.

Ralston, N.V.C., Blackwell III, J.L., and Raymond, L.J. (2007) Importance of molar ratios in selenium-dependent protection against methylmercury toxicity. *Biol Trace Elem Res*, 119, 255–268.

Ralston, N.V.C., Ralston, C.R., Blackwell III, J.L., and Raymond, L.J. (2008) Dietary and tissue selenium in relation to methylmercury toxicity. *Neurotoxicology*, 29, 802–811.

Ralston, N.V.C. and Raymond, L.J. (2010) Dietary selenium's protective effects against methylmercury toxicity. *Toxicology*, 278, 112–123.

Rawls, J.F., Mellgren, E.M. and Johnson, S.L. (2001) How the zebrafish gets its stripes. *Dev Biol*, 240, 301–314.

Raymond, L.J., Deth, R.C., and Ralston, N.V.C. (2014) Potential role of selenoenzymes and antioxidant metabolism in relation to autism etiology and pathology. Autism Research and Treatment, 2014, 1–15.

Raymond, L.J. and Ralston, N.V.C. (2009) Selenium's importance in regulatory issues regarding mercury. *Fuel Process Technol*, 90, 1333–1338.

Ready, D., Pratten, J., Mordan, N., Watts, E., and Wilson, M. (2007). The effect of amalgam exposure on mercury- and antibiotic-resistant bacteria. *Int J Antimicrob Ag*, 30(1), 34–39.

Risher, J.F., and Amler, S.N. (2005) Mercury exposure: Evaluation and intervention: The inappropriate use of chelating agents in the diagnosis and treatment of putative mercury poisoning. *Neurotoxicology*, 26, 691–699.

Rooney, J.P.K. (2007) The role of thiols, dithiols, nutritional factors and interacting ligands in the toxicology of mercury. *Toxicology*, 234, 145–156.

Sakamoto, M., Yasutake, A., Kakita, A., Ryufuku, M., Chan, H.M., Yamamoto, M., Oumi, S., Kobayashi, S., and Watanabe, C. (2013) Selenomethionine Protects against Neuronal Degeneration by methylmercury in the developing rat cerebrum. *Environ Sci Technol*, 47, 2862–2868.

Sandahl, J.F., Baldwin, D.H., Jenkins, J.J., and Scholz, N.L. (2007) A sensory system at the interface between urban stormwater runoff and salmon survival. *Environ Sci Technol*, 41 (8), 2998–3004.

Scharpf, M., Schweizer, U., Arzberger, T., Roggendorf, W., Schomburg, L., and Köhrle, J. (2007) Neuronal and ependymal expression of selenoprotein P in the human brain, *J Neural Transm*, 114, 877–884.

Sener, H.G., Sehirli, A.O., and Ayanoglu-Dülger, G. (2003) Melatonin protects against mercury(II)-induced oxidative tissue damage in rats. *Pharmacol Toxicol*, 93, 290–296.

Sigel, A. and Sigel, H. Eds. (1997) Metal Ions in Biological Systems: Mercury and its Effects on Environment and Biology. New York: Marcel Dekker Inc.

Sillen, L.G. (1964) In Stability constants of metal-ion complexes (Sillen, L. G., and Martell, A. E., Eds.), 2nd ed., pp. 64, The Royal Chemical Society, London.

SMAK Software. Retrieved online June 2015 at: http://ssrl.slac.stanford.edu/~swebb/

Song, F., Watanabe, S., Floreancig, P.E., and Koide, K. (2009) Oxidation-resistant fluorogenic probe for mercury based on alkyne oxymercuration. *J Am Chem Soc*, 130(49), 16460–61.

Sprovieri, F., Pirrone, N., Ebinghaus, R., Kock, H., and Dommergue, A. (2010) A review of worldwide atmospheric mercury measurements. *Atmos Chem Phys*, 10, 8245–65.

Stein, W.D., and Lieb, W.R. (1986) In Transport and Diffusion across Cell Membranes, 1st ed., pp. 69-107, Academic Press, Orlando.

Strasdeit, H., von Döllen, A., Saak, W., and Wilhelm, M. (2000) Intracellular degradation of diorganomercury compounds by biological thiols-insights from model reactions. *Angew Chem Int Ed Engl*, 39, 784–786.

Sullivan-Brown, J., Bisher, M.E., and Burdine, R.D. (2011). Embedding, serial sectioning and staining of zebrafish embryos using JB-4 resin. *Nat Methods*, 6, 46–55.

Summers, A.O., Wireman, J., Vimy, M.J., Lorscheider, F.L., Marshall, B., Levy, S.B., Bennett, S., and Billard, L. (1993) Mercury released from dental "silver" fillings provokes an increase in mercury- and antibiotic-resistant bacteria in oral and intestinal floras of primates. *Antimicrob Agents Ch*, 37(4), 825–834.

Suzuki, K.T., Sasakura, C., and Yoneda, S. (1998) Binding sites for the (Hg-Se) complex on selenoprotein P, *Biochim Biophys Acta*, 1429, 102–112.

Sylvain, N.J., Brewster, D.L., and Ali, D.W. (2010) Zebrafish embryos exposed to alcohol undergo abnormal development of motor neurons and muscle fibers. *Neurotoxicol Teratol*, 32(4), 472–480.

Thanigaimalai, P., Lee, K-C., Sharma, V.K., Joo, C., Cho, W-J., Roh, E., Kim, Y., and Jung, S-H. (2011) Structural requirement of phenylthiourea analogs for their inhibitory activity of melanogenesis and tyrosinase. *Bioorg Med Chem Lett*, 21, 6824–6828.

Thomas, J.K. and Janz, D.M. (2011) Dietary selenomethionine exposure in adult zebrafish alters swimming performance, energetics and the physiological stress response. *Aquat Toxicol*, 102, 79–86.

Thomas, J.K. and Janz, D.M. (2014) In ovo exposure to selenomethionine via maternal transfer increases developmental toxicities and impairs swim performance in F1 generation zebrafish (*Danio rerio*). *Aquat Toxicol*, 152, 20–29.

Thompson, A.C. (Ed.) (2009) X-ray data booklet 3rd edition. Berkley California: Lawrence Berkley National Laboratory.

Tilton, F., Du, J.K., and Tanguay, R.L. (2008) Sulfhydryl systems are a critical factor in the zebrafish developmental toxicity of the dithiocarbamate sodium metam (NaM). *Aquat Toxicol*, 90, 121–127.

Trasande, L., Cortes, J.E., Landrigan, P.J., Abercrombie, M.I., Bopp, R.F., and Cifuentes, E. (2010) Methylmercury exposure in a subsistence fishing community in Lake Chapala, Mexico: an ecological approach. *Environ Health*, 9, 1.

Tujebajeva, R.M., Ransom, D.G., Harney, J.W., and Berry, M.J. (2000) Expression and characterization of nonmammalian selenoprotein P in the zebrafish, *Danio rerio*. *Genes Cells*, 5, 897–903.

United Nations Environment Programme UNEP. (2006) Summary of Supply, Trade and Demand Information on Mercury.

United Nations Environment Programme UNEP. (2008) The Global Atmospheric Mercury Assessment: Sources, Emissions and Transport. Geneva.

United Nations Environment Programme UNEP. (2013) Global Mercury Assessment: Sources, Emmissions, Releases and Environmental Transport. Geneva.

van den Berg, B.M., Nieuwdorp, M., Stroes, E.S.G., and Vink, H. (2006) Glycocalyx and endothelial (dys) function: from mice to men. *Pharmacol Rep*, 58, 75–80.

Wang, E.E., Mahajan, N., Wills, B., and Leikin, J. (2007) Successful treatment of potentially fatal heavy metal poisonings. *J Emerg Med*, 32, 289–294.

Wang, X., Andrews, L., Riedel, S., and Kaupp, M. (2007) Mercury is a transition metal: the first experimental evidence for HgF_4. *Angew Chem Int Ed*, 46(44), 8371–8375.

Webb, J.L. (1966) In Enzyme and Metabolic Inhibitors, 1st ed., pp.729-751, Academic Press, New York.

Weekley, C.M., and Harris, H.H. (2013) Which form is that? The importance of selenium speciation and metabolism in the prevention and treatment of disease. *Chem Soc Rev*, 42, 8870–8894.

Weinstein, M. and Bernstein, S. (2003) Pink ladies: mercury poisoning in twin girls. *Can Med Assoc J*, 168(2), 201.

Westerfield, M. (1995) The zebrafish book: a guide for the laboratory use of zebrafish (Brachydanio rerio). University of Oregon Press, Eugene.

White, R.M., Sessa, A., Burke, C., Bowman, T., LeBlanc, J., Ceol, C., Bourque, C., Dovey, M., Goessling, W., Burns, C.E., and Zon, L.I. (2008) Transparent adult zebrafish as a tool for in vivo transplantation analysis. *Cell Stem Cell*, 2, 183–189.

Whittaker, J.R. (1966) An analysis of melanogenesis in differentiating pigment cells of ascidian embryos. *Dev Biol*, 14, 1–39.

Winick, H. (Ed.) (1994) Synchrotron Radiation Sources, A Primer. Singapore: World Scientific.

World Health Organization WHO. (1991) International Programme on Chemical Safety. Environmental Health Criteria 118: Inorganic mercury. Geneva: World Health Organization.

World Health Organization WHO. (2003) Concise International Chemical Assessment Document (CICAD) 50. Elemental mercury and inorganic mercury compounds: human health aspects. Geneva: World Health Organization.

World Health Organization WHO. (2008) Environmental Burden of Disease Series, No. 16. Mercury Assessing the environmental burden of disease at national and local levels. Geneva: World Health Organization.

Yamamoto, A., Akanuma, S., Tachikawa, M., and Hosoya, K. (2010) Involvement of LAT1 and LAT2 in the high- and low-affinity transport of L-leucine in human retinal pigment epithelial cells (ARPE-19 cells). *J Pharm Sci*, 99, 2475–2482.

Yamashita, M., Yamashita, Y., Suzuki, T., Kani, Y., Mizusawa, N., Imamura, S., Takemoto, K., Hara, T., Hossain, M.A., Yabu, T., and Touhata, K. (2013) Selenoneine, a novel selenium-containing compound, mediates detoxification mechanisms against methylmercury accumulation and toxicity in zebrafish embryo. *Mar Biotechnol*, 15, 559-570.

Yang, G., Liu, G-F., Zheng, S-L., and Chen, X-M. (2001) Synthesis and structures of dichlorotetrakis(phenylthiourea) Cadmium(II) and catena-bis(thiocyanate) bis(phenylthiourea) Cadmium(II). *J Coord Chem*, 53, 269–279.

Yang, L., Ho, N.Y., Alshut, R., Legradi, J., Weiss, C., Reischl, M., Mikut, R., Liebel, U., Müller, F., and Strähle, U. (2009) Zebrafish embryos as models for embryotoxic and teratological effects of chemicals. *Reprod Toxicol*, 28, 245–253.

Yoneda, S., and Suzuki, K.T. (1997) Equimolar Hg-Se complex binds selenoprotein P. *Biochem Biophys Res Commun*, 231, 7–11.

Yoon, S., Albers, A.E., Wong, A.P., and Chang, C.J. (2005) Screening mercury levels in fish with a selective fluorescent chemosensor. *J Am Chem Soc*, 127(46), 16030–16031.

Yoon, S., Miller, E.W., He, Q., Do, P.H., and Chang, C.J. (2007) A bright and specific fluorescent sensor for mercury in water, cells and tissue. *Angew Chem Int Ed*, 46, 6658–61.

Zalups, R.K., and Bridges, C.C. (2010) Seventy-five percent nephrectomy and the disposition of inorganic mercury in 2,3-dimercaptopropanesulfonic acid-treated rats lacking functional multidrug-resistance protein 2. *J Pharmacol Exp Ther*, 332, 866–875.

Zalups, R. K., and Bridges, C.C. (2012) Relationships between the renal handling of DMPS and DMSA and the renal handling of mercury. *Chem Res Toxicol*, 25, 1825–1838.

Zalups, R.K., Joshee, L., and Bridges, C.C. (2014) Novel Hg^{2+}-induced nephropathy in rats and mice lacking Mrp2: evidence of axial heterogeneity in the handling of Hg^{2+} along the proximal tubule. *Toxicol Sci* 142, 250–260.

Zecca, L., Pietra, R., Goj, C., Mecacci, C., Radice, D., and Sabbioni, E. (1994) Iron and other metals in neuromelanin, substantia nigra, and putamen of human brain. *J Neurochem*, 62, 1097–1101.

APPENDIX A – SUPPLEMENTARY MATERIAL FOR CHAPTER 3

Supplementary Table 3.1 All components of mercury treatment solutions in millimolar concentrations included in speciation calculations using MINTEQA2 software.

Formulation	Cl^-	CO_3^{2-}	SO_4^{2-}	Na^+	NO^{3-}	K^+	Mg^{2+}	Ca^{2+}	$HEPES^-$	Hg^{2+}	CH_3Hg^+	RS^-	PO_4^{3-}
1 µM $HgCl_2$	0.3123	2.426	1.041	1.218	0.0274	0.0818	0.740	0.948	-	0.001	-	-	-
1 µM CH_3HgCl	0.3113	2.426	1.041	1.218	0.0274	0.0818	0.740	0.948	-	-	0.001	-	-
200 µM $HgCl_2$ 500 µM L-Cys	0.648	1.941	0.833	0.974	0.0219	0.0655	0.592	0.758	10	0.2	-	0.5	-
2 µM CH_3HgOH 2.4 µM L-Cys	0.5402	2.426	1.041	1.529	0.0274	0.0818	0.74	0.948	-	-	0.002	0.0024	0.0446

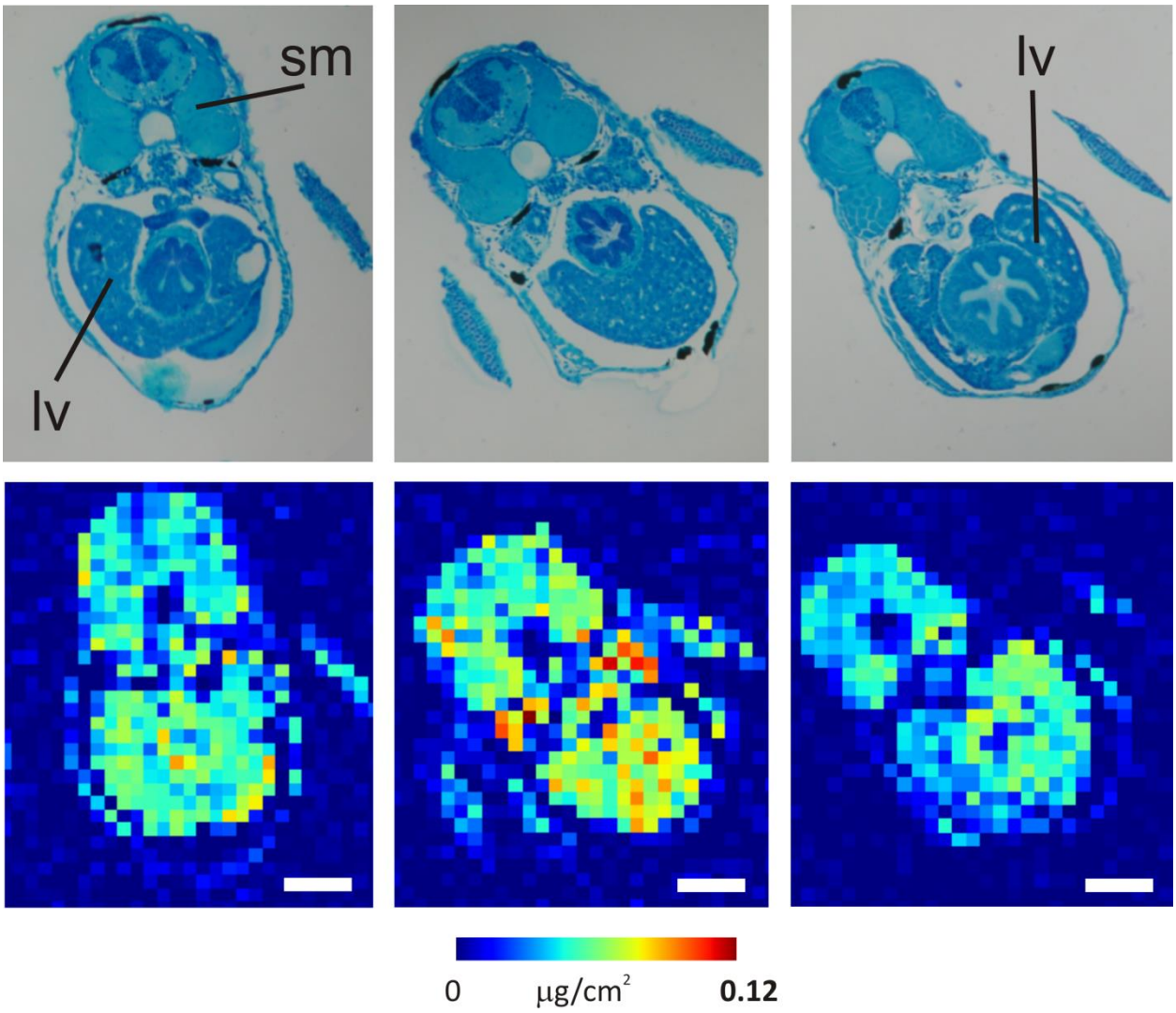

Supplementary Figure 3.1. Quantitative mercury distributions in 7 dpf zebrafish larvae following the same treatment with methylmercury L-cysteineate. Histological images (upper panel) of the liver region are compared with the mercury distributions of the adjacent sections (lower panel). The mercury maps are scaled to the highest level of mercury among all three images. Scale bar 100 µm, *sm*-somitic muscles, *lv*-liver.

Supplementary Table 3.2 Variation in cellular mercury concentrations in liver and somitic muscles between three zebrafish larvae from Supplementary Figure 3.1.

Fish from Supplementary Figure 1	Average Hg concentration in liver ($\mu g/cm^2$)	Average Hg concentration in somitic muscles ($\mu g/cm^2$)	Deviation from the average value in liver/muscles
A	0.053	0.046	3%/10%
B	0.060	0.058	10%/14%
C	0.051	0.048	7%/6%
Average	0.055	0.051	

APPENDIX B – SUPPLEMENTARY MATERIAL FOR CHAPTER 4

Supplementary Table 4.1 Statistical significance values for comparison of deaths in $HgCl_2$ versus $HgCl_2$ with phenylthiourea groups

	2 μM $HgCl_2$ *vs* 2 μM $HgCl_2$ + 100 μM PTU	4 μM $HgCl_2$ *vs* 4 μM $HgCl_2$ + 100 μM PTU
Day 1	$P < 0.001$	$P < 0.0001$
Day 2	$P < 0.0001$	$P < 0.0001$
Day 3	$P < 0.0001$	$P < 0.0001$

Supplementary Table 4.2 Statistical significance values for comparison of deaths in CH_3HgCl versus CH_3HgCl with phenylthiourea groups

	0.5 μM CH_3HgCl *vs* 0.5 μM CH_3HgCl + 100 μM PTU
Day 1	Not significant
Day 2	$P < 0.0001$
Day 3	$P < 0.0001$

Supplementary Table 4.3 T-test values

	4 μM $HgCl_2$	**4 μM $HgCl_2$ + PTU**	**0.2 μM CH_3HgCl**	**0.2 μM CH_3HgCl + PTU**
Fish 1	0.1297	0.00200	0.04589	0.07668
Fish 2	0.1225	0.00161	0.06792	0.12224
Fish 3	0.1132	0.00234	0.05066	0.08737
Mean	0.1218	0.00198	0.05482	0.09421
P value	0.001662		0.028974	